Finite Element Heterogeneous Multiscale Methods for the Wave Equation

Inauguraldissertation

zur
Erlangung der Würde eines Doktors der Philosophie
vorgelegt der
Philosophisch-Naturwissenschaftlichen Fakultät
der Universität Basel

von

Christian Stohrer

aus Basel, Basel-Stadt

Basel, 2013

creative commons

Namensnennung-Keine kommerzielle Nutzung-Keine Bearbeitung 2.5 Schweiz

---

Sie dürfen:

das Werk vervielfältigen, verbreiten und öffentlich zugänglich machen

Zu den folgenden Bedingungen:

Namensnennung. Sie müssen den Namen des Autors/Rechteinhabers in der von ihm festgelegten Weise nennen (wodurch aber nicht der Eindruck entstehen darf, Sie oder die Nutzung des Werkes durch Sie würden entlohnt).

Keine kommerzielle Nutzung. Dieses Werk darf nicht für kommerzielle Zwecke verwendet werden.

Keine Bearbeitung. Dieses Werk darf nicht bearbeitet oder in anderer Weise verändert werden.

- Im Falle einer Verbreitung müssen Sie anderen die Lizenzbedingungen, unter welche dieses Werk fällt, mitteilen. Am Einfachsten ist es, einen Link auf diese Seite einzubinden.
- Jede der vorgenannten Bedingungen kann aufgehoben werden, sofern Sie die Einwilligung des Rechteinhabers dazu erhalten.
- Diese Lizenz lässt die Urheberpersönlichkeitsrechte unberührt.

Quelle: http://creativecommons.org/licenses/by-nc-nd/2.5/ch/ Datum: 3.4.2009

Genehmigt von der Philosophisch-Naturwissenschaftlichen Fakultät
auf Antrag von

Prof. Dr. Marcus J. Grote
Prof. Dr. Olof Runborg

Basel, den 21. Mai 2013

Prof. Dr. Jörg Schibler
Dekan

To Annina and my parents

Abstract

Wave phenomena appear in a wide range of applications such as full-waveform seismic inversion, medical imaging, or composite materials. Often, they are modeled by the acoustic wave equation. It can be solved by standard numerical methods such as, e.g., the finite element (FE) or the finite difference method. However, if the wave propagation speed varies on a microscopic length scale denoted by ε, the computational cost becomes infeasible, since the medium must be resolved down to its finest scale. In this thesis we propose multiscale numerical methods which approximate the overall macroscopic behavior of the wave propagation with a substantially lower computational effort. We follow the design principles of the heterogeneous multiscale method (HMM), introduced in 2003 by E and Engquist. This method relies on a coarse discretization of an a priori unknown effective equation. The missing data, usually the parameters of the effective equation, are estimated on demand by solving microscale problems on small sampling domains. Hence, no precomputation of these effective parameters is needed. We choose FE methods to solve both the macroscopic and the microscopic problems.

For limited time the overall behavior of the wave is well described by the homogenized wave equation. We prove that the FE-HMM method converges to the solution of the homogenized wave equation. With increasing time, however, the true solution deviates from the classical homogenization limit, as a large secondary wave train develops. Neither the homogenized solution, nor the FE-HMM capture these dispersive effects. To capture them we need to modify the FE-HMM. Inspired by higher order homogenization techniques we additionally compute a correction term of order ε^2. Since its computation also relies on the solution of the same microscale problems as the original FE-HMM, the computational effort remains essentially unchanged. For this modified version we also prove convergence to the homogenized wave equation, but in contrast to the original FE-HMM the long-time dispersive behavior is recovered.

The convergence proofs for the FE-HMM follow from new Strang-type results for the wave equation. The results are general enough such that the FE-HMM with and without the long-time correction fits into the setting, even if numerical quadrature is used to evaluate the arising L^2 inner product.

In addition to these results we give alternative formulations of the FE-HMM, where the elliptic micro problems are replaced by hyperbolic ones. All the results are supported by numerical tests. The versatility of the method is demonstrated by various numerical examples.

Contents

List of Figures

Acknowledgement

I would like to thank Prof. Dr. Marcus J. Grote for giving me the opportunity to do my PhD at the Department for Mathematics and Computer Since at the University of Basel. I appreciate his support, guidance, advice, and confidence during my study. I owe him my gratitude for awakening my interest for numerical analysis and my fascination for wave phenomena.

I would like to thank Prof. Dr. Olof Runborg for kindly agreeing to take part as a co-referee in the thesis committee. My sincere thanks go to Prof. Dr. Assyr Abdulle not only for acting as an additional expert during my PhD examination, but also for many helpful discussions, inspiring ideas, and his interest in my work.

My thanks also go to Dr. Achim Nonnenmacher and Dr. Henrik Holst for providing me access to their multiscale code. They were suppliers of ideas from which my own implementation profited.

I wish to thank my colleagues and the administrative staff at the Mathematical Institute. In particular I thank the current and former members of the Numerical Analysis group: Prof. Dr. David Cohen, Dr. Loredana Gaudio, Dr. Marie Kray, Dr. Teodora Mitkova Michaela Mehlin, Uri Nahum, Dr. Vivana Palumberi, and Dr. Imbo Sim for many discussions, mutual assistance, and the open working atmosphere. I am indebted to my office mate Johannes Huber for many hours of inspirational and animating discussions, countless coding hints, and, speaking figuratively, for his permanent helping hands and open ears.

This thesis would not have been possible without the support and encouragement of my family and friends. I heartily thank my parents Susi and Dieter Stohrer for their support, care, and love during my whole life. I cannot find appropriate words to express my deepest gratitude.

Finally, from the bottom of my heart I thank my beloved girlfriend, Annina Nef, for her understanding, patience, emotional hold, and, most of all, for her love.

This thesis was partly supported by the Swiss National Science Foundation.

One

Introduction

> Wave phenomena are ubiquitous in science and engineering. From the obvious and long-standing applications in hydrodynamics, through seismics, acoustic noise propagation and radio wave propagation, waves underlie many important scientific and engineering areas.
>
> Jan S. Hesthaven, Houssem Haddar, [51]

> There is a growing need to develop systematic modeling and simulation approaches for multiscale problems.
>
> Russel E. Caflisch, [18]

Many natural and artificial materials are heterogeneous. Often their properties, such as bulk modulus, thermal conductivity, and wave propagation speed vary within the domain. If these variations occur on a microscopic scale, they cause serious computational challenges when simulating physical phenomena in those materials. They are known as composite materials and consist of at least two finely mixed components. Typical examples are concrete, a mixture of tiny stones and cement or fiber-reinforced plastic, consisting of carbon, glass, or other fibers in a polymeric surrounding material, called the matrix. Within this mixture the components are not dissolved into each other, but are combined such that one can distinguish them at a microscopic level. Even if we are only interested in the overall behavior of a physical process on a larger, macroscopic scale we can not simply neglect the microscopic structure of the underlying material. On the contrary, using classical numerical methods such as the finite difference (FD) or the finite element (FE) method one needs to resolve the medium down to its finest scale to obtain satisfactory simulation results. However, the full resolution of a problem is often very costly or even not feasible due to CPU or memory restrictions.

1.1 Homogenization theory

Although composites consist of materials with different properties, at the macroscopic level they behave like a homogeneous material, if the mixture is fine enough. The so-called effective or homogenized material displays properties differing from the properties of the original components. Homogenization theory describes this process mathematically. Its goal is to describe the macroscopic behavior of solutions of multiscale problems. Let us consider the following general multiscale problem: Find the solution u^ε in an appropriate function space such that

$$L^\varepsilon(u^\varepsilon) = 0. \tag{1.1}$$

Here, L^ε is a multiscale operator reflecting material variations on a microscale of typical length ε. The parameter ε can be seen as a measure of the fineness of the mixture in the composite material. For composite materials the multiscale structure of the operator L^ε is caused by the microscale nature of the material. We denote this by $L^\varepsilon(\cdot) = L^\varepsilon(\cdot, d^\varepsilon)$, where d^ε are given microscale data on which the multiscale operator depends.

We assume that the multiscale problem (1.1) is well-posed and has a unique solution u^ε for every $\varepsilon > 0$. Homogenization theory answers the question, does the sequence of solutions u^ε converges if $\varepsilon \to 0$ and if so, is there an effective or homogenized equation

$$L^{\text{eff}}(u^{\text{eff}}) = 0$$

such that its solution u^{eff} is the limit of the u^ε, possibly in a weak sense. Often the answer is positive.

Remark. Because $u^\varepsilon \to u^{\text{eff}}$ as $\varepsilon \to 0$, the effective solution is commonly denoted by u^0 and the corresponding effective operator by L^0. We reserve the superscript 0 for the classical homogenization limit. To study long-time wave propagation, however, we will use a different effective model; therefore, we prefer the superscript "eff" here.

The effective equation typically has the following form: Find u^{eff} such that

$$L^{\text{eff}}(u^{\text{eff}}, d^{\text{eff}}) = 0,$$

where the homogenized data d^{eff} can be computed analytically only in exceptional cases, but the structure of L^{eff} is known. For a better understanding consider, e.g, heat conduction in a material with highly oscillatory thermal conductivity k^ε. The heat distribution in the heterogeneous material is modeled by the heat equation. The overall distribution can be well described by the homogenization limit of this problem. It turns out that the homogenized equation is again a heat equation. Nevertheless the homogenized thermal conductivity k^0 needed for a complete description can only be computed analytically in some special cases, e.g., if k^ε is ε-periodic. We will see later in the thesis that we are in the same situation for the wave equation with highly oscillatory propagation speed. Again the limit equation stays of the same type as the original multiscale problem. Thus we know its structure, but the homogenized wave speed can only rarely be computed analytically, too.

1.2 Heterogeneous multiscale methods

The heterogeneous multiscale method (HMM) introduced in [30] provides a framework for the design of multiscale algorithms for problems given in the general setting of the previous section. We now describe its main idea. Further details about HMM can be found in the review articles [4, 31]. Specific details for particular cases are given throughout the thesis. The goal of HMM is to approximate the effective behavior of the solution of a multiscale problem without fully resolving the whole computational domain. HMM follows a top-down approach, beginning with the effective equation.

Assuming that we know the structure of the effective equation, we first choose a numerical method to discretize it. The method chosen is called the macro solver and its discretization parameter, e.g., the mesh size, is denoted by H. The discretized effective equation is written as

$$L_H^{\text{eff}}(u_H^{\text{eff}}, d^{\text{eff}}) = 0. \tag{1.2}$$

Note that this equation is incomplete since we do not know d^{eff}. Every time we need it for the evaluation of the macro solver, we estimate these missing data by solving a micro problem

$$L^{\text{mic}}(u^{\text{mic}}, d^{\text{mic}}) = 0.$$

The micro problem is often identical with the original multiscale problem (1.1), yet this is not necessary. The purpose of the micro problem is to estimate the missing data in (1.2). Note that we do not precompute d^{eff} everywhere, but we compute it on demand. In addition the micro problem is constrained by d^{mic} to be consistent with the macroscopic solution. These constraints are often realized by special initial or boundary conditions. To solve the micro problem we need to apply another numerical method which we call the micro solver. We denote the discretization parameter of the micro solver by h and consider the micro problem

$$L_h^{\text{mic}}(u_h^{\text{mic}}, d^{\text{mic}}) = 0.$$

From the numerical solution u_h^{mic} we estimate the missing data. This is often done by an averaging process. Replacing d^{eff} with the estimate data d^{est} we finally get our HMM scheme L_H:

$$L_H(u_H) = L_H^{\text{eff}}(u_H, d^{\text{est}}) = 0.$$

In Figure 1.1 the concept of the HMM framework is shown schematically.

The HMM scheme is computationally affordable since it does not resolve the whole computational domain with the micro mesh size h. Only some small sampling domains needed to estimate the missing data are fully resolved. The macroscopic discretization can be much coarser and does not need to resolve the fine scale structure of the medium, i.e., $H \gg \varepsilon$ is allowed. The goal of this thesis is to develop and analyze HMM schemes for the wave equation. In particular we are looking for FE heterogeneous multiscale methods (FE-HMM), where both the macro and the micro problem are solved with FE methods.

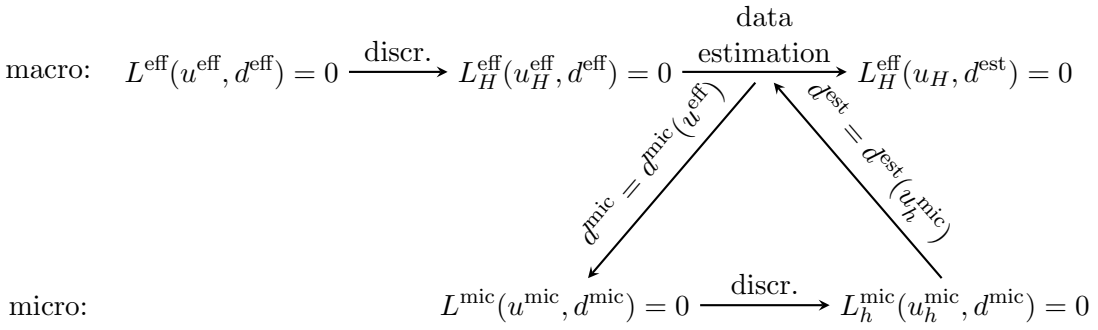

Figure 1.1: Schematics of the HMM.

1.3 Numerical methods for waves in multiscale materials

We consider the acoustic wave equation

$$\partial_{tt} u(t;x) - \nabla \cdot (a(x) \nabla u(t;x)) = f(t;x) \qquad \text{in } \Omega \times (0,T), \tag{1.3}$$

where Ω denotes a bounded open set in $\mathbb{R}^d$, $T > 0$ the final time, and $a(x)$ is the squared wave propagation field. For a well-posedness of the system, appropriate initial and boundary conditions must be specified as well. We postpone a more detailed mathematical introduction to Section 2.2. If the material the wave is propagating through is highly oscillatory, we denote this by replacing $a(x)$ with $a^\varepsilon(x)$. Only the propagation speed may vary on the microscale. The source f and the initial and boundary conditions depend only on the macroscale.

In the following we give an overview of multiscale methods developed to simulate wave propagation in highly heterogeneous media. Here we do not discuss purely analytical approaches where effective equations are developed. Because these effective models are the starting point of an HMM scheme, they will be discussed in more detail in Chapter 4.

While there are many multiscale methods for elliptic and parabolic problems, only a few of them are designed for the acoustic wave equation (1.3). The method most similar to the one presented in this thesis is the FD-HMM scheme proposed in [35, 37]. Although both methods follow the general HMM approach described in Section 1.2, they differ essentially in the following aspects: On the first approach finite differences are used to solve the macro and the micro problem, whereas we use finite elements. Since the macroscopic solvers are not the same, different effective data must be estimated: an effective flux for FD-HMM and an effective bilinear form for FE-HMM. For the FD-HMM this estimation relies on the numerical solution of a wave equation in a small space-time sampling domain as contrasted with the elliptic micro problem of FE-HMM. In Section 5.5 we give alternative formulations of the standard FE-HMM which are more similar to the FD-HMM scheme. In [36, 39] the FD-HMM was modified slightly such that it is able to capture long-time dispersive effects of wave propagation. The modifications are described in Section 6.4.

In the following we give an overview of multiscale methods beyond HMM: In [56] the multiscale finite element method (MsFEM) was used to solve the acoustic wave equation with continuum spatial scales. MsFEM relies on the computation of multiscale basis functions. See, e.g., the monograph [33] for further details. In [66] another FE method relying on global change of variables is proposed. This techniques has been used to solve elliptic and parabolic multiscale problems in [64, 65]. The approach is general since it does not assume any scale separation of the medium and can be applied to strongly nonlocal media. However, the computation of the change of coordinates is rather challenging and computationally intensive. The computation of the coarse scale models requires the solution of fully resolved problems throughout the whole computation domain. Similar in this aspect are the methods presented in [58, 71, 72]. These operator based upscaling methods calculate effective media property. Because of the full resolution, the computational cost scales at a comparable rate to any fully resolved standard FD or FE method. The computational gain lies in the possibility that these computations can be made in parallel. Based on an asymptotic expansion, a numerical method for the acoustic wave equation with rapidly oscillating coefficients was proposed in [27]. Yet it assumes not only periodicity, but also internal symmetry in the periodic cells.

1.4 Outline of the thesis

The thesis is divided into three parts. In the first preliminary part we introduce the accurate function spaces for the wave equation. Afterwards we consider, on one hand, wave propagation, but without exploiting the multiscale nature of the medium. On the other hand, we then consider elliptic problems in highly oscillating media. First, in Chapter 2, we recall well-known analytical results, which we will use later on. The numerical methods on which the FE-HMM is based, i.e., FEM for the wave equation and HMM, are introduced in Chapter 3. In Section 3.1 we prove an a priori error estimate, which we apply to show convergence results for the FE-HMM schemes proposed in the following part.

In the second part we combine these topics and consider wave propagation in highly oscillatory media. In Chapter 4 we recall first the result from homogenization theory for the wave equation. We consider both the finite-time and the long-time regime and show the differences between them. In Chapter 5 we propose an FE-HMM scheme for the wave equation, show convergence results and give various numerical examples. We conclude this chapter by proposing two alternative formulations of the FE-HMM and comment on the implementation that we used for the numerical examples. The following Chapter 6 is structured similarly, but here we consider longer times, where dispersive effects develop unexpectedly.

In the last and short part we summarize our results, draw conclusions, and give an outlook on further research.

1.5 Notation

We introduce here the notation that we use throughout this thesis.

Let the computational spatial domain $\Omega \subset \mathbb{R}^d$ be an open bounded set in the d-dimensional real Euclidean space, where $d \in \{1, 2, 3\}$. For a domain $\mathcal{O} \subset \Omega$, $|\mathcal{O}|$ denotes the measure of $\mathcal{O}$. The time domain is given by $(0, T)$ with $T > 0$. The l^2 scalar product of $x, y \in \mathbb{R}^d$ is given by $x \cdot y = \sum_{i=1}^{d} x_i y_i$ and $|x|$ denotes the Euclidean norm of x. Hence we have $|x|^2 = x \cdot x$ for all $x \in \mathbb{R}^d$.

For a function

$$f : \begin{cases} (0,T) \times \Omega \to \mathbb{R}, \\ \qquad (t, x) \mapsto f(t; x), \end{cases}$$

we mean by writing $f(t) : \Omega \to \mathbb{R}$ the function given by $(f(t))(x) = f(t; x)$. If $f(t)$ belongs to a certain function space X, the function f can be identified with a function from $(0, T)$ to X. For more information on Banach space valued functions, see Section 2.1.

Partial derivatives with respect to time are written as $\frac{\partial}{\partial t}$, $\frac{\partial^2}{\partial t^2}$, and $\frac{\partial^k}{\partial t^k}$ or more briefly as ∂_t, ∂_{tt} and ∂_t^k, respectively. Partial derivatives with respect to spatial variables are denoted accordingly. Moreover we use $\nabla = (\partial_{x_1}, \ldots, \partial_{x_d})^T$ to abbreviate the gradient of a scalar-valued function and the divergence of a vector-valued function by the suggestive notation ∇f and $\nabla \cdot g$, respectively. The Jacobian of a function

$$g : \begin{cases} \mathbb{R}^d \to \mathbb{R}^d, \\ \quad x \mapsto \left(g^1(x), \ldots, g^d(x) \right)^T, \end{cases}$$

is given by

$$(Dg)_{ij} = \partial_{x_j} g^i.$$

Thus for a scalar-valued function f, we have $Df = (\nabla f)^T$. We want to emphasize that ∇ and D are taken with respect to the spatial variable only.

The function spaces $L^p(\Omega)$ and $W^{k,p}(\Omega)$ denote the standard Lebesque and Sobolev spaces. For $p = 2$ we use the notation $H^k(\Omega)$ and $H_0^k(\Omega)$ as usual. The associated norm are written as $\|\cdot\|_{L^p(\Omega)}$, $\|\cdot\|_{W^{k,p}(\Omega)}$ and $\|\cdot\|_{H^k(\Omega)}$, respectively, where the explicit indication of the domain may be dropped, if no confusion can occur. If Ω is cuboidal, we denote the subspace of H^1 consisting of functions with Ω-periodic trace and vanishing mean value by

$$H^1_{\mathrm{per}}(\Omega) = \{v \in W^{1,2}_{\mathrm{per}}(\Omega);\ \int_\Omega v \, dx = 0\},$$

where $W^{1,2}_{\mathrm{per}}(\Omega)$ is defined as the closure of $C^\infty_{\mathrm{per}}(\Omega)$, the subset of Ω-periodic functions of $C^\infty(\Omega)$, with respect to the $W^{1,2}$ norm. In addition to standard Sobolev norms, we introduce the broken Sobolev norm. Let $\mathcal{T}_H$ be a partition of Ω into disjoint elements K, as in Section 3.1. Provided that $v : \Omega \to \mathbb{R}$ is such that $\|v\|_{H^\ell(K)}$ is finite for all

$K \in \mathcal{T}_H$, the broken Sobolev norm is given by

$$\|v\|_{\bar{H}^\ell(\Omega)} = \left(\sum_{K \in \mathcal{T}_H} \|v\|^2_{H^\ell(K)} \right)^{\frac{1}{2}}.$$

Note that if $v \in H^\ell(\Omega)$ the identity $\|v\|_{\bar{H}^\ell} = \|v\|_{H^\ell}$ holds.

The constant $C > 0$ is generic and not necessarily the same at any two occurrences.

Part I

Preliminaries

Two

Analytical background

In this chapter we summarize important analytical propositions and theorems without giving detailed proofs. They can be found in the referenced literature. We first introduce the accurate function spaces for time dependent functions and recall the existence and uniqueness theorems for the wave equation. Then we provide a short overview of the homogenization theory for elliptic equations.

2.1 Banach space valued functions

In this section we follow [41, Section 5.9.2]. Let X be a Banach space with norm $\|\cdot\|_X$. The Bochner space $L^p(0,T;X)$, $1 \leq p \leq \infty$, consists of measurable functions $v\colon [0,T] \to X$ such that

$$\|v\|_{L^p(0,T;X)} = \begin{cases} \left(\int_\Omega \|v(t)\|_X^p \, dx \right)^{\frac{1}{p}} & \text{for } 1 \leq p < \infty, \\ \operatorname*{ess\,sup}_{t\in[0,T]} \|v(t)\|_X & \text{for } p = \infty \end{cases}$$

is finite. It is well known that with this norm $L^p(0,T;X)$ is a Banach space.

The set of all continuous functions $v\colon [0,T] \to X$ satisfying

$$\|v\|_{C(0,T;X)} = \max_{t\in[0,T]} \|v(t)\|_X \leq \infty$$

is denoted by $C(0,T;X)$.

Theorem 2.1 (see [41, Section 5.9.2, Theorem 2])**.** *Let X be a Banach space. After a possible modification on a set of measure zero, the following inclusion holds:*

$$W^{1,p}(0,T;X) = \{v | v \in L^p(0,T;X), \partial_t v \in L^p(0,T;X)\} \subset C(0,T;X)$$

for all $1 \leq p \leq \infty$, where $\partial_t v$ is the weak derivative with respect to time. Moreover, there is a constant $C > 0$ such that

$$\|v\|_{C(0,T;X)} \leq C \left(\|v\|_{L^p(0,T;X)} + \|\partial_t v\|_{L^p(0,T;X)} \right)$$

for all $v \in W^{1,p}(0,T;X)$.

We will use this theorem to bound $v(t)$, where $v \in W^{1,p}(0,T;X)$ and $t \in [0,T]$. We have

$$\|v(t)\|_X \leq \|v\|_{C(0,T;X)} \leq C\left(\|v\|_{L^p(0,T;X)} + \|\partial_t v\|_{L^p(0,T;X)}\right).$$

2.2 Wave equation

We consider the linear wave equation, which is a typical example for second order hyperbolic partial differential equations. There are various physical areas where the wave equation arises. The most prominent examples are acoustics, electromagnetism, and elasticity theory. In this section, we summarize classical existence, uniqueness, and regularity results for the wave equation. The results presented here are general, since no special assumption on the medium is needed.

A weak solution of the wave equation (1.3) is a solution of the following variational problem: Find $u\colon [0,T] \to H_0^1(\Omega)$ such that

$$\begin{cases} (\partial_{tt} u(t), v) + B(u(t), v) = (f(t), v) & \text{for all } v \in H_0^1(\Omega),\ 0 \leq t \leq T, \\ u(0) = u_I & \text{in } \Omega, \\ \partial_t u(0) = v_I & \text{in } \Omega, \end{cases} \tag{2.1}$$

where $(\cdot,\cdot)$ denotes the standard L^2 scalar product. The bilinear form B is given by

$$B(v,w) = \int_\Omega a(x) \nabla v \cdot \nabla w \, dx,$$

where $a(x)$ is symmetric, uniformly elliptic, and bounded. Note that due to the symmetry of a, the bilinear form B is symmetric, too. To be more precise we introduce a set of admissible matrix-valued functions $\mathcal{M}(\lambda,\Lambda)$ and assume from now on that $a \in \mathcal{M}(\lambda,\Lambda)$.

Definition 2.2. Let $0 < \lambda \leq \Lambda$ and $d \in \mathbb{N}$. The set $\mathcal{M}(\lambda,\Lambda)$ consists of all $a(x) \in (L^\infty(\Omega))^{d\times d}$ such that for all $\xi \in \mathbb{R}^d$ and for almost every $x \in \Omega$

$$\lambda |\xi|^2 \leq a(x)\xi \cdot \xi$$

and

$$|a(x)\xi| \leq \Lambda |\xi|. \tag{2.2}$$

Remark. There are (at least) two alternative definitions of $\mathcal{M}(\lambda,\Lambda)$ available in the literature (see, e.g., [22, 62]), where the boundedness, i.e. (2.2), is replaced by either

$$a(x)\xi \cdot \xi \leq \Lambda |\xi|^2 \qquad \text{or} \qquad a^{-1}(x)\xi \cdot \xi \geq L |\xi|^2.$$

It can be shown that these definitions are equivalent, but only if $a(x)$ is symmetric, which we always assume.

The given functions f, u_I, and v_I describe the source term and the initial conditions, respectively. We always assume that the standard assumptions

$$f \in L^2(0,T;L^2(\Omega)), \tag{2.3}$$
$$u_I \in H_0^1(\Omega), \tag{2.4}$$
$$v_I \in L^2(\Omega), \tag{2.5}$$

hold.

From [61, Chap. 3, Theorems 8.1 and 8.2] we have the following existence and uniqueness theorem.

Theorem 2.3. *Let $\Omega \subset \mathbb{R}^d$, and $a(x) \in \mathcal{M}(\lambda,\Lambda)$. Given the assumptions (2.3)–(2.5), the wave equation (2.1) has a unique weak solution $u \in L^2(0,T;H_0^1(\Omega))$ with $\partial_t u \in L^2(0,T;L^2(\Omega))$. The solution is actually more regular. After a possible modification on a set of measure zero, we have*

$$u \in C(0,T;H_0^1(\Omega)) \quad \textit{and} \quad \partial_t u \in C(0,T;L^2(\Omega)).$$

Properties of the wave equation

In the following we highlight two characteristic properties of the wave equation. The first property is the conservation of energy. Assume that $f \equiv 0$ and let $u(t)$ be the weak solution of the wave equation. Choosing formally $v = \partial_t u(t)$ in (2.1) we find

$$(\partial_{tt} u, \partial_t u) + B(u, \partial_t u) = \frac{1}{2}\frac{d}{dt}\left(\|\partial_t u\|^2_{L^2(\Omega)} + B(u,u)\right) = 0,$$

where we used that B is symmetric. Hence, the energy defined by

$$E(t) = \frac{1}{2}\left(\|\partial_t u(t)\|^2_{L^2(\Omega)} + B(u(t),u(t))\right) \tag{2.6}$$

is constant. Knowing the initial conditions we can compute

$$E(t) = E(0) = \frac{1}{2}\left(\|v_I\|^2_{L^2(\Omega)} + B(u_I,u_I)\right).$$

For a rigorous proof we refer to [61, Chapter 3, Section 8].

The second property of the wave equation is the finite speed of disturbances. We consider first the one-dimensional wave equation in $\mathbb{R}$ in a homogeneous medium, i.e., $a(x) = c^2 0$ for all $x \in \mathbb{R}$. Here this property is immediately comprehensible. For the ease of presentation we assume here that u_I and v_I are smooth. Then the solution of

$$\begin{cases} \partial_{tt} u(t;x) - c^2 \partial_{xx} u(t;x) = 0 & \text{in } (0,T)\times\mathbb{R}, \\ u(0) = u_I \text{ and } \partial_t u(0) = v_I & \text{in } \Omega, \end{cases}$$

with $c > 0$ is given by d' Alembert's formula

$$u(t;x) = \frac{1}{2}\left(u_I(x+ct) + u_I(x-ct)\right) + \frac{1}{2c}\int_{x-ct}^{x+ct} v_I(\xi)\,d\xi. \tag{2.7}$$

From this formula we can conclude that $u(t;x)$ only depends on the values of u_I and v_I in the interval $[x-ct, x+ct]$; or vice versa, that the initial data at x_0 only influence values in the cone $\{(x,t); x_0 - ct \le x \le x_0 + ct\}$. These considerations can be generalized to the multidimensional, non-homogeneous case. For the wave equation (2.1) with $a \in \mathcal{M}(\lambda, \Lambda)$, we have that the initial data at x_0 do not influence $u(t;x)$, if $x \notin x_0 + [-\sqrt{\Lambda}t, \sqrt{\Lambda}t]^d$. In other words, information travels with a speed less than $\sqrt{\Lambda}$. Note that these are not sharp bounds. A precise statement can be found in [41, Section 7.2.4].

2.3 Homogenization for elliptic problems

Here we recall some classical results from homogenization theory for the most fundamental case, which is the homogenization of a second order elliptic partial differential equation. Further results and details can be found, e.g., in the monographs [13, 22, 57]. Homogenization of the wave equation is described in more detail in Chapter 4.

We consider

$$\begin{cases} -\nabla\cdot(a^\varepsilon(x)\nabla v^\varepsilon(x)) = g(x) & \text{in } \Omega, \\ v^\varepsilon(x) = 0 & \text{on } \partial\Omega, \end{cases} \tag{2.8}$$

with $g \in H^{-1}(\Omega)$. The tensor a^ε describes the characteristics of the medium, varying on a length scale $\varepsilon > 0$, where ε is much smaller than the diameter of Ω. Assuming that $a^\varepsilon \in \mathcal{M}(\lambda, \Lambda)$ for all ε, problem (2.8) has a unique solution v^ε for every ε. We consider now the sequence $(v^\varepsilon)_\varepsilon$ of these solutions, which is uniformly bounded since λ and Λ do not depend on ε. Hence there is a subsequence, still denoted by $(v^\varepsilon)_\varepsilon$, that weakly converges to v^0 as ε tends to zero. To examine the limit function, we are looking for an equation such that its solution equals v^0. We name this equation the homogenized or effective equation, and accordingly v^0 is called the homogenized or effective solution.

H-convergence

The existence of a homogenized equation can be studied using the notion of H-convergence, introduced in [62].

Definition 2.4 (see [22, Definition 13.3])**.** A sequence of matrix-valued functions $(a^\varepsilon)_\varepsilon$, satisfying $a^\varepsilon \in \mathcal{M}(\lambda, \Lambda)$ for all ε, H-converges to $a^0 \in \mathcal{M}(\lambda', \Lambda')$, if for any $g \in H^{-1}(\Omega)$, the solution v^ε of the elliptic problem (2.8) is such that

$$v^\varepsilon \rightharpoonup v^0 \text{ weakly in } H_0^1(\Omega) \qquad \text{and} \qquad a^\varepsilon \nabla v^\varepsilon \rightharpoonup a^0 \nabla v^0 \text{ weakly in } (L^2(\Omega))^d,$$

where v^0 is the unique weak solution of the homogenized problem

$$\begin{cases} -\nabla\cdot\left(a^0(x)\nabla v^0(x)\right) = g(x) & \text{in } \Omega, \\ v^0(x) = 0 & \text{on } \partial\Omega. \end{cases} \tag{2.9}$$

Remark. It is well known, that every sequence $(a^\varepsilon)_\varepsilon \subset \mathcal{M}(\lambda, \Lambda)$ has an H-converging subsequence. If additionally a^ε is symmetric it can be shown that the H-limit $a^0 \in \mathcal{M}(\lambda, \Lambda)$ is symmetric, too. In this case H-convergence coincides with G-convergence introduced in [70].

Note that in general there are no formulas to compute the limit a^0 of an H-converging sequence explicitly. By contrast such formulas are available for periodic materials.

Periodic material

Here we restrict ourselves to symmetric, ε-periodic tensors a^ε. Let $Y = [-1/2, 1/2]^d$ be the d-dimensional centered unit cube and $a\colon \mathbb{R}^d \to \mathbb{R}$ be a Y-periodic function in $\mathcal{M}(\lambda, \Lambda)$. We set

$$a^\varepsilon(x) = a\left(\frac{x}{\varepsilon}\right) \qquad \text{for all } x \in \Omega. \tag{2.10}$$

Note that $a^\varepsilon \in \mathcal{M}(\lambda, \Lambda)$ is εY-periodic. In this particular setting, preciser statements are available. Often they can be justified by a (formal) asymptotic expansion, where the macroscale and the microscale are separated; see [13]. Additional techniques such as the notion of two-scale convergence [10, 63] provide a broader access to understand homogenization in periodic materials. Following [22] we summarize the results for periodic homogenization.

Theorem 2.5. *Let $g \in H^{-1}(\Omega)$, $a \in \mathcal{M}(\lambda, \Lambda)$ be Y-periodic, a^ε be given as in* (2.10)*, and v^ε be the solution of* (2.8)*. Then*

$$v^\varepsilon \rightharpoonup v^0 \text{ weakly in } H^1_0(\Omega) \qquad \text{and} \qquad a^\varepsilon \nabla v^\varepsilon \rightharpoonup a^0 \nabla v^0 \text{ weakly in } (L^2(\Omega))^d,$$

where $v^0 \in H^1_0(\Omega)$ is the weak solution of the homogenized problem (2.9) *with the constant matrix a^0 given by*

$$a^0_{r,s} = \int_Y \left(a_{r,s}(y) + \sum_{k=1}^d a_{r,s}(y) \frac{\partial \hat{\psi}^s}{\partial y_k} \right) dy. \tag{2.11}$$

Here $\hat{\psi}^s$ is the unique solution of the following cell problem: Find $\hat{\psi}^s \in H^1_{\mathrm{per}}(Y)$ such that

$$\int_Y a(y) \nabla \hat{\psi}^s \cdot \nabla z \, dy = -\int_Y a(y) e_s \cdot z \, dy \qquad \text{for all } z \in H^1_{\mathrm{per}}(Y), \tag{2.12}$$

where e_s is the s-th canonical basic vector.

The first statement in this theorem guarantees that the whole sequence $(v^\varepsilon)_\varepsilon$ H-converges. The second one provides a formula to compute the homogenized tensor a^0 analytically. We will rewrite (2.11) into a closed matrix formulation. The homogenized tensor is equivalently given by

$$a^0 = \int_Y a(y) \left(Id + D^T \hat{\psi}(y) \right) dy, \tag{2.13}$$

where $\hat{\psi} = (\hat{\psi}^1, \ldots, \hat{\psi}^d)^T$ and Id is the identity matrix.

In one dimension, i.e., $d = 1$ and $Y = [-1/2, 1/2]$, the homogenized tensor a^0 can be computed explicitly. In this case we have (see, e.g., [22, Section 5.3])

$$a^0 = \left(\int_{-\frac{1}{2}}^{\frac{1}{2}} \frac{1}{a(y)} \, dy \right)^{-1}. \tag{2.14}$$

Moreover, there are explicit formulas for a layered material in two dimensions. By layered we mean that $a(x)$ only depends on the first component of $x = (x_1, x_2)^T$, i.e., $a(x) = a(x_1)$. In this case we have (see, e.g., [22, Section 5.4])

$$a^0 = \begin{pmatrix} a^0_{1,1} & a^0_{1,2} \\ a^0_{2,1} & a^0_{2,2} \end{pmatrix}, \tag{2.15}$$

with

$$\begin{aligned}
a^0_{1,1} &= \left(\int_{-\frac{1}{2}}^{\frac{1}{2}} \frac{1}{a_{1,1}} \, dy_1 \right)^{-1}, \\
a^0_{1,2} &= a^0_{1,1} \int_{-\frac{1}{2}}^{\frac{1}{2}} \left(\frac{a_{1,2}}{a_{1,1}} \right) \, dy_1, \\
a^0_{2,1} &= a^0_{1,1} \int_{-\frac{1}{2}}^{\frac{1}{2}} \left(\frac{a_{2,1}}{a_{1,1}} \right) \, dy_1, \\
a^0_{2,2} &= \frac{a^0_{1,2} a^0_{2,1}}{a^0_{1,1}} + \int_{-\frac{1}{2}}^{\frac{1}{2}} a_{2,2} - \frac{a_{1,2} a_{2,1}}{a_{1,1}} \, dy_1.
\end{aligned}$$

Remark. All formulas in this subsection can be generalized to media not only oscillating periodically in the microscale, but also depending on the macroscale, i.e.,

$$a^\varepsilon(x) = a\left(x, \frac{x}{\varepsilon}\right),$$

where $a \colon \Omega \times \mathbb{R}^d \to \mathbb{R}^{d \times d}$ is Y-periodic in the second variable. Contrary to the purely periodic case, it is now no longer sufficient to solve only a single cell problem. Due to the variation in the macroscale, a cell problem must now be solved for every $x \in \Omega$.

Three

Fundamentals from numerical analysis

The method developed in this thesis to simulate wave propagation through a highly heterogeneous medium is based on two numerical methods. On the one hand we use the well-known finite element method and on the other hand the heterogeneous multiscale method introduced in [30]. The latter should rather be seen as methodology or framework to develop multiscale algorithms than as a method itself. The algorithms following the design principles of HMM consist of two different solvers to tackle the macroscale and the microscale problems as described in the introduction of this thesis. We prefer for both scales to use FEM, because of its flexibility when applied to various geometries and of its rigorous analytical foundation. In this chapter we introduce both methods, FEM and HMM.

3.1 FEM for the wave equation

The use of finite elements to solve the wave equation (2.1) numerically can be considered as well established. The method consists of two steps: First, a Galerkin projection onto a finite dimensional space leads to a system of ordinary differential equations that is solved numerically in the second step, using a time stepping scheme. In addition to the introduction of the method itself, we prove a new error estimate in an abstract setting.

Space discretization

We consider a regular partition $\mathcal{T}_H$ of Ω into simplicial or quadrilateral elements K, where $H = \max_{K\in\mathcal{T}_H} H_K$ and H_K denotes the diameter of K. By regular we mean that there is a constant σ such that ${}^{H_K}/_{\rho_K} \leq \sigma$ for all $K \in \mathcal{T}_H$, where ρ_K is the diameter of the largest circle contained in K. Additionally we assume that all elements in $\mathcal{T}_H$ are affine equivalent to a reference element $\hat{K}$. The associated affine mapping is denoted by $F_K \colon \hat{K} \to K$. For the ease of presentation, we restrict ourself to a polygonal domain Ω, which is covered exactly by the partition $\mathcal{T}_H$.

For $\ell > 1$ let $S^\ell_{BC}(\Omega, \mathcal{T}_H)$ be the finite element space defined by

$$S^\ell_{BC}(\Omega, \mathcal{T}_H) = \left\{ v_H \in H^1_{BC}(\Omega); v_H|_K \in \mathcal{R}^\ell(K) \; \forall K \in \mathcal{T}_H \right\},$$

where BC encodes the boundary condition and $\mathcal{R}^\ell(K)$ is the space $\mathcal{P}^\ell(K)$ of polynomial on K of total degree at most ℓ for simplicial elements or the space $\mathcal{Q}^\ell(K)$ of polynomials on K of degree at most ℓ in each variable for rectangular elements. In this thesis we consider a homogeneous Dirichlet boundary condition, denoted by $BC = 0$, and a periodic boundary condition, denoted by $BC = \text{per}$.

The time-continuous finite element approximation of the wave equation (2.1) is given by the following: Find $u_H \colon [0,T] \to S^\ell_0(\Omega, \mathcal{T}_H)$ such that

$$\begin{cases} (\partial_{tt} u_H, v_H) + B(u_H, v_H) = (f, v_H) & \text{for all } v_H \in S^\ell_0(\Omega, \mathcal{T}_H),\ 0 \le t \le T, \\ u_H(0) = I_H(u_I) & \text{in } \Omega, \\ \partial_t u_H(0) = I_H(v_I) & \text{in } \Omega, \end{cases} \tag{3.1}$$

with a suitable interpolation operator $I_H : H^1_0(\Omega) \to S^\ell_0(\Omega, \mathcal{T}_H)$; see (3.13) for further details.

Let N be the dimension of $S^\ell_0(\Omega, \mathcal{T}_H)$ and $\{\phi_1, \dots, \phi_N\}$ be the standard finite element basis. Then u_H can be written as

$$u_H(t) = \sum_{j=1}^{N} u_{Hj}(t) \phi_j,$$

with time dependent coefficients u_{Hj}. The problem (3.1) is equivalent to

$$\begin{cases} \partial_{tt} M U_H(t) + A U_H(t) = F(t) & \text{for all } 0 \le t \le T, \\ U_H(0) = I_H(u_I) & \text{in } \Omega, \\ \partial_t U_H(0) = I_H(v_I) & \text{in } \Omega, \end{cases} \tag{3.2}$$

where $U_H = (u_{H1}, \dots, u_{HN})^T$. The mass matrix M, the stiffness matrix A, and the load vector F are given by

$$M_{i,j} = (\phi_j, \phi_i), \qquad A_{i,j} = B(\phi_j, \phi_i), \qquad F_i = (f, \phi_i),$$

for $i, j = 1, \dots, N$.

Remark. Provided that u_H is sufficiently smooth, we can test (3.1) with $\partial_t u_H$, which yields for $f = 0$ that the energy defined in (2.6) with u replaced by u_H is still conserved. Using the mass and the stiffness matrix we can rewrite this energy as

$$E(t) = M \partial_t U_H(t) \cdot \partial_t U_H(t) + A U_H(t) \cdot U_H(t).$$

The proof relies on the symmetry of M and A, which is obviously given, since $(\cdot\,, \cdot)$ and B are both symmetric.

To achieve a discrete scheme in space, the integrals are computed numerically. Therefore, let $(\hat{x}_j, \hat{\omega}_j)$ for $j = 1, \dots, J$ be a quadrature formula on the reference element $\hat{K}$ given by its integration nodes and its corresponding weights. By setting

$$x_{K,j} = F_K(\hat{x}_j) \quad \text{and} \quad \omega_{K,j} = \hat{\omega}_j \det(DF_K) \tag{3.3}$$

for all j, we get a quadrature formula for every $K \in \mathcal{T}_H$ and by summation a quadrature formula for the whole computational domain.

The FEM with numerical integration is given by

$$\begin{cases} (\partial_{tt} u_H, v_H)_{\mathrm{QF}} + B_{\mathrm{QF}}(u_H, v_H) = (f, v_H) & \text{for all } v_H \in S_0^\ell(\Omega, \mathcal{T}_H),\ 0 \le t \le T, \\ u(0) = I_H(u_I) & \text{in } \Omega, \\ \partial_t u(0) = I_H(v_I) & \text{in } \Omega, \end{cases}$$

where

$$B_{\mathrm{QF}}(v_H, w_H) = \sum_{K \in \mathcal{T}_H} \sum_{j=1}^{J} \omega_{K,j} a(x_{K,j}) \nabla v_H(x_{K,j}) \cdot \nabla w_H(x_{K,j})$$

and

$$(v_H, w_H)_{\mathrm{QF}} = \sum_{K \in \mathcal{T}_H} \sum_{j=1}^{J} \omega_{K,j} v_H(x_{K,j}) w_H(x_{K,j})$$

for all $v_H, w_H \in S_0^\ell(\Omega, \mathcal{T}_H)$.

Remark. Note that there is no need to use the same quadrature formula to approximate both the L^2 inner product and the bilinear form. On the contrary, sometimes it is advantageous to use different quadrature formulas, as we will see later and as was mentioned in [67]. Additionally we could use a third quadrature formula to approximate the right-hand side. For the ease of presentation we assume that the right-hand side is computed exactly. At the end of the next section we briefly comment on the changes needed in the general setting to cover this case, too.

General error analysis

The first a priori error estimates can be traced back to the 1970s [11, 29]. In [12] error estimates for (3.1) taking into account numerical integration were derived. Using a quadrature formula to evaluate both the bilinear form B and the L^2 scalar product, the method is no longer conforming in the sense of [20]. For nonconforming FE methods Strang-type lemmas are essential; see [20, Chapter 4]. The first Strang lemma [20, Section 4.1, Theorem 4.1.1], on which the analysis of the finite element method with numerical quadrature for elliptic problems relies, can be seen as a generalization of Céa's lemma. In [5] a Strang-type lemma for the wave equation was derived. In [6] an improved version for the setting of FE-HMM-L, the finite element HMM scheme for long time wave propagation described in Chapter 6 was used. The theorems presented below can be seen as similar results, in a more general setting. We consider the solution $\tilde{u}$ of the wave equation (2.1), where B is replaced by any symmetric, coercive, and bounded

bilinear form $\tilde{B}$. Its approximation is computed with a finite element method which is nonconforming, since not only a Galerkin projection is used but in addition the bilinear form is altered. Moreover, we assume that the L^2 inner product is not computed exactly, but only approximately.

Let $\tilde{u} : [0,T] \to H_0^1(\Omega)$ and $\tilde{u}_H : [0,T] \to S_0^\ell(\Omega, \mathcal{T}_H)$ be the unique solutions of

$$\begin{cases} (\partial_{tt}\tilde{u}, v) + \tilde{B}(\tilde{u}, v) = (f, v) & \text{for all } v \in H_0^1(\Omega),\ 0 \le t \le T, \\ \tilde{u}(0) = u_I & \text{in } \Omega, \\ \partial_t \tilde{u}(0) = v_I & \text{in } \Omega, \end{cases} \tag{3.4}$$

and

$$\begin{cases} \{\partial_{tt}\tilde{u}_H, v_H\} + \tilde{B}_H(\tilde{u}_H, v_H) = (f, v_H) & \text{for all } v_H \in S_0^\ell(\Omega, \mathcal{T}_H),\ 0 \le t \le T, \\ \tilde{u}(0) = I_H(u_I) & \text{in } \Omega, \\ \partial_t \tilde{u}(0) = I_H(v_I) & \text{in } \Omega, \end{cases} \tag{3.5}$$

where $(\cdot\,,\cdot)$ is the standard L^2 inner product and $\{\cdot\,,\cdot\}$ is a possibly different inner product, which is symmetric and coercive, which means, that there is a C such that

$$\|v_H\|_{L^2}^2 \le C\{v_H, v_H\}. \tag{3.6}$$

Moreover, there is an α independent of H such that

$$|\{v_H, w_H\}| \le C \|v_H\|_{L^2} \|w_H\|_{L^2} + \alpha \|\nabla v_H\|_{L^2} \|\nabla w_H\|_{L^2} \tag{3.7}$$

and

$$\begin{aligned} |(v_H, w_H) - \{v_H, w_H\}| \le & C H^{\ell+\mu} \|v_H\|_{\bar{H}^{\ell+\mu}} \|w_H\|_{\bar{H}^{1+\mu}} \\ & + \alpha \|\nabla v_H\|_{L^2} \|\nabla w_H\|_{L^2} \end{aligned} \tag{3.8}$$

for all $v_H, w_H \in S_0^\ell(\Omega, \mathcal{T}_H)$. We use this assumption either for $\mu = 0$ or $\mu = 1$.

We assume that both bilinear forms $\tilde{B}$ and $\tilde{B}_H$ are symmetric, elliptic, and bounded, i.e., there are $0 < \gamma \le \Gamma$ such that

$$\gamma \|v\|_{H^1}^2 \le \tilde{B}(v,v), \qquad \left|\tilde{B}(v,w)\right| \le \Gamma \|v\|_{H^1} \|w\|_{H^1}, \tag{3.9}$$

$$\gamma \|v_H\|_{H^1}^2 \le \tilde{B}_H(v_H, v_H), \qquad \left|\tilde{B}_H(v_H, w_H)\right| \le \Gamma \|v_H\|_{H^1} \|w_H\|_{H^1}. \tag{3.10}$$

Furthermore, the difference between the bilinear forms can be bounded as

$$\begin{aligned} \left|\tilde{B}(v_H, w_H) - \tilde{B}_H(v_H, w_H)\right| \le & C H^{\ell+\mu} \|v_H\|_{\bar{H}^{\ell+\mu}} \|w_H\|_{\bar{H}^{1+\mu}} \\ & + \beta \|\nabla v_H\|_{L^2} \|\nabla w_H\|_{L^2} \end{aligned} \tag{3.11}$$

and

$$\begin{aligned} \left|\tilde{B}(v_H, w_H) - \tilde{B}_H(v_H, w_H)\right| \le & C H \|v_H\|_{H^1} \|w_H\|_{H^1} \\ & + \beta \|\nabla v_H\|_{L^2} \|\nabla w_H\|_{L^2}. \end{aligned} \tag{3.12}$$

In addition, we assume that for any integer k with $2 \le k \le \ell + 1$, there is a linear interpolation operator $I_H : H^k(\Omega) \cap H_0^1(\Omega) \to S_0^\ell(\Omega, \mathcal{T}_H)$ such that

$$\|I_H v - v\|_{\bar{H}^m} \le C H^{k-m} \|v\|_{H^k} \qquad \text{for all } v \in H^k(\Omega) \cap H_0^1(\Omega) \tag{3.13}$$

and for all $0 \le m \le k$. Note that for $m = k$ we have for all $v \in H^k(\Omega)$

$$\|I_H v\|_{\bar{H}^k} \le \|I_H v - v\|_{\bar{H}^k} + \|v\|_{\bar{H}^k} \le C \|v\|_{H^k},$$

which shows the boundedness of I_H.

Using these assumptions we can now state the two main results of this chapter.

Theorem 3.1. *Let $H \le H_0$ and $\tilde{u}$ and $\tilde{u}_H$ be the unique solutions of* (3.4) *and* (3.5)*, respectively. Suppose that the inner product $\{\cdot\,,\cdot\}$ satisfies* (3.6)–(3.8) *and the two bilinear forms satisfy* (3.9)–(3.12) *for $\mu = 0$. Provided that there is an interpolation operator I_H satisfying* (3.13) *and that*

$$\begin{aligned} &\partial_t^k \tilde{u} \in L^2(0,T; H^{\ell+1}(\Omega)),\ \partial_t^{2+k} \tilde{u} \in L^2(0,T; H^\ell(\Omega)) && \text{for } k = 0,1,2, \\ &u_I \in H^{\ell+1}(\Omega),\ v_I \in H^{\tilde{\ell}}(\Omega) && \text{with } \tilde{\ell} = \max\{\ell, 2\}, \end{aligned}$$

and $\partial_t u_H \in L^2(0,T; H^1(\Omega))$, then

$$\|\partial_t(\tilde{u} - \tilde{u}_H)\|_{L^\infty(0,T;L^2(\Omega))} + \|\tilde{u} - \tilde{u}_H\|_{L^\infty(0,T;H^1(\Omega))} \le C \left(H^\ell + \alpha + \beta \right).$$

Theorem 3.2. *Let $H \le H_0$ and $\tilde{u}$ and $\tilde{u}_H$ be the unique solutions of* (3.4) *and* (3.5)*, respectively. Suppose that the inner product $\{\cdot\,,\cdot\}$ satisfies* (3.6)–(3.8) *and the two bilinear forms satisfy* (3.9)–(3.12) *for $\mu = 1$. Provided that there is an interpolation operator I_H satisfying* (3.13) *and that*

$$\begin{aligned} &\partial_t^k \tilde{u} \in L^2(0,T; H^{\ell+1}(\Omega)) && \text{for } k = 0,1,2,3, \\ &\partial_t^4 \tilde{u} \in L^2(0,T; H^\ell(\Omega)), && \\ &u_I \in H^{\ell+1}(\Omega),\ v_I \in H^{\tilde{\ell}}(\Omega) && \text{with } \tilde{\ell} = \max\{\ell, 2\}, \end{aligned}$$

and $\partial_t u_H \in H^1\big(0,T; H^1(\Omega)\big)$, then

$$\|\tilde{u} - \tilde{u}_H\|_{L^\infty(0,T;L^2(\Omega))} \le C \left(H^{\ell+1} + \alpha + \beta \right).$$

Following the lines of the proof we see that the regularity assumptions on u_H are not needed if $\alpha = 0$, which means, among other things, that $\{\cdot\,,\cdot\}$ induces a norm equivalent to the standard L^2-norm for $v_H \in S_0^\ell(\Omega, \mathcal{T}_H)$.

Corollary 3.3. *If $\alpha = 0$, Theorem 3.1 remains valid without the assumption $\partial_t u_H \in L^2(0,T; H^1(\Omega))$. Similarly Theorem 3.2 remains valid without the assumption $\partial_t u_H \in H^1\big(0,T; H^1(\Omega)\big)$, if $\alpha = 0$.*

The proofs of both theorems follow ideas from [12] and rely on the following elliptic projection $\pi_H \tilde{u}$ defined by

$$\tilde{B}_H(\pi_H \tilde{u}, v_H) = \tilde{B}(\tilde{u}, v_H) + (\partial_{tt}\tilde{u}, v_H) - \{I_H(\partial_{tt}\tilde{u}), v_H\}, \tag{3.14}$$

for all $v_H \in S_0^\ell(\Omega, \mathcal{T}_H)$. The projections $\pi_H(\partial_t^k \tilde{u})$ for $k > 1$ are defined accordingly by differentiating (3.14). Since $\tilde{B}_H$ is coercive and bounded and the right-hand side of (3.14) is linear, $\pi_H \tilde{u} \in S_0^\ell(\Omega, \mathcal{T}_H)$ is uniquely defined. Note that since neither the bilinear forms nor the inner products depend on time, we have provided sufficient regularity,

$$\partial_t^k(\pi_H \tilde{u}) = \pi_H(\partial_t^k \tilde{u}).$$

Inserting $v_H = \pi_H \tilde{u}$ into (3.14) we find that $\|\pi_H \tilde{u}\|_{L^2(H^1)}$ is bounded using (3.7), the ellipticity of $\tilde{B}_H$, and the boundedness of $\tilde{B}$.

Before proving Theorems 3.1 and 3.2 we establish bounds for the difference between $\tilde{u}$ and $\pi_H \tilde{u}$ in the following two auxiliary lemmas.

Lemma 3.4. *Assume that the solution $\tilde{u}$ of (3.4) has the regularity*

$$\partial_t^k \tilde{u} \in L^2(0, T; H^{\ell+1}(\Omega)) \text{ and } \partial_t^{2+k} \tilde{u} \in L^2(0, T; H^\ell(\Omega))$$

for $k = 0, 1, 2$. Then, provided that (3.13) and (3.8)–(3.11) hold for $\mu = 0$, we have

$$\left\| \partial_t^k \tilde{u} - \pi_H(\partial_t^k \tilde{u}) \right\|_{L^2(H^1)} \leq C \left(H^\ell + \alpha + \beta \right).$$

Proof. We give here the proof only for $k = 0$. For higher k it follows by differentiating (3.14). We find

$$\begin{aligned}
\tilde{B}_H(\pi_H \tilde{u} - I_H \tilde{u}, v_H) = {} & \tilde{B}(\tilde{u} - I_H \tilde{u}, v_H) + \tilde{B}(I_H \tilde{u}, v_H) - \tilde{B}_H(I_H \tilde{u}, v_H) \\
& + (\partial_{tt}\tilde{u} - I_H(\partial_{tt}\tilde{u}), v_H) + (I_H(\partial_{tt}\tilde{u}), v_H) \\
& - \{I_H(\partial_{tt}\tilde{u}), v_H\}
\end{aligned}$$

and hence we have

$$\begin{aligned}
\left| \tilde{B}_H(\pi_H \tilde{u} - I_H \tilde{u}, v_H) \right| \leq {} & \Gamma \|\tilde{u} - I_H \tilde{u}\|_{H^1} \|v_H\|_{H^1} + C H^\ell \|I_H \tilde{u}\|_{\bar{H}^\ell} \|v_H\|_{\bar{H}^1} \\
& + \beta \|\nabla(I_H \tilde{u})\|_{L^2} \|\nabla v_H\|_{L^2} \\
& + \|\partial_{tt}\tilde{u} - I_H(\partial_{tt}\tilde{u})\|_{L^2} \|v_H\|_{L^2} \\
& + C H^\ell \|I_H(\partial_{tt}\tilde{u})\|_{\bar{H}^\ell} \|v_H\|_{\bar{H}^1} \\
& + \alpha \|\nabla(I_H(\partial_{tt}\tilde{u}))\|_{L^2} \|\nabla v_H\|_{L^2} \\
\leq {} & C \|v_H\|_{H^1} \big(H^\ell \|\tilde{u}\|_{H^{\ell+1}} + H^\ell \|\tilde{u}\|_{H^\ell} + \beta \|\tilde{u}\|_{H^1} \\
& + H^\ell \|\partial_{tt}\tilde{u}\|_{H^\ell} + H^\ell \|\partial_{tt}\tilde{u}\|_{H^\ell} + \alpha \|\partial_{tt}\tilde{u}\|_{H^1} \big),
\end{aligned}$$

where we used the Cauchy-Schwartz inequality, the boundedness of $\tilde{B}$, and additionally (3.8) and (3.11) for $\mu = 0$ in the first, and (3.13) in the second inequality. Now we set $v_H = \pi_H \tilde{u} - I_H \tilde{u}$, use the ellipticity of $\tilde{B}_H$, and integrate from 0 to T to get

$$\begin{aligned}
\|\pi_H \tilde{u} - I_H \tilde{u}\|_{L^2(H^1)} \leq {} & C\big(H^\ell (\|\tilde{u}\|_{L^2(H^{\ell+1})} + \|\tilde{u}\|_{L^2(H^\ell)} + \|\partial_{tt}\tilde{u}\|_{L^2(H^\ell)}) \\
& + \beta \|\tilde{u}\|_{L^2(H^1)} + \alpha \|\partial_{tt}\tilde{u}\|_{L^2(H^1)} \big).
\end{aligned}$$

Finally, the use of the regularity assumptions on $\tilde{u}$ and the triangle inequality

$$\|\pi_H \tilde{u} - \tilde{u}\|_{L^2(H^1)} \leq \|\pi_H \tilde{u} - I_H \tilde{u}\|_{L^2(H^1)} + \|I_H \tilde{u} - \tilde{u}\|_{L^2(H^1)}$$

give the result. □

Lemma 3.5. *Assume that the solution $\tilde{u}$ of (3.4) has the regularity*

$$\partial_t^k \tilde{u} \in L^2(0,T;H^{\ell+1}(\Omega)) \text{ and } \partial_t^{2+k} \tilde{u} \in L^2(0,T;H^{\ell+1}(\Omega))$$

for $k = 0, 1, 2$. Then, provided that (3.13) and (3.8)–(3.12) hold for $\mu = 1$, we have

$$\left\| \partial_t^k \tilde{u} - \pi_H(\partial_t^k \tilde{u}) \right\|_{L^2(L^2)} \leq C \left(H^{\ell+1} + \alpha + \beta \right)$$

for $H \leq H_0$.

We apply a duality argument known as the Aubin-Nitsche Trick, see, e.g., [20, Section 3.2] or [15, Section 7.6], which is commonly used to prove optimal convergence rates for FEM in the L^2-norm.

Proof. Again we only show the proof for $k = 0$. The proofs for higher k follow by differentiation. For any $g \in L^2(0,T;L^2(\Omega))$ let $\varphi_g(t) \in H_0^1(\Omega)$ be the solution of

$$\tilde{B}(v, \varphi_g(t)) = (v, g(t)) \qquad \text{for all } v \in H_0^1(\Omega).$$

From the made assumptions it follows, that $\varphi_g \in L^2(0,T;H^2(\Omega) \cap H_0^1(\Omega))$ and that

$$\|\varphi_g\|_{L^2(H^2)} \leq C \|g\|_{L^2(L^2)}. \tag{3.15}$$

For $v = \pi_H \tilde{u} - \tilde{u}$, using (3.14) we find

$$\begin{aligned}
(\pi_H \tilde{u} - \tilde{u}, g) &= \tilde{B}(\pi_H \tilde{u} - \tilde{u}, \varphi_g) - \tilde{B}_H(\pi_H \tilde{u}, v_H) + \tilde{B}(\tilde{u}, v_H) \\
&\quad + (\partial_{tt} \tilde{u}, v_H) - \{I_H(\partial_{tt} \tilde{u}), v_H\} \\
&= \tilde{B}(\pi_H \tilde{u} - \tilde{u}, \varphi_g - v_H) \\
&\quad + \tilde{B}(\pi_H \tilde{u} - I_H \tilde{u}, v_H) - \tilde{B}_H(\pi_H \tilde{u} - I_H \tilde{u}, v_H) \\
&\quad + \tilde{B}(I_H \tilde{u}, v_H) - \tilde{B}_H(I_H \tilde{u}, v_H) \\
&\quad + (\partial_{tt} \tilde{u} - I_H(\partial_{tt} \tilde{u}), v_H) \\
&\quad + (I_H(\partial_{tt} \tilde{u}), v_H) - \{I_H(\partial_{tt} \tilde{u}), v_H\}.
\end{aligned}$$

Let $v_H = I_H \varphi_g$. By integrating from 0 to T we get

$$\begin{aligned}
\left| \int_0^T (\pi_H \tilde{u} - \tilde{u}, g)\, dt \right| &\leq \int_0^T \left| \tilde{B}(\pi_H \tilde{u} - \tilde{u}, \varphi_g - I_H \varphi_g) \right| dt \\
&\quad + \int_0^T \left| \tilde{B}(\pi_H \tilde{u} - I_H \tilde{u}, I_H \varphi_g) - \tilde{B}_H(\pi_H \tilde{u} - I_H \tilde{u}, I_H \varphi_g) \right| dt \\
&\quad + \int_0^T \left| \tilde{B}(I_H \tilde{u}, I_H \varphi_g) - \tilde{B}_H(I_H \tilde{u}, I_H \varphi_g) \right| dt \\
&\quad + C H^{\ell+1} \|\partial_{tt} \tilde{u}\|_{L^2(H^{\ell+1})} \|\varphi_g\|_{L^2(L^2)} \\
&\quad + C \Big(H^{\ell+1} \|\partial_{tt} \tilde{u}\|_{L^2(H^{\ell+1})} \|\varphi_g\|_{L^2(H^2)} + \alpha \|\partial_{tt} \tilde{u}\|_{L^2(H^1)} \|\varphi_g\|_{L^2(H^1)} \Big),
\end{aligned}$$

where we used (3.13) and (3.8) with $\mu = 1$ to bound the last two terms. We now estimate the three remaining integrals.

$$\begin{aligned}\int_0^T \left|\tilde{B}(\pi_H\tilde{u} - \tilde{u}, \varphi_g - I_H\varphi_g)\right| dt &\leq C\int_0^T \|\pi_H\tilde{u} - \tilde{u}\|_{H^1} \|\varphi_g - I_H\varphi_g\|_{H^1} \, dt \\ &\leq CH \|\pi_H\tilde{u} - \tilde{u}\|_{L^2(H^1)} \|\varphi_g\|_{L^2(H^2)} \\ &\leq CH\left(H^\ell + \alpha + \beta\right)\|\varphi_g\|_{L^2(H^2)} \\ &\leq C\left(H^{\ell+1} + \alpha + \beta\right)\|\varphi_g\|_{L^2(H^2)},\end{aligned}$$

where we used (3.13), that $\varphi_g \in H^2(\Omega)$, Lemma 3.4, and $H \leq H_0$. For the second integral we compute

$$\begin{aligned}&\int_0^T \left|\tilde{B}(\pi_H\tilde{u} - I_H\tilde{u}, I_H\varphi_g) - \tilde{B}_H(\pi_H\tilde{u} - I_H\tilde{u}, I_H\varphi_g)\right| dt \\ &\quad\leq C\int_0^T H\|\pi_H\tilde{u} - I_H\tilde{u}\|_{H^1}\|\varphi_g\|_{H^1} + \beta\|\pi_H\tilde{u} - I_H\tilde{u}\|_{H^1}\|\varphi_g\|_{H^1} \, dt \\ &\quad\leq CH\|\pi_H\tilde{u} - I_H\tilde{u}\|_{L^2(H^1)}\|\varphi_g\|_{L^2(H^1)} \\ &\qquad + C\beta\|\pi_H\tilde{u} - I_H\tilde{u}\|_{L^2(H^1)}\|\varphi_g\|_{L^2(H^1)} \\ &\quad\leq C\left(H\left(H^\ell + \alpha + \beta\right) + \beta\|\pi_H\tilde{u} - I_H\tilde{u}\|_{L^2(H^1)}\right)\|\varphi_g\|_{L^2(H^2)},\end{aligned}$$

where we used (3.12) in the first and once again Lemma 3.4 and the regularity of $\tilde{u}$ in the last inequality. Furthermore we find a bound of $\pi_H\tilde{u}$ by inserting $v_H = \pi_H\tilde{u}$ into (3.14) and using the ellipticity of $\tilde{B}_H$ and the boundedness of the right-hand side. Hence,

$$\|\pi_H\tilde{u} - I_H\tilde{u}\|_{L^2(H^1)} \leq \|\pi_H\tilde{u}\|_{L^2(H^1)} + \|I_H\tilde{u}\|_{L^2(H^1)} \leq C.$$

Finally, we find for the second integral

$$\begin{aligned}&\int_0^T \left|\tilde{B}(\pi_H\tilde{u} - I_H\tilde{u}, I_H\varphi_g) - \tilde{B}_H(\pi_H\tilde{u} - I_H\tilde{u}, I_H\varphi_g)\right| dt \\ &\qquad\leq C\left(H^{\ell+1} + \alpha + \beta\right)\|\varphi_g\|_{L^2(H^2)}.\end{aligned}$$

The third integral can be bounded similarly using (3.11) with $\mu = 1$:

$$\begin{aligned}&\int_0^T \left|\tilde{B}(I_H\tilde{u}, I_H\varphi_g) - \tilde{B}_H(I_H\tilde{u}, I_H\varphi_g)\right| dt \\ &\quad\leq C\left(H^{\ell+1}\|\tilde{u}\|_{L^2(H^{\ell+1})}\|\varphi_g\|_{L^2(H^2)} + \beta\|\tilde{u}\|_{L^2(H^1)}\|\varphi_g\|_{L^2(H^1)}\right) \\ &\quad\leq C\left(H^{\ell+1} + \beta\right)\|\varphi_g\|_{L^2(H^2)}.\end{aligned}$$

To finish the proof, we note that

$$\|\pi_H\tilde{u} - \tilde{u}\|_{L^2(L^2)} = \sup_{\substack{g\in L^2(L^2)\\ g\neq 0}} \frac{\left|\int_0^T(\pi_H\tilde{u} - \tilde{u}, g)\, dt\right|}{\|g\|_{L^2(L^2)}},$$

and recall (3.15). Putting all together we have

$$\|\tilde{u} - \pi_H \tilde{u}\|_{L^2(L^2)} \leq C \left(H^{\ell+1} + \alpha + \beta \right). \qquad \square$$

We will now give the proofs of Theorems 3.1 and 3.2.

Proof of Theorem 3.1. Set $\zeta_H = \tilde{u}_H - \pi_H \tilde{u}$ and consider

$$\begin{aligned}
\{\partial_{tt}\zeta_H, v_H\} + \tilde{B}_H(\zeta_H, v_H) &= (f, v_H) - \{\pi_H(\partial_{tt}\tilde{u}), v_H\} - \tilde{B}_H(\pi_H\tilde{u}, v_H) \\
&= \tilde{B}(\tilde{u}, v_H) + (\partial_{tt}\tilde{u}, v_H) - \{\pi_H(\partial_{tt}\tilde{u}), v_H\} - \tilde{B}_H(\pi_H\tilde{u}, v_H) \\
&= \{I_H(\partial_{tt}\tilde{u}) - \pi_H(\partial_{tt}\tilde{u}), v_H\},
\end{aligned}$$

where we used (3.14) and that $\tilde{u}$ and $\tilde{u}_H$ solve (3.4) and (3.5), respectively. Setting $v_H = \partial_t \zeta_H$ and exploiting the symmetry of $\{\cdot\,,\cdot\}$ and $\tilde{B}_H$ we get

$$\frac{1}{2}\frac{d}{dt}\left(\{\partial_t\zeta_H, \partial_t\zeta_H\} + \tilde{B}_H(\zeta_H, \zeta_H) \right) = \{I_H(\partial_{tt}\tilde{u}) - \pi_H(\partial_{tt}\tilde{u}), \partial_t\zeta_H\}.$$

Define

$$\eta(t) = \{\partial_t\zeta_H, \partial_t\zeta_H\} + B_H(\zeta_H, \zeta_H),$$

and proceed by

$$\begin{aligned}
\frac{1}{2}\frac{d}{dt}\eta(t) &= \{I_H(\partial_{tt}\tilde{u}) - \pi_H(\partial_{tt}\tilde{u}), \partial_t\zeta_H\} \\
&\leq C\Big(\|I_H(\partial_{tt}\tilde{u}) - \pi_H(\partial_{tt}\tilde{u})\|_{L^2} \|\partial_t\zeta_H\|_{L^2} \\
&\quad + \alpha \|\nabla(I_H(\partial_{tt}\tilde{u}) - \pi_H(\partial_{tt}\tilde{u}))\|_{L^2} \|\nabla(\partial_t\zeta_H)\|_{L^2} \Big) \\
&\leq \frac{C}{2}\Big(\|I_H(\partial_{tt}\tilde{u}) - \pi_H(\partial_{tt}\tilde{u})\|_{L^2}^2 + \|\partial_t\zeta_H\|_{L^2} \\
&\quad + \|\nabla(I_H(\partial_{tt}\tilde{u}) - \pi_H(\partial_{tt}\tilde{u}))\|_{L^2}^2 + \alpha^2 \|\nabla(\partial_t\zeta_H)\|_{L^2} \Big).
\end{aligned}$$

Since $\partial_t\tilde{u}_H \in L^2(0,T;H^1(\Omega))$ by assumption, we find that $\|\partial_t\zeta_H\|_{L^2(H^1)}$ is bounded. The continuous embedding of $C(0,T;H^1(\Omega))$ into $H^1\big(0,T;H^1(\Omega)\big)$ yields a bound for $\|\nabla(\partial_t\zeta_H(t))\|_{L^2}$ for every t. Moreover, due to (3.6) and adding $B_H(\zeta_H,\zeta_H) \geq 0$ to the right-hand side of the above inequality, we find

$$\frac{d}{dt}\eta(t) \leq C\Big(\eta(t) + \|I_H(\partial_{tt}\tilde{u}) - \pi_H(\partial_{tt}\tilde{u})\|_{H^1}^2 + \alpha^2\Big).$$

Using Gronwall's Lemma we obtain

$$\sup_{0\leq t\leq T} \eta(t) \leq C\Big(\eta(0) + \|I_H(\partial_{tt}\tilde{u}) - \pi_H(\partial_{tt}\tilde{u})\|_{L^2(H^1)}^2 + \alpha^2\Big).$$

Because of (3.13) and the regularity assumptions on $\tilde{u}$ we have

$$\|I_H(\partial_{tt}\tilde{u}) - \partial_{tt}\tilde{u}\|_{L^2(H^1)}^2 \leq CH^{2\ell},$$

and because of Lemma 3.4 for $k = 2$,

$$\|\partial_{tt}\tilde{u} - \pi_H(\partial_{tt}\tilde{u})\|^2_{L^2(H^1)} \leq C(H^{2\ell} + \alpha^2 + \beta^2),$$

which yields by applying the triangle inequality

$$\|I_H(\partial_{tt}\tilde{u}) - \pi_H(\partial_{tt}\tilde{u})\|^2_{L^2(H^1)} \leq C(H^{2\ell} + \alpha^2 + \beta^2).$$

It remains to bound $\eta(0)$:

$$\begin{aligned}\eta(0) &= \{\partial_t\zeta_H(0), \partial_t\zeta_H(0)\} + B_H(\zeta_H(0), \zeta_H(0)) \\ &\leq C\left(\|\partial_t\zeta_H(0)\|^2_{L^2} + \alpha\,\|\partial_t\zeta_H(0)\|^2_{H^1} + B_H(\zeta_H(0), \zeta_H(0))\right).\end{aligned}$$

By the initial condition of (3.4) and (3.5) we find

$$\begin{aligned}\left|\tilde{B}_H(\zeta_H(0), \zeta_H(0))\right| &\leq C\,\|\zeta_H(0)\|^2_{H^1} \leq C\left(\|I_H u_I - u_I\|^2_{H^1} + \|u_I - \pi_H\tilde{u}(0)\|^2_{H^1}\right) \\ &\leq C\left(H^{2\ell}\,\|u_I\|^2_{H^{\ell+1}} + \|\tilde{u}(0) - \pi_H\tilde{u}(0)\|^2_{H^1}\right) \\ &\leq C\left(H^{2\ell} + \|\tilde{u} - \pi_H\tilde{u}\|^2_{L^2(H^1)} + \|\partial_t(\tilde{u} - \pi_H\tilde{u})\|^2_{L^2(H^1)}\right) \\ &\leq C\left(H^{2\ell} + \alpha^2 + \beta^2\right).\end{aligned}$$

In the third inequality we used the continuous embedding of $H^1\big(0,T;H^1(\Omega)\big)$ into $C(0,T;H^1(\Omega))$, see Theorem 2.1, and in the last one Lemma 3.4 for $k = 0, 1$. Similarly using the embedding $H^1\big(0,T;L^2(\Omega)\big)$ into $C(0,T;L^2(\Omega))$ yields

$$\begin{aligned}\|\partial_t\zeta_H(0)\|_{L^2} &= \|I_H v_I - \pi_H(\partial_t\tilde{u}(0))\|_{L^2} \\ &\leq \|I_H v_I - v_I\|_{L^2} + \|\partial_t\tilde{u}(0) - \pi_H(\partial_t\tilde{u}(0))\|_{L^2} \\ &\leq C\left(H^{\tilde{\ell}}\,\|g\|_{H^{\tilde{\ell}}} + \|\partial_t\tilde{u} - \pi_H(\partial_t\tilde{u})\|_{L^2(L^2)} + \|\partial_{tt}\tilde{u} - \pi_H(\partial_{tt}\tilde{u})\|_{L^2(L^2)}\right) \\ &\leq C\left(H^{\tilde{\ell}} + \alpha + \beta\right),\end{aligned}$$

and by the same arguments we find

$$\|\nabla(\partial_t\zeta_H(0))\|_{L^2} \leq C\left(H^{\tilde{\ell}-1} + H^{\ell} + \alpha + \beta\right).$$

All together we have the following bound

$$\eta(0) \leq C\left(H^{2\ell} + \alpha^2 + \beta^2 + \alpha(H^{2\tilde{\ell}-2} + H^{2\ell} + \alpha^2 + \beta^2)\right),$$

which can be simplified to

$$\eta(0) \leq C\left(H^{2\ell} + \alpha^2 + \beta^2\right),$$

as either $\alpha \leq H^2$ and hence $\alpha H^{2\tilde{\ell}-2} \leq H^{2\ell}$ or $\alpha \geq H^2$ inducing that α^2 is dominant. Since

$$c\left(\|\partial_t\zeta_H\|^2_{L^\infty(L^2)} + \|\zeta_H\|^2_{L^\infty(H^1)}\right) \leq \sup_{0\leq t\leq T}\eta(t),$$

we finally obtain the result using once more the triangle inequality. □

Proof of Theorem 3.2. As before let $\zeta_H = \tilde{u}_H - \pi_H \tilde{u}$. Additionally define

$$\Psi_H = I_H(\partial_t \tilde{u}) - \pi_H(\partial_t \tilde{u}) - \partial_t \zeta_H$$

and

$$\Phi_H = I_H(\partial_t \tilde{u}) - \pi_H(\partial_t \tilde{u}).$$

In the proof of Theorem 3.1 we saw that

$$\{\partial_{tt}\zeta_H, v_H\} + \tilde{B}_H(\zeta_H, v_H) = \{I_H(\partial_{tt}\tilde{u}) - \pi_H(\partial_{tt}\tilde{u}), v_H\}.$$

For all $v_H \in L^2(0,T; S_0^\ell(\Omega, \mathcal{T}_H))$ with $\partial_t v_H \in L^2(0,T; S_0^\ell(\Omega, \mathcal{T}_H))$ we can rewrite this identity as

$$\begin{aligned} -\{\partial_t \zeta_H, \partial_t v_H\} + \tilde{B}_H(\zeta_H, v_H) &= -\{\partial_t \zeta_H, \partial_t v_H\} + \{\partial_t \Psi_H, v_H\} \\ &= -\{\partial_t \zeta_H, \partial_t v_H\} + \frac{d}{dt}\{\Psi_H, v_H\} - \{\Psi_H, \partial_t v_H\} \\ &= \frac{d}{dt}\{\Psi_H, v_H\} - \{\Phi_H, \partial_t v_H\}. \end{aligned}$$

For $0 < s \leq T$ let

$$v_H(t;x) = \int_t^s \zeta_H(\tau;x)\, d\tau.$$

Since $\partial_t v_H = -\zeta_H$, the above identity becomes

$$\frac{1}{2}\frac{d}{dt}\left(\{\zeta_H, \zeta_H\} - \tilde{B}_H(v_H, v_H)\right) = \frac{d}{dt}\{\Psi_H, v_H\} + \{\Phi_H, \zeta_H\}.$$

Note that $v_H(s) = 0$ and $\Psi_H(0) = 0$, too. Now we integrate from 0 to s to get

$$\frac{1}{2}\left(\{\zeta_H(s), \zeta_H(s)\}^2 - \{\zeta_H(0), \zeta_H(0)\}^2 + \tilde{B}_H(v_H(0), v_H(0))\right) = \int_0^s \{\Phi_H, \zeta_H\}\, d\tau.$$

We can bound the integral on the right-hand side by

$$\begin{aligned} \int_0^s \{\Phi_H, \zeta_H\}\, d\tau &\leq \int_0^s \left(\|\Phi_H\|_{L^2} \|\zeta_H\|_{L^2} + \alpha \|\nabla \Phi_H\|_{L^2} \|\nabla \zeta_H\|_{L^2}\right) d\tau \\ &\leq \int_0^T \left(\|\Phi_H\|_{L^2} \|\zeta_H\|_{L^2} + \alpha \|\Phi_H\|_{H^1} \|\zeta_H\|_{H^1}\right) d\tau \\ &\leq \left(\|\Phi_H\|_{L^2(L^2)} \|\zeta_H\|_{L^\infty(L^2)} + \alpha \|\Phi_H\|_{L^2(H^1)} \|\zeta_H\|_{L^2(H^1)}\right). \end{aligned}$$

Using (3.6), (3.7), (3.10), and the Cauchy inequality leads to

$$\begin{aligned} \|\zeta_H(s)\|_{L^2}^2 \leq\ & C\left(\|\zeta_H(0)\|_{L^2}^2 + \alpha \|\nabla \zeta_H(0)\|_{L^2}^2\right) \\ & + \frac{C}{\kappa} \|I_H(\partial_t \tilde{u}) - \pi_H(\partial_t \tilde{u})\|_{L^2(L^2)}^2 + C\kappa \|\zeta_H\|_{L^\infty(L^2)}^2 \\ & + C\alpha\left(\|I_H(\partial_t \tilde{u}) - \pi_H(\partial_t \tilde{u})\|_{L^2(H^1)}^2 + \|\zeta_H\|_{L^2(H^1)}^2\right) \end{aligned}$$

for all $\kappa > 0$. Thus taking the supremum over s, we obtain for κ small enough

$$\begin{aligned}\|\zeta_H(s)\|^2_{L^\infty(L^2)} \le C &\left(\|\zeta_H(0)\|^2_{L^2} + \|I_H(\partial_t\tilde{u}) - \pi_H(\partial_t\tilde{u})\|^2_{L^2(L^2)}\right)\\ &+ C\alpha\left(\|\nabla\zeta_H(0)\|^2_{L^2} + \|I_H(\partial_t\tilde{u}) - \pi_H(\partial_t\tilde{u})\|^2_{L^2(H^1)} + \|\zeta_H\|^2_{L^2(H^1)}\right).\end{aligned}$$

We have

$$\begin{aligned}\|\zeta_H(0)\|_{L^2} &\le \|\pi_H u_I - u_I\|_{L^2} + \|u_I - I_H u_I\|_{L^2}\\ &\le \|\pi_H\tilde{u} - \tilde{u}\|_{L^2(L^2)} + \|\pi_H(\partial_t\tilde{u}) - \partial_t\tilde{u}\|_{L^2(L^2)} + \|\tilde{u}(0) - I_H\tilde{u}(0)\|_{L^2}\\ &\le C\left(H^{\ell+1} + \alpha + \beta\right),\end{aligned}$$

using the continuous embedding from $H^1\big(0,T;L^2(\Omega)\big)$ into $C(0,T;L^2(\Omega))$ and Lemma 3.5 for $k = 0, 1$. From the same lemma together with (3.13) it follows that

$$\begin{aligned}\|I_H(\partial_t\tilde{u}) - \pi_H(\partial_t\tilde{u})\|_{L^2(L^2)} &\le \|I_H(\partial_t\tilde{u}) - \partial_t\tilde{u}\|_{L^2(L^2)} + \|\partial_t\tilde{u} - \pi_H(\partial_t\tilde{u})\|_{L^2(L^2)}\\ &\le C\left(H^{\ell+1} + \alpha + \beta\right).\end{aligned}$$

From Lemma 3.4 it follows similarly that

$$\|I_H(\partial_t\tilde{u}) - \pi_H(\partial_t\tilde{u})\|_{L^2(H^1)} \le C\left(H^{\ell} + \alpha + \beta\right).$$

Moreover, using the embedding from $H^1\big(0,T;H^1(\Omega)\big)$ into $C(0,T;H^1(\Omega))$ and Lemma 3.4 for $k = 0, 1$,

$$\begin{aligned}\|\nabla\zeta_H(0)\|_{L^2} &\le \|I_H u_I - u_I\|_{H^1} + \|\tilde{u}(0) - \pi_H\tilde{u}(0)\|_{H^1}\\ &\le C\left(H^{\ell} + \|\tilde{u} - \pi_H\tilde{u}\|_{L^2(H^1)} + \|\partial_t\tilde{u} - \pi_H(\partial_t\tilde{u})\|_{L^2(H^1)}\right)\\ &\le C\left(H^{\ell} + \alpha + \beta\right).\end{aligned}$$

Finally, $\|\zeta_H\|_{L^2(H^1)}$ can be bounded by Theorem 3.1. Summing up, we have

$$\|\zeta_H(s)\|^2_{L^\infty(L^2)} \le C\left(H^{2\ell+2} + \alpha^2 + \beta^2 + \alpha(H^{2\ell} + \alpha^2 + \beta^2)\right),$$

from where the theorem follows by the same argument as in the proof before. □

Remark. The case where the right hand-side of (3.5) is computed with a quadrature formula as well, can be incorporated into the general setting as follows: Replace (f, v_H) in (3.5) with $[f, v_H]$, where $[\cdot,\cdot]$ is an additional inner product satisfying (3.6)–(3.8). Since $f \in L^2(0,T;L^2(\Omega))$ the pointwise evaluation, which is needed to apply a quadrature formula, is not well definied. Hence we should either consider a conforming interpolation or assume that f is continuous. In the latter case the projection π_H should be defined by

$$\tilde{B}_H(\pi_H\tilde{u}, v_H) = [f, v_H] - \{I_H(\partial_{tt}\tilde{u}), v_H\}.$$

Note that this is equivalent to (3.14) if $[\cdot,\cdot]$ is the standard L^2 inner product. Mutatis mutandis, the proofs in this section would remain valid. However an additional term, coming from the difference between $[\cdot,\cdot]$ and $(\cdot\,,\cdot)$ would remain in the estimates.

A priori error estimates

We can apply Theorems 3.1 and 3.2 to get a priori error estimates for FEM with and without numerical integration. In the absence of numerical integration we have $\{\cdot\,,\cdot\} = (\cdot\,,\cdot)$ and $\tilde{B}_H = B$. Hence (3.6)–(3.7), (3.11), and (3.12) hold with $\alpha = \beta = 0$. The coercivity and the boundedness follow since $a \in \mathcal{M}(\lambda, \Lambda)$. For FEM without numerical integration we get under appropriate regularity assumptions on u

$$\begin{aligned}\|\partial_t(u-u_H)\|_{L^\infty(0,T;L^2(\Omega))} + \|u-u_H\|_{L^\infty(0,T;H^1(\Omega))} &\le CH^\ell,\\ \|u-u_H\|_{L^\infty(0,T;L^2(\Omega))} &\le CH^{\ell+1},\end{aligned}$$

where u and u_H are the solutions of (2.1) and (3.1), respectively. Very similar results can be found in [29] and [11].

In the presence of numerical integration we set $\{\cdot\,,\cdot\} = (\cdot\,,\cdot)_{\mathrm{QF}}$ and $\tilde{B}_H = B_{\mathrm{QF}}$. We now give sufficient assumptions on the quadrature formula such that the assumptions (3.6)–(3.12) hold again with $\alpha = \beta = 0$. We assume that

$$\hat{\omega}_j > 0 \qquad \text{for } j = 1, \dots, J, \tag{3.16}$$

that there is a $\hat{\lambda} > 0$ such that

$$\sum_{j=1}^{J} \hat{\omega}_j \, |\nabla \hat{p}(\hat{x}_j)|^2 \ge \hat{\lambda} \, \|\nabla \hat{p}\|^2_{L^2(\hat{K})} \qquad \text{for all } \hat{p} \in \mathcal{R}^\ell(\hat{K}), \tag{3.17}$$

$$\int_{\hat{K}} \hat{p}(\hat{x}) \, d\hat{x} = \sum_{j=1}^{J} \hat{\omega}_j \hat{p}(\hat{x}_j) \qquad \text{for all } \hat{p} \in \mathcal{R}^\sigma(\hat{K}), \tag{3.18}$$

where $\sigma = \max(2\ell - 2, \ell)$ if $\hat{K}$ is a simplicial element, or $\sigma = \max(2\ell - 1, \ell + 1)$ if $\hat{K}$ is a quadrilateral element. Additionally, we assume that

$$\sum_{j=1}^{J} \hat{\omega}_j \, |\hat{p}(\hat{x}_j)|^2 \ge \hat{\lambda} \, \|\hat{p}\|^2_{L^2(\hat{K})} \qquad \text{for all } \hat{p} \in \mathcal{R}^\ell(\hat{K}), \tag{3.19}$$

which implies (3.17).

Remark. If $a \in W^{\ell+\mu,\infty}(\Omega)$ for $\mu = 0, 1$, then the conditions (3.7)–(3.12) with $\alpha = \beta = 0$ follow from (3.16)–(3.18); see [20, 21]. But for (3.6), i.e., the coercivity of $(\cdot\,,\cdot)_{\mathrm{QF}}$, the stricter assumption (3.19) is necessary. Here we see, why it might be advantageous to use two different quadrature formulas. If the pointwise evaluation of a is computationally costly, we should minimize the number of quadrature nodes needed such that (3.16)–(3.18) hold. A more accurate quadrature formula for which assumption (3.19) holds, may have more nodes and should therefore be used only for the computation of $(\cdot\,,\cdot)_{\mathrm{QF}}$.

Now we can use again Theorems 3.1 and 3.2 to recover the error estimates from [12]:

$$\begin{aligned}\|\partial_t(u-u_H)\|_{L^\infty(0,T;L^2(\Omega))} + \|u-u_H\|_{L^\infty(0,T;H^1(\Omega))} &\le CH^\ell,\\ \|u-u_H\|_{L^\infty(0,T;L^2(\Omega))} &\le CH^{\ell+1}.\end{aligned}$$

Time discretization

As seen in Section 3.1, the Galerkin projection leads to a system of second order ordinary differential equations (3.2). We solve this system by applying a time stepping scheme with step size Δt. Let $N_T = {}^{T}/_{\Delta t}$ be the number of time steps always assumed to be an integer, which means that T is a multiple of Δt. The approximation of $u_H(t_k)$ is denoted by u_H^k, where $t_k = k\Delta t$. The time stepping schemes we use are the well-known second order leap-frog scheme and the fourth order modified equation scheme, introduced in [69].

Leap-frog scheme

Applying the leap-frog scheme to (3.1) leads to the following time-discrete FE scheme for the wave equation.

$$\begin{cases} \left(\tilde{\partial}_{tt} u_H^n, v_H\right) + B(u_H^n, v_H) = (f(t_n), v_H) \quad \text{for all } v_H \in S_0^\ell(\Omega, \mathcal{T}_H),\ 1 \le n \le N_T - 1, \\ u_H^0 = I_H(u_I), \quad u_H^1 = u_H^0 + \Delta t I_H(v_I) + \dfrac{\Delta t^2}{2} \ddot{u}_H^0, \end{cases} \tag{3.20}$$

where

$$\tilde{\partial}_{tt} u_H^n = \frac{u_H^{n+1} - 2u_H^n + u_H^{n-1}}{\Delta t^2},$$

and $\ddot{u}_H^0$ is given by

$$\left(\ddot{u}_H^0, v_H\right) = (f(0), v_H) - B\left(u_H^0, v_H\right) \quad \text{for all } v_H \in S_0^\ell(\Omega, \mathcal{T}_H).$$

Similarly to the time-continuous FE scheme (3.1), numerical integration can be applied to evaluate the integrals of the L^2 inner product and the bilinear form B. The matrix formulation of (3.20) reads as

$$M\left(\frac{U_H^{m+1} - 2U_H^m + U_H^{m-1}}{\Delta t^2}\right) + AU_H^m = F^m \quad \text{for } m = 1, \ldots, N_T - 1.$$

We recall that the wave equation and the time-continuous finite element approximation conserve the energy $E(t)$ defined in (2.6). It is easy to prove that the leap-frog scheme conserves the following discretized energy

$$E_H^{m+1/2} = \frac{1}{2}\left(\left(\frac{U_H^{m+1} - U_H^m}{\Delta t}\right)^T M \left(\frac{U_H^{m+1} - U_H^m}{\Delta t}\right) + U_H^{m+1} A U_H^m\right). \tag{3.21}$$

Note that $E_H^{m+1/2} \ge 0$ for all m and that $E_H^{m+1/2} = 0$ if and only if $U_H^{m+1} = U_H^m = 0$. The conservation of the discretized energy (3.21) holds if A and M are symmetric. To show that the energy is positive definite, one needs in addition the positive definiteness of the matrix $M - {}^{\Delta t^2}/_4 A$, which is given for Δt small enough.

In addition we want to mention that the mesh size H and the time step Δt should be refined simultaneously. The necessary condition

$$\frac{\Delta t}{H} \leq C_{\mathrm{CFL}} \tag{3.22}$$

to ensure stability of the leap-frog scheme is known as CFL-condition, named after Courant, Friedrichs and Lewy, the authors of [24]. Note that the constant C_{CFL} depends only on the space discretization and on a^ε.

Modified equation scheme

We give the modified equation scheme directly in the matrix formulation:

$$M\left(\frac{U_H^{m+1} - 2U_H^m + U_H^{m-1}}{\Delta t^2}\right) + \left(A - \frac{\Delta t^2}{12} A M^{-1} A\right) U_H^m = F^m$$

for $m = 1, \ldots, N_T - 1$. To determine U_H^0 and U_H^1 we need a Taylor expansion with four terms such that we do not destroy the order of convergence. Besides the higher order of convergence another advantage of the ME scheme over the leap-frog scheme is the weaker CFL condition. In [47] it is proven that the ME scheme is stable if

$$\frac{\Delta t}{H} \leq \sqrt{3} C_{\mathrm{CFL}},$$

where C_{CFL} is the constant given in (3.22).

The modified equation scheme can be seen as a leap-frog scheme, where A is replaced by

$$\tilde{A} = A - {}^{\Delta t^2}/_{12} A M^{-1} A.$$

Note that $\tilde{A}$ is again symmetric and positive definite for Δt small enough. Hence, the modified equation scheme conserves a discrete energy, given by (3.21), replacing A with $\tilde{A}$.

Mass lumping

Regardless of whether we use the leap-frog or the modified equation scheme, the mass matrix must be inverted in every time step. To reduce the needed computational cost, the mass matrix can be replaced by a diagonal approximation. Then both time stepping schemes become fully explicit. This diagonalization of the mass matrix can be achieved by evaluating the L^2 inner product with a suitable quadrature formula, where quadrature nodes correspond to the FE nodes. Note that FEM with rectangular elements and mass lumping is very similar to the spectral element method. This case is much easier than mass lumping for triangular elements. More details about mass lumping for the wave equation can be found in [23, Chapters 11–13].

3.2 FE-HMM for elliptic problems

In this short description of FE-HMM for elliptic homogenization problems we follow basically the lines of [2] and [4, Section 4]. The results and their proofs can be found in [1–3, 32]. The goal is to approximate the macroscale behavior of the solution of the elliptic problem (2.8) without fully resolving the microscale of the medium given by a^ε. The variational formulation of (2.8) reads as follows: Find $v^\varepsilon \in H^1_0(\Omega)$ such that

$$B^\varepsilon(v^\varepsilon, w) = (g, w) \qquad \text{for all } w \in H^1_0(\Omega),$$

where $(\cdot\,,\cdot)$ is the standard scalar product in $L^2(\Omega)$ and the bilinear form B^ε is given by

$$B^\varepsilon(v, w) = \int_\Omega a^\varepsilon(x)\nabla v \cdot \nabla w \, dx \qquad \text{for all } v, w \in H^1_0(\Omega). \tag{3.23}$$

Recall that HMM is designed following a top-down approach. This means that we have to choose the macroscale solver first and to identify the missing data, before we can choose an appropriate microscale problem and its solver to estimate the missing data.

Macroscale solver

From homogenization theory, see Section 2.3, we know that an appropriate macroscale problem is again an elliptic second order PDE with a diffusion tensor a^0 not depending on the microscale. If a^0 were explicitly known we could directly apply standard FE to the variational formulation of the homogenized problem (2.9): Find $v^0 \in H^1_0(\Omega)$ such that

$$B^0\big(v^0, w\big) = (g, w) \qquad \text{for all } w \in H^1_0(\Omega), \tag{3.24}$$

where the homogenized bilinear form B^0 is given by

$$B^0(v, w) = \int_\Omega a^0(x)\nabla v \cdot \nabla w \, dx \qquad \text{for all } v, w \in H^1_0(\Omega).$$

The Galerkin projection of problem (3.24) into the space $S^\ell_0(\Omega, \mathcal{T}_H)$ using a quadrature formula to evaluate the integral in the bilinear form reads as follows: Find $v^0_H \in S^\ell_0(\Omega, \mathcal{T}_H)$ such that

$$B^0_{\mathrm{QF}}\big(v^0_H, w_H\big) = (g, w_H) \qquad \text{for all } w_H \in S^\ell_0(\Omega, \mathcal{T}_H),$$

where B^0_{QF} is given by

$$B^0_{\mathrm{QF}}(v_H, w_H) = \sum_{K \in \mathcal{T}_H} \omega_{K,j} a^0(x_{K,j}) \nabla v_H(x_{K,j}) \cdot \nabla w_H(x_{K,j}) \tag{3.25}$$

for all $v_H, w_H \in S^\ell_0(\Omega, \mathcal{T}_H)$, where $x_{K,j}$ and $\omega_{K,j}$ are defined as in (3.3). Since a^0 only depends on the macroscale, $H > \varepsilon$ is allowed. Hence we refer to $S^\ell_0(\Omega, \mathcal{T}_H)$ as the macro FE space. However, since a^0 is usually not known, we need to estimate B^0_{QF} or more precisely the value $a^0(x_{K,j})\nabla v_H(x_{K,j}) \cdot \nabla w_H(x_{K,j})$ for all quadrature nodes $x_{K,j}$. This is done by solving numerically a micro problem in a sampling domain of size δ centered at the corresponding quadrature node.

Micro problem and micro solver

Let us first introduce the needed notation. Recall that we denote the unit cell centered at the origin by $Y = [-1/2, 1/2]^d$. For $\delta > 0$ the sampling domain is given by

$$I_\delta = I_\delta(x_{K,j}) = x_{K,j} + \delta Y.$$

Note that $\delta \geq \varepsilon$ with both variables being of the same order, i.e., $\delta/\varepsilon = \mathcal{O}(1)$. Since we use again a finite element method to solve the micro problems defined in (3.26), we consider for every sampling domain a (micro) partition $\mathcal{T}_h$ of $I_\delta(x_{K,j})$ into simplicial or quadrilateral elements Q and a micro FE space

$$S^q_{\mathrm{per}}(I_\delta, \mathcal{T}_h) = \left\{ v_h \in H^1_{\mathrm{per}}(I_\delta); v_h|_Q \in \mathcal{R}^q(Q) \ \forall Q \in \mathcal{T}_h \right\}.$$

By choosing the Sobolev space $H^1_{\mathrm{per}}(I_\delta(x_{K,j}))$ we use a periodic coupling between macroscale and microscale. For a coupling through Dirichlet boundary conditions we choose the FE space

$$S^q_0(I_\delta, \mathcal{T}_h) = \left\{ v_h \in H^1_0(I_\delta); v_h|_Q \in \mathcal{R}^q(Q) \ \forall Q \in \mathcal{T}_h \right\}.$$

Writing only $S^q(I_\delta, \mathcal{T}_h)$ without any specification about the coupling, the statements are valid for both choices. A detailed description about different coupling methods can be found in [75].

The micro problem is given as follows: Find v_h such that $v_h - v_{H,\mathrm{lin}} \in S^q(I_\delta, \mathcal{T}_h)$ and

$$\int_{I_\delta} a^\varepsilon(x) \nabla v_h \cdot \nabla z_h \, dx = 0 \qquad \text{for all } z_h \in S^q(I_\delta, \mathcal{T}_h), \tag{3.26}$$

where

$$v_{H,\mathrm{lin}}(x) = v_H(x_{K,j}) + (x - x_{K,j}) \cdot \nabla v_H(x_{K,j}) \tag{3.27}$$

is the linearization of v_H at the quadrature node $x_{K,j}$. We do not indicate the dependence of $v_{H,\mathrm{lin}}$ and v_h on $x_{K,j}$ to avoid cluttered notation.

Multiscale method

Find $v_H \in S^\ell_0(\Omega, \mathcal{T}_H)$ such that

$$B_H(v_H, w_H) = (g, w_H) \qquad \text{for all } w_H \in S^\ell_0(\Omega, \mathcal{T}_H), \tag{3.28}$$

where B_H is given by

$$B_H(v_H, w_H) = \sum_{K \in \mathcal{T}_H} \sum_{j=1}^{J} \frac{\omega_{K,j}}{|I_\delta(x_{K,j})|} \int_{I_\delta} a^\varepsilon(x) \nabla v_h(x) \cdot \nabla w_h(x) \, dx \tag{3.29}$$

for all $v_H, w_H \in S^\ell_0(\Omega, \mathcal{T}_H)$, where v_h and w_h are the solutions of the micro problem (3.26) with the obvious modification for w_h.

The FE-HMM bilinear form can be rewritten as

$$B_H(v_H, w_H) = \sum_{K\in\mathcal{T}_H} \sum_{j=1}^{J} \omega_{K,j} a_K^0(x_{K,j}) \nabla v_H(x_{K,j}) \cdot \nabla(x_{K,j}),$$

where

$$\left(a_K^0(x_{K,j})\right)_{r,s} = \frac{1}{|I_\delta|} \int_{I_\delta} \left(a^\varepsilon(x)(e_s + \nabla\psi_h^s(x))\right) \cdot e_r \, dx, \tag{3.30}$$

and ψ_h^s is the solution of the problem: Find $\psi_h^s \in S^q(I_\delta, \mathcal{T}_h)$ such that

$$\int_{I_\delta} a^\varepsilon(x) \nabla\psi_h^s \cdot \nabla z_h \, dx = -\int_{I_\delta} a^\varepsilon(x) e_s \cdot z_h \, dx \qquad \text{for all } z_h \in S^q(I_\delta, \mathcal{T}_h). \tag{3.31}$$

Again we do not indicate that ψ_h^s depends on $x_{K,j}$. The tensor a_K^0 can be seen as a numerically homogenized tensor.

Remark. Comparing (3.30) with (2.11) and (3.31) with (2.12), we see the close relation between the FE-HMM and the homogenized bilinear form. The micro problem can be seen as a scaled version of the cell problem. But contrary to homogenization, there is no restriction to periodic materials only. Similar to (2.13) the numerically homogenized tensor is given equivalently by

$$a_K^0(x_{K,j}) = \frac{1}{|I_\delta|} \int_{I_\delta(x_{K,j})} a^\varepsilon(x) \left(Id + D^T\psi_h(x)\right) \, dx,$$

where $\psi_h = (\psi_h^1, \ldots, \psi_h^d)^T$.

Error analysis

For the a priori error estimates we need the following lemma.

Lemma 3.6 (Coercivity and boundedness of B_H)**.** *There are constants γ and Γ such that the FE-HMM bilinear form satisfies*

$$\gamma \|v_H\|_{H^1(\Omega)}^2 \le B_H(v_H, v_H)$$

and

$$|B_H(v_H, w_H)| \le \Gamma \|v_H\|_{H^1(\Omega)} \|w_H\|_{H^1(\Omega)}$$

for all $v_H, w_H \in S_0^\ell(\Omega, \mathcal{T}_H)$.

The following error bounds hold.

Theorem 3.7. *Let v^0 and v_H be the solution of* (3.24) *and* (3.28)*, respectively. Suppose that $a^\varepsilon \in \mathcal{M}(\lambda, \Lambda)$ and that the regularity $v^0 \in H^{\ell+1}(\Omega)$ and $a^0 \in W^{\ell+\mu,\infty}(\Omega)$ for $\mu = 0, 1$ hold. Provided that the quadrature formula $(\hat{x}_j, \hat{\omega}_j)_{j=1}^J$ satisfies* (3.16)–(3.18)*, we have*

$$\left\|v^0 - v_H\right\|_{H^1(\Omega)} \le C(H^\ell + e_{\mathrm{HMM}}),$$
$$\left\|v^0 - v_H\right\|_{L^2(\Omega)} \le C(H^{\ell+1} + e_{\mathrm{HMM}}),$$

where C is independent of H and h, and

$$e_{\mathrm{HMM}} = \sup_{\substack{K\in\mathcal{T}_H\\ j=1,\dots,J}} \left\|a^0(x_{K,j}) - a^0_K(x_{K,j})\right\|_F,$$

where $\|\cdot\|_F$ is the Frobenius norm.

The proof uses standard error estimates for FEM, the first Strang lemma [20, Section 4.1, Theorem 4.1.1], and that

$$\left|B^0_{\mathrm{QF}}(v_H, w_H) - B_H(v_H, w_H)\right| \le C e_{\mathrm{HMM}} \left\|\nabla v_H\right\|_{L^2} \left\|\nabla w_H\right\|_{L^2}. \tag{3.32}$$

Note that there are no assumptions, such as periodicity on the spatial structure of a^ε. However, to give further estimates for e_{HMM} additional assumptions are needed. The error of the HMM scheme can be decomposed in a micro error e_{MIC} and a modeling error e_{MOD}. Roughly speaking, the micro error comes from solving the micro problem numerically and the modeling error from the difference between the exact homogenized tensor a^0 and its approximation.

For a precise statement let us introduce the semidiscrete numerically homogenized tensor

$$\bar{a}^0_K(x_{K,j}) = \frac{1}{|I_\delta(x_{K,j})|}\int_{I_\delta} a^\varepsilon(x)\left(Id + D^T\psi(x)\right)\,dx,$$

where $\psi = (\psi^1, \dots, \psi^d)^T$ and ψ^s is the solution of the problem: Find $\psi^s \in H^1_{\mathrm{per}}(I_\delta)$ such that

$$\int_{I_\delta} a^\varepsilon(x)\nabla\psi^s\cdot\nabla z_h\,dx = -\int_{I_\delta} a^\varepsilon(x)e_s\cdot z\,dx \qquad \text{for all } z\in H^1_{\mathrm{per}}(I_\delta), \tag{3.33}$$

if a periodic coupling condition is used. For Dirichlet coupling replace $H^1_{\mathrm{per}}(I_\delta)$ with $H^1_0(I_\delta)$. Note that (3.33) is the nondiscretized version of (3.31). Now the micro and the modeling error are given by

$$e_{\mathrm{MIC}} = \sup_{\substack{K\in\mathcal{T}_H\\ j=1,\dots,J}} \left\|\bar{a}^0_K(x_{K,j}) - a^0_K(x_{K,j})\right\|_F,$$
$$e_{\mathrm{MOD}} = \sup_{\substack{K\in\mathcal{T}_H\\ j=1,\dots,J}} \left\|a^0(x_{K,j}) - \bar{a}^0_K(x_{K,j})\right\|_F,$$

and we obviously have

$$e_{\mathrm{HMM}} \le e_{\mathrm{MIC}} + e_{\mathrm{MOD}}.$$

These errors can be bounded as follows.

Theorem 3.8 (Micro error)**.** *Suppose that $a^\varepsilon \in \mathcal{M}(\lambda,\Lambda)$ and that $|\psi^s|_{H^{q+1}(I_\delta)} \le C\varepsilon^{-q}\sqrt{|I_\delta|}$, then*

$$e_{\mathrm{MIC}} \le C\left(\frac{h}{\varepsilon}\right)^{2q},$$

where C is independent of H, h, and ε.

Theorem 3.9 (Modeling error)**.** *Suppose that $a^\varepsilon(x) = a(x, x/\varepsilon)$, with a matrix valued function $a(x, y)$, which is Y-periodic in y, and that*

$$a_{ij}(x, y) \in C(\bar{\Omega}; W^{1,\infty}_{\text{per}}(Y))$$

for all $i, j = 1, \ldots, d$. Then

$$e_{\text{MOD}} \leq C \left(\frac{\varepsilon}{\delta} + \delta \right),$$

where the size of the sampling $\delta > \varepsilon$ and C is independent of H, h, and ε.

If additionally $\delta/\varepsilon \in \mathbb{N}$, periodic coupling is used and if the slow variable x is collocated at the quadrature point $x_{K,j}$, then the modeling error vanishes.

By collocation we mean that we replace $a^\varepsilon(x) = a(x, x/\varepsilon)$ by $a(x_{K,j}, x/\varepsilon)$ in (3.26) and (3.29).

Part II

Wave Propagation in Heterogeneous Media

Four

Homogenization of the wave equation

In this part, consisting of Chapters 4, 5, and 6, we are focusing on wave propagation in heterogeneous media. In this context we write the wave equation (2.1) as

$$\begin{cases} (\partial_{tt} u(t), v) + B^\varepsilon(u(t), v) = (f(t), v) & \text{for all } v \in H_0^1(\Omega),\ 0 \le t \le T, \\ u(0) = u_I & \text{in } \Omega, \\ \partial_t u(0) = v_I & \text{in } \Omega, \end{cases} \tag{4.1}$$

where B^ε is given as in (3.23). In this chapter we give an overview of analytical homogenization results; in the two following chapters we introduce and analyze FE-HMM schemes to solve (4.1). First of all, we introduce a model example, which will be used repeatedly as illustrative motivation and as a test case.

4.1 Model example

Let $\Omega = (-1, 1)$. Remember that the one-dimensional wave equation with periodic boundary condition is given by

$$\begin{cases} \partial_{tt} u^\varepsilon(t;x) - \partial_x(a^\varepsilon(x)\partial_x u^\varepsilon(t;x)) = f(t;x) & \text{in } \Omega \times (0,T), \\ u^\varepsilon(t;-1) = u^\varepsilon(t;1) & \text{for all } t \in (0,T), \\ u^\varepsilon(0;x) = u_I(x) & \text{in } \Omega, \\ \partial_t u^\varepsilon(x,0) = v_I(x) & \text{in } \Omega. \end{cases}$$

We consider no internal sources, i.e., $f \equiv 0$ and we choose a Gaussian pulse with zero velocity as initial condition. More precisely we have

$$u_I(x) = \exp\bigl(-100x^2\bigr) \text{ and } v_I(x) = 0.$$

For this model example we choose a smooth ε-periodic wave speed, given by

$$a^\varepsilon(x) = \sqrt{2} + \sin\Bigl(2\pi\frac{x}{\varepsilon}\Bigr). \tag{4.2}$$

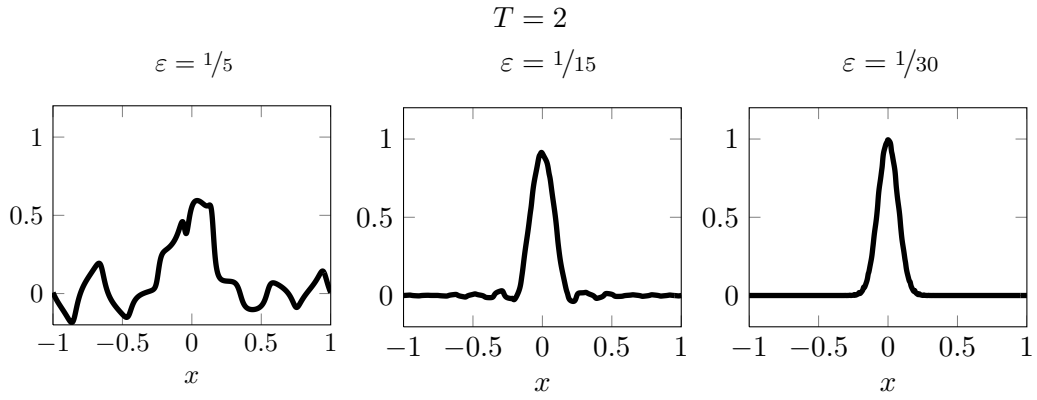

Figure 4.1: Reference solution of the model example at $T = 2$ for $\varepsilon = 1/5, 1/15, 1/30$.

In Figure 4.1 the reference solution u^ε at $T = 2$ is shown for three different ε. The end time corresponds to one evolution of the main pulse. The reference solution is computed on a mesh that resolves the microscale. More specifically, we use cubic finite elements with Gauss-Lobatto mesh points on a mesh with $H = 2^{-13} = 1.22 \cdot 10^{-4}$, where H denotes the length of an element. Hence the number of degree of freedoms is 49,153. Furthermore, we use the leap-frog scheme with $\Delta t = H/8$ for time stepping. We see that the oscillations in the solution diminish as ε gets smaller.

From the model example we can see that undersampling or simple averaging techniques do not yield a reliable approximation of the macroscopic behavior of the solution. In Figure 4.2 we plot a DNS of the model example at $T = 2$ with $\varepsilon = 50$, computed with the same parameter setting as before. In addition we depict the solution of the wave equation, where a^ε is replaced by its average $\bar{a} = \sqrt{2}$. Third we show the FEM solution with the correct squared wave speed a^ε but on a too coarse mesh. For this computation the size of an element is set to $H = 2^{-6}$. We see that the averaged and the undersampled solutions both deviate from the reference solution. Therefore more involved techniques, such as classical homogenization theory, are needed to recover the macroscopic wave propagation.

4.2 Homogenization for the wave equation

For finite time the effective behavior is well described by classical homogenization theory. Before we give the precise results, we make a formal asymptotic expansion showing the relation between homogenization of elliptic and hyperbolic homogenization problems.

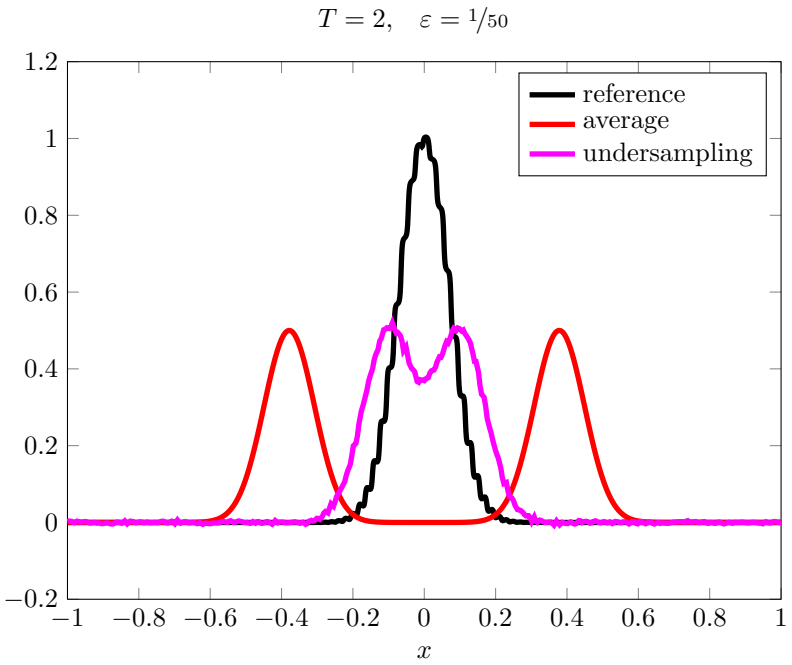

Figure 4.2: Reference, averaged, and undersampled solutions of the model example at $T = 2$ for $\varepsilon = 1/50$.

Asymptotic expansion

As is commonly done for an asymptotic expansion we consider only periodic media. Therefore, let $a^\varepsilon(x)$ be given as in (2.10). First, we separate the scales by the ansatz

$$u^\varepsilon(t;x) = u\left(t;x,\frac{x}{\varepsilon}\right).$$

Because of the periodicity of a^ε, we assume that $u(t;x,y)$ is Y-periodic in the y variable. Note that we have

$$\nabla u^\varepsilon(t;x) = \nabla_x u(t;x,y) + \frac{1}{\varepsilon}\nabla_y u(t;x,y). \tag{4.3}$$

Now we expand u in an ε-power series

$$u(t;x,y) = \sum_{k=0}^{\infty} \varepsilon^k u^k(t;x,y) \tag{4.4}$$

with $u^k(t;x,y) \in H^1_{\text{per}}(Y)$ for fixed t and x. We want to recover u^0, which describes the macroscopic behavior. We insert (4.4) into the wave equation (1.3) and compare the like terms in ε.

From order ε^{-2} we deduce that u^0 is independent of y. At order ε^{-1} we find the elliptic problem

$$-\nabla_y \cdot (a(y)(\nabla_x u^0 + \nabla_y u^1)) = 0. \tag{4.5}$$

We notice that u^1 depends linearly on u^0. Hence we can write

$$u^1(t;x,y) = \nabla_x u^0(t;x) \cdot \hat{\psi}(y) + c(t;x)$$

with $\hat{\psi}(y) = (\hat{\psi}^1(y), \hat{\psi}^2(y), \dots, \hat{\psi}^d(y))^T$, where $\hat{\psi}^s$ is given as in (2.12).

Up to this point the time dependence has no crucial influence on the asymptotic expansion. Only for the equations of order 0 or higher in ε does the time derivative come into effect. Using (4.3) we get

$$\partial_{tt} u^0 - \nabla_x \cdot (a(y)\nabla_x u^0) - \nabla_x \cdot (a(y)\nabla_y u^1) - \nabla_y \cdot (a(y)\nabla_x u^1) - \nabla_y \cdot (a(y)\nabla_y u^2) = f,$$

from where the following elliptic problem for u^2 follows:

$$-\nabla_y \cdot (a(y)\nabla_y u^2) = f - \partial_{tt} u^0 + \nabla_x \cdot (a(y)(\nabla_x u^0 + \nabla_y u^1)) + \nabla_y \cdot (a(y)\nabla_x u^1).$$

For fixed x and t this is a partial differential equation for $u^2(t;x,\cdot) \in H^1_{\mathrm{per}}(Y)$, which is well-posed if the mean over Y of the right-hand side vanishes. Since $|Y| = 1$, by the periodicity of a and u^1 this reads

$$\int_Y f - \partial_{tt} u^0 + \nabla_x \cdot (a(y)(\nabla_x u^0 + \nabla_y u^1)) = 0.$$

Note that f and u^0 are independent of y and that $\nabla_y u^1 = (D^T \hat{\psi}) \nabla_x u^0$ due to (4.5). This leads to

$$\partial_{tt} u^0 - \nabla_x \cdot \left(\left(\int_Y a(y) \left(Id + D^T \hat{\psi}(y) \right) dy \right) \nabla_x u^0 \right) = f,$$

which simplifies to

$$\partial_{tt} u^0 - \nabla_x \cdot \left(a^0 \nabla_x u^0 \right) = f,$$

using a^0 as given in (2.13).

This formal asymptotic expansion shows that the effective behavior is described by a wave equation, where the homogenized coefficient a^0 is given as for the elliptic homogenization. The following theorem explicates this statement; its proof can be found for example in [13, Chapter 3, Section 2].

Theorem 4.1 (Homogenization for the wave equation)**.** *Let $(a^\varepsilon)_\varepsilon \subset \mathcal{M}(\lambda, \Lambda)$ be a sequence of matrix-valued functions that H-converges to a^0. Provided that the regularity assumptions* (2.3)–(2.5) *on the source term and the initial data hold, then the sequence of solutions u^ε of the wave equation* (2.1) *converges in the following sense:*

$$\begin{aligned} u^\varepsilon &\rightharpoonup u^0, && \text{weak-}\star \text{ in } L^\infty(0,T;H^1_0(\Omega)), \\ \partial_t u^\varepsilon &\rightharpoonup \partial_t u^0, && \text{weak-}\star \text{ in } L^\infty(0,T;L^2(\Omega)), \end{aligned}$$

where u^0 is the solution of the homogenized wave equation given by

$$\begin{cases} \left(\partial_{tt} u^0(t), v\right) + B^0\left(u^0(t), v\right) = (f(t), v) & \text{for all } v \in H^1_0(\Omega),\ 0 \le t \le T, \\ u^0(0) = u_I & \text{in } \Omega, \\ \partial_t u^0(0) = v_I & \text{in } \Omega, \end{cases} \tag{4.6}$$

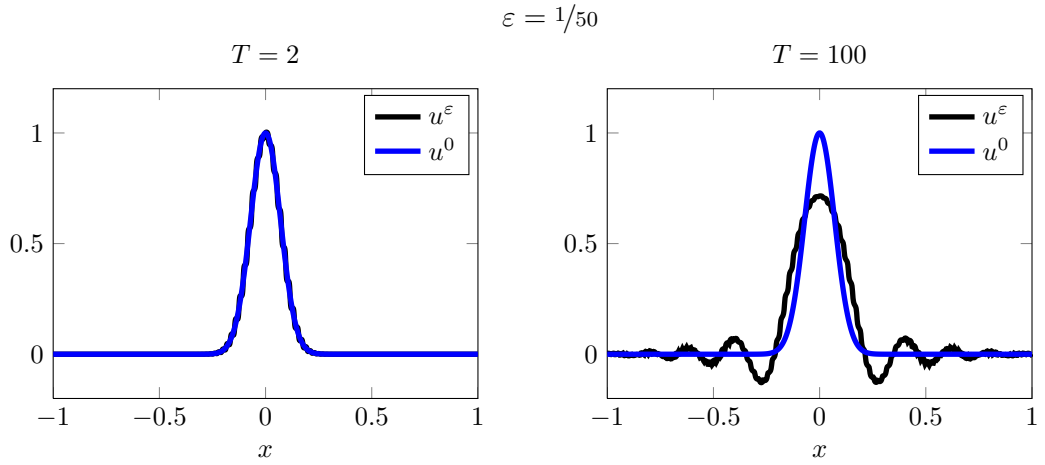

Figure 4.3: Reference solution u^ε and homogenized solution u^0 of the model example at $T = 2$ (left) and $T = 100$ (right) for $\varepsilon = 1/50$.

and the homogenized bilinear form B^0 *is defined by*

$$B^0(v, w) = \int_\Omega a^0(x) \nabla v \cdot \nabla w \, dx. \tag{4.7}$$

In [16] it is pointed out that the energy E^ε of u^ε does not converge to the energy E^0 of the homogenized solution in general as $\varepsilon \to 0$. For $v_I \equiv 0$ we have, for example,

$$\lim_{\varepsilon \to 0} E^\varepsilon = \frac{1}{2} \lim_{\varepsilon \to 0} B^\varepsilon(u_I, u_I) > \frac{1}{2} B^0(u_I, u_I) = E^0.$$

We return to our model example; see Section 4.1. For a^ε given as in (4.2) the formula (2.14) can be applied and the homogenized coefficient can be computed as

$$a^0 = \left(\int_0^1 \frac{1}{\sqrt{2} + \sin(2\pi y)} \, dy \right)^{-1} = 1.$$

In Figure 4.3 on the left the reference solution for $\varepsilon = 1/50$ coincides with the homogenized solution, which we computed analytically using d' Alembert's formula (2.7). The energy of u^ε is $E^\varepsilon \approx 8.86$, whereas the homogenized energy $E^0 \approx 6.27$.

4.3 Long-time dispersive effects

In the previous section we have seen that for limited time the propagation of waves in a highly oscillatory medium is well described by the nondispersive homogenized wave equation. With increasing time, however, the true solution deviates from the classical homogenization limit, as a large secondary wave train develops unexpectedly. The dispersion can be well observed in the model example as seen on the right of Figure 4.3.

To capture these dispersive effects different methods have been applied: In [68] a Bloch expansion [14,74], in [19,42–46] an asymptotic expansion into multiple fast spatial and slow temporal scales, and the construction of an adaption operator in [59, 60] were used to devise a dispersive effective equation. While the former three references contain formal calculations, rigorous proofs were given in the two latter references for a purely periodic medium in one dimension. Very recently the results of [59, 60] were generalized to higher dimensions in [25]. All developed effective equations resemble each other in that a small fourth order term, either $\partial_{xxxx} u^{\text{eff}}$ or $\partial_{tt}\partial_{xx} u^{\text{eff}}$, is added to the homogenized wave equation. This leads to the following one-dimensional effective equations, often referred to as linearized Boussinesq equations [55, 73]:

$$\partial_{tt} u^{\text{eff}} - a^0 \partial_{xx} u^{\text{eff}} - \varepsilon^2 b^0 \partial_{xxxx} u^{\text{eff}} = f, \tag{4.8}$$

$$\partial_{tt} u^{\text{eff}} - a^0 \partial_{xx} u^{\text{eff}} - \varepsilon^2 \frac{b^0}{a^0} \partial_{tt}\partial_{xx} u^{\text{eff}} = f. \tag{4.9}$$

Note that for $f \equiv 0$ there are exponentially growing solutions for (4.8). For example,

$$u(t;x) = \cos(kx) \exp\left(\sqrt{k^4 - k^2}\, t\right)$$

with $|k| > 1$ is a solution of (4.8) with $f \equiv 0$ and $a^0 = \varepsilon^2 b^0 = 1$. This is the reason why (4.8) is called the linearized "bad" Boussinesq equation. On the contrary (4.9) is well-posed and called the linearized "improved" Boussinesq equation [34, 54].

Summarizing the results from this chapter we point out that the homogenized wave equation (4.6) is an accurate effective model to describe the macroscopic behavior of wave propagation in a highly oscillatory medium. The homogenized tensor a^0 is the same as for homogenization of elliptic problems. For longer time, however, the addition of a fourth-order term is needed to capture long-time dispersive effects. This additional term leads to a Boussinesq-type effective model. In Figure 4.4 the solution of the effective model (4.9) is shown. Not only for short, but also for longer time it describes well the macroscopic behavior of the reference solution. The coefficient $a^0 = 1$ and $b^0 = 9.09632625 \cdot 10^{-3}$ are computed with the MAPLE program given in [53, Section 3].

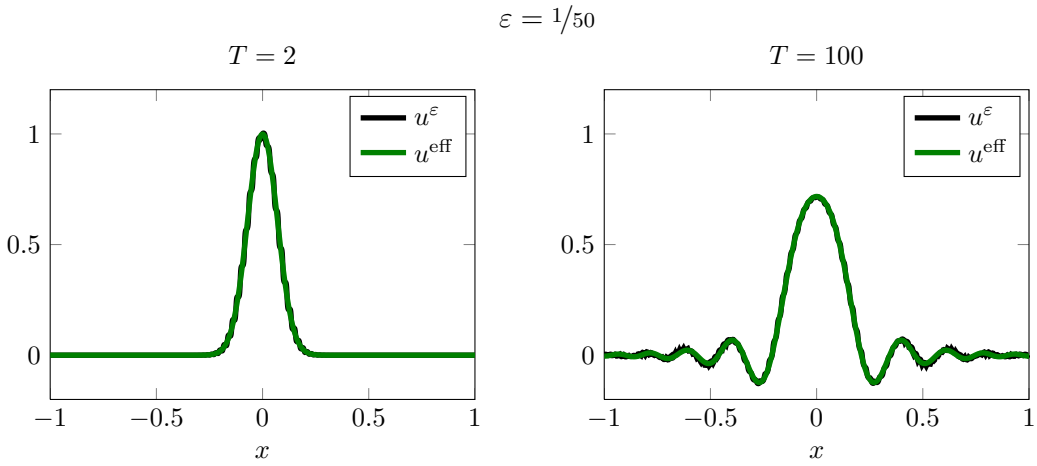

Figure 4.4: Reference solution u^ε and solution of the improved linearized Boussinesq equation u^{eff} of the model example at $T = 2$ (left) and $T = 100$ (right) for $\varepsilon = 1/50$.

Five

FE-HMM for the wave equation for finite time

Since HMM follows a top-down philosophy from macro- to microscale, we have first to identify an appropriate macroscale model. As seen in the previous chapter classical homogenization theory provides a suitable model for finite time. For elliptic problems the homogenized tensor a^0 and the cell problems are the same. Hence we can benefit from the FE-HMM theory developed for elliptic problems, described in Section 3.2. We adapt the FE-HMM to the time dependent wave equation, as was done in [5].

5.1 Description of the multiscale method

We give here a description of the FE-HMM for the wave equation. In view of the equality of the homogenized tensor for elliptic and hyperbolic problems, we can use the same computation to approximate an effective bilinear form. The notation used here is in accordance with the notation introduced in Section 3.2.

Let $\Omega \subset \mathbb{R}^d$ be the computational domain. The wave speed $a^\varepsilon \in \mathcal{M}(\lambda, \Lambda)$ has a micro-scale nature of a typical length ε (e.g., period, correlation length). First, we generate a macro triangulation $\mathcal{T}_H$. By macro we mean that $H \gg \varepsilon$ is allowed. Choosing a quadrature formula in the reference element $\hat{K}$, we get by (3.3) a quadrature formula $\{x_{K,j}, \omega_{K,j}\}$ on every macro element $K \in \mathcal{T}_H$. The HMM solution u_H is given by he following variational problem: Find $u_H \colon [0,T] \to S_0^\ell(\Omega, \mathcal{T}_H)$ such that

$$\begin{cases} (\partial_{tt} u_H, v_H) + B_H(u_H, v_H) = (f, v_H) & \text{for all } v_H \in S_0^\ell(\Omega, \mathcal{T}_H),\ 0 \le t \le T, \\ u_H(0) = I_H(u_I) & \text{in } \Omega, \\ \partial_t u_H(0) = I_H(v_I) & \text{in } \Omega, \end{cases} \tag{5.1}$$

where B_H given in (3.29) is an approximation of the discretized homogenized bilinear B^0_{QF}, defined in (3.25). Since B_H is elliptic and bounded, the FE-HMM is well defined for all $H, h > 0$.

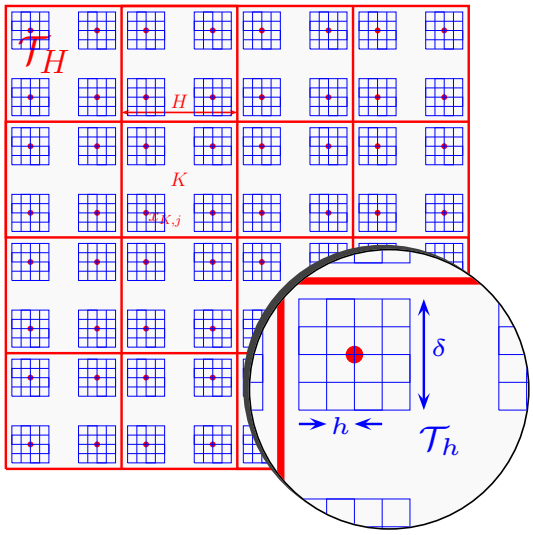

Figure 5.1: Visualization of the FE-HMM: Macro mesh shown in red and micro mesh in blue.

Remember that we estimate the bilinear form by solving an elliptic micro problem within sampling domains I_δ of diameter $\delta = \mathcal{O}(\varepsilon)$ around each quadrature node. For this we use triangulations $\mathcal{T}_h$ of the sampling domains. Here the mesh must resolve the micro scale, i.e., $h < \varepsilon$. However, since the sampling domains scale in size with ε, the computational work is independent of ε. In Figure 5.1 the different meshes used in the FE-HMM are depicted.

The inner products can also be computed using numerical integration. Replacing $(\cdot\,,\cdot)$ with $(\cdot\,,\cdot)_{\mathrm{QF}}$ we get a scheme, which is fully discretized in space. The application of mass lumping techniques as described on page 31 leads to a diagonal mass matrix, which is easy to invert. Note that the quadrature used to evaluate the L^2 inner product may differ from the quadrature formula used to define the FE-HMM bilinear form.

Regardless of whether numerical integration is used to compute the L^2 inner product or not, the FE-HMM scheme (5.1) is equivalent to a system of second order ordinary differential equations; c.f. Section 3.1. To solve it, we apply either the leap-frog scheme or the modified equation scheme. There is no restriction that forbids use of any other time stepping scheme.

5.2 Convergence analysis

In [5] a convergence proof of the FE-HMM scheme (5.1) was given. Here we apply Theorems 3.1 and 3.2 to give a slightly more general proof, as it generalizes immediately to the case where numerical quadrature is used to evaluate the L^2-inner product on the left-hand side. In contrast to [5] no regularity assumption on u_H is needed.

Theorem 5.1. *Let u^0 and u_H be the unique solutions of the homogenized wave equation* (4.6) *and the FE-HMM scheme* (5.1)*, respectively. Suppose that the quadrature formula satisfies* (3.16)–(3.18)*. Provided that $a^\varepsilon \in \mathcal{M}(\lambda, \Lambda)$, $a^0 \in W^{\ell,\infty}(\Omega)$, and the following regularity assumptions hold,*

$$\begin{aligned} &\partial_t^k u^0 \in L^2(0,T;H^{\ell+1}(\Omega)),\ \partial_t^{2+k} u^0 \in L^2(0,T;H^\ell(\Omega)) && \text{for } k=0,1,2,\\ &u_I \in H^{\ell+1}(\Omega),\ v_I \in H^{\tilde{\ell}}(\Omega), && \text{with } \tilde{\ell} = \max\{\ell, 2\}, \end{aligned}$$

we have

$$\left\|\partial_t(u^0 - u_H)\right\|_{L^\infty(0,T;L^2(\Omega))} + \left\|u^0 - u_H\right\|_{L^\infty(0,T;H^1(\Omega))} \leq C\left(H^\ell + e_{\mathrm{HMM}}\right)$$

for all $H \leq H_0$.

If the stronger regularity conditions, $a^0 \in W^{\ell+1,\infty}(\Omega)$ and

$$\begin{aligned} &\partial_t^k u^0 \in L^2(0,T;H^{\ell+1}(\Omega)),\ \partial_t^{4} u^0 \in L^2(0,T;H^\ell(\Omega)) && \text{for } k=0,1,2,3,\\ &u_I \in H^{\ell+1}(\Omega),\ v_I \in H^{\tilde{\ell}}(\Omega), && \text{with } \tilde{\ell} = \max\{\ell, 2\}, \end{aligned}$$

hold we have additionally

$$\left\|u^0 - u_H\right\|_{L^\infty(0,T;L^2(\Omega))} \leq C\left(H^{\ell+1} + e_{\mathrm{HMM}}\right).$$

Moreover, if the quadrature formula also satisfies (3.19)*, we get the same error estimates, even if we replace $(\cdot\,,\cdot)$ with $(\cdot\,,\cdot)_{\mathrm{QF}}$ on the left-hand side of* (5.1)*.*

Proof. In order to apply Theorems 3.1 and 3.2 with $\tilde{B} = B^0$, $\tilde{B}_H = B_H$, and $\{\cdot\,,\cdot\} = (\cdot\,,\cdot)$ we have to verify their assumptions for these choices. The assumptions (3.6)–(3.8) on the inner product are trivially fulfilled. In addition the coercivity and boundedness of both bilinear forms follow since $a^\varepsilon, a^0 \in \mathcal{M}(\lambda, \Lambda)$; see the remark on page 15 and Lemma 3.6. It remains to estimate the difference between B^0 and B_H. We treat this difference by splitting it as follows:

$$\begin{aligned} \left|B^0(v_H, w_H) - B_H(v_H, w_H)\right| \leq{}& \left|B^0(v_H, w_H) - B^0_{\mathrm{QF}}(v_H, w_H)\right| \\ &+ \left|B^0_{\mathrm{QF}}(v_H, w_H) - B_H(v_H, w_H)\right|. \end{aligned}$$

Since $a^0 \in W^{\ell+\mu,\infty}(\Omega)$, $\mu = 0, 1$ it follows from the remark on page 29 that

$$\left|B^0(v_H, w_H) - B^0_{\mathrm{QF}}(v_H, w_H)\right| \leq CH^{\ell+\mu} \left\|v_H\right\|_{\bar{H}^{\ell+\mu}} \left\|w_H\right\|_{\bar{H}^{1+\mu}}$$

and

$$\left|B^0(v_H, w_H) - B^0_{\mathrm{QF}}(v_H, w_H)\right| \leq CH \left\|v_H\right\|_{H^1} \left\|w_H\right\|_{H^1}.$$

Moreover, from (3.32) we have that

$$\left|B^0(v_H, w_H) - B^0_{\mathrm{QF}}(v_H, w_H)\right| \leq Ce_{\mathrm{HMM}} \left\|\nabla v_H\right\|_{L^2} \left\|\nabla w_H\right\|_{L^2}.$$

Hence we can apply 3.1 and Theorem 3.2 with $\alpha = 0$ and $\beta = e_{\mathrm{HMM}}$. Note that we do not need any assumptions on u_H because $\alpha = 0$; see Corollary 3.3.

If numerical integration is used to evaluate the inner product on the left-hand side, we can conclude this result similarly. The additional assumption (3.19) is needed to guarantee the coercivity of $(\cdot\,,\cdot)_{\mathrm{QF}}$; see the remark on page 29. □

Note that we can decompose e_{HMM} into micro and modeling error, which can be bounded by Theorems 3.8 and 3.9. From Theorem 3.8 we deduce that the micro mesh size h and the macro mesh size H must be refined simultaneously such that the convergence order is not destroyed.

Numerical confirmation

We recover the theoretical order of convergence by the following experiment: We consider (4.1) in $\Omega = (-1, 1)$ until the final time $T = 0.6$ with the initial conditions $u_I(x) = \sin(\pi x)$ and $v_I(x) = 0$. The squared velocity field is given as for the model example (4.2) with $\varepsilon = 1/50$. Since we can compute analytically that $a^0 = 1$, the homogenized solution is given by $u^0 = \sin(\pi x)\cos(\pi t)$. We compute the L^2- and the H^1-error between the homogenized solution u^0 and its FE-HMM approximation u_H for different discretization levels. We choose equidistant meshes for the macro and the micro mesh, and use linear, quadratic, or cubic FEM as macro- and micro solver. We set the size δ of the sampling domain I_δ equal to the periodicity length ε. For linear FEM we choose the leap-frog time stepping scheme and for quadratic and cubic FEM the modified equation scheme. The discretization parameters are given as follows:

$$H = \frac{1}{2^k}, \qquad h = \frac{\delta}{5 \cdot 2^k}, \qquad \Delta t = \frac{1}{10 \cdot 2^k},$$

for $k = 2, \dots, 8$. In Figure 5.2 we observe the expected overall convergence order for the L^2- and the H^1-error for all linear, quadratic, and cubic finite elements, though fixing the micro mesh size destroys the convergence as expected; see Figure 5.3.

5.3 Complexity of the FE-HMM

In this section we compare the computation load for the FE-HMM scheme presented in Section 5.1 with the fully resolved standard FEM. In general the overall computational cost of an HMM scheme consists of the cost of the macroscopic solver and the cost of the microscopic solver times the number of micro problems that we need to solve.

The macroscopic solver consists of two steps as is usually the case solving the wave equation with standard FEM. First the mass and the stiffness matrix need to be computed and afterwards the time stepping scheme is applied. The computation of the mass matrix and the time stepping scheme are the same as for standard FEM with the macro triangulation $\mathcal{T}_H$. Only the computation of the HMM stiffness matrix given by $A_{i,j} = B_H(\phi_j, \phi_i)$ becomes more expensive. Recall that $\{\phi_1, \dots, \phi_N\}$ denotes the standard FEM basis for $S_0^\ell(\Omega, \mathcal{T}_H)$. By N_{elem} we denote the degree of freedom for each element $K \in \mathcal{T}_H$. This is the number of basis functions ϕ_i such that the intersection of the support of ϕ_i and K is nonempty. Furthermore, let N_{mac} be the number of macroscopic elements. For quasi-uniform meshes we have $N_{\mathrm{mac}} \in \mathcal{O}\big(H^{-d}\big)$, where d is the spatial dimension. Assembling the stiffness matrix elementwise, we need to evaluate the HMM bilinear form $JN_{\mathrm{elem}}^2 N_{\mathrm{mac}}$ times, where J denotes the number of quadrature nodes per macro element. Having computed the micro solutions ϕ_{ih}, $i = 1, \dots, N$ of the

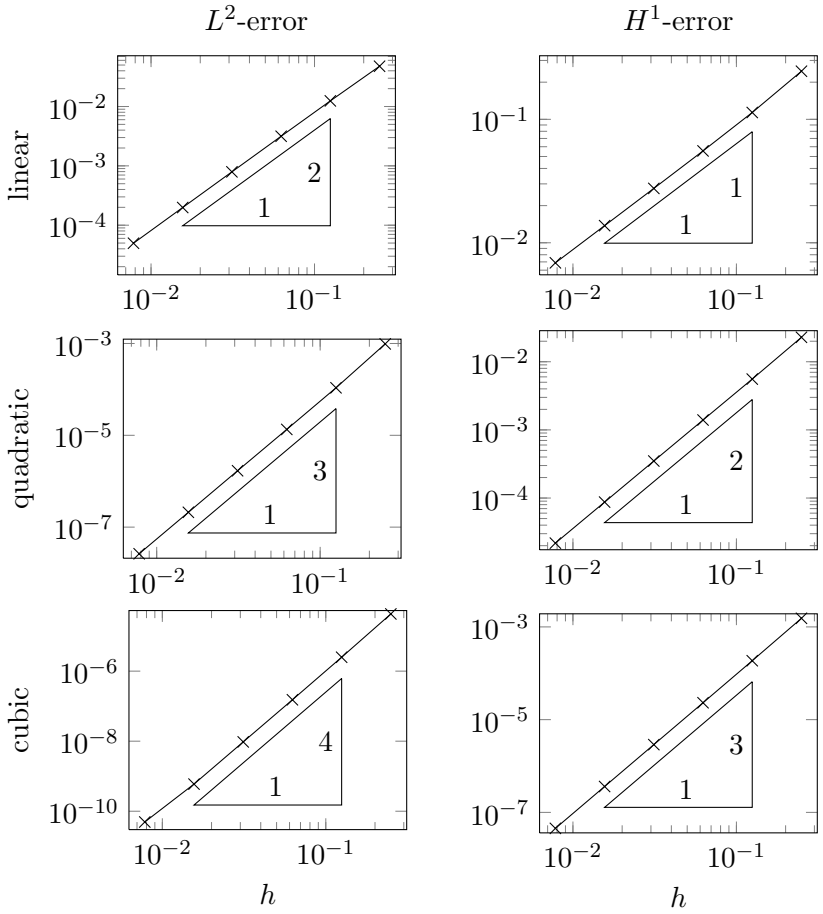

Figure 5.2: L^2- and the H^1-error of the FE-HMM with linear, quadratic, and cubic FEM for the macro and the micro solver. The expected orders of convergence are achieved if the macro and micro mesh are refined simultaneously.

micro problem (3.26) corresponding to the basis function ϕ_i, we need to multiply the micro stiffness matrix with two coefficient vectors of two micro solutions. Since the micro stiffness matrix needs to be assembled to solve the micro problems, the main additional work consists of solving the micro problems. Saving the solutions of the micro problems temporally, we need to solve N_{elem} micro problems per quadrature node. Overall $JN_{\text{elem}}N_{\text{mac}}$ micro problems need to be solved. Since the micro problems are elliptic, their solution requires the solution of one sparse linear system per sampling domain.

Remark. In [28] it was shown that the number of microscale problems that need to be solved can be reduced by choosing a special quadrature formula with quadrature nodes on the boundary of the element. Thus one can use one micro problem and its solution for several elements. Furthermore, to speed up the implementation one could solve the micro problems in parallel since they do not depend on each other.

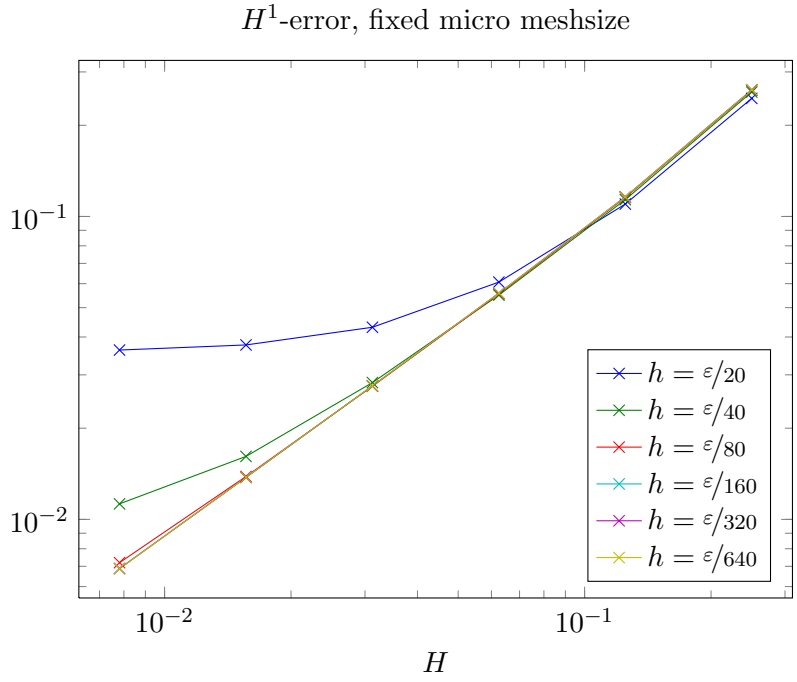

Figure 5.3: H^1-error of the FE-HMM with linear FEM for the macro and micro solver and with fixed micro mesh size h. The convergence is harmed if h is not refined.

As mentioned above, we use a standard explicit time stepping scheme. A fully resolved spatial domain enforces very small time steps because of the CFL condition. Hence, being allowed to use a coarser mesh, as is the case for the FE-HMM scheme, leads to a less restrictive CFL condition and to an additional computational gain.

To demonstrate the deliberations above we compare the computational cost of solving the model problem introduced in Section 4.1 with $\varepsilon = 2^{-10}$ and $T = 2$. First we use a standard fully resolved quadratic FE solution and afterwards the FE-HMM scheme with quadratic FE for the macro and the micro solver. The size δ of the sampling domains I_δ is set to one period of the underlying material, i.e., $\delta = \varepsilon$. All integrals are approximated in both schemes elementwise with a Simpson quadrature formula.

Furthermore, we use uniform meshes with $H = 2^{-5}$ and $h = 2^{-13}$. Here H denotes the length of an element of the macroscopic partition $\mathcal{T}_H$ and h the length of an element of the microscopic partition $\mathcal{T}_h$. Moreover we used the same mesh size h for the fully resolved FEM. The mesh sizes H and h are chosen such that the L^2 differences between the approximations and the analytically computed homogenized solution are of the same order; see the last row in Table 5.1. Note that we cannot coarsen the mesh size of the fully resolved FEM: If we double the mesh size, we would undersample the fine scale structure of the medium. The error between this coarsened FEM solution and the homogenized solution would increase over fifty-fold to 0.0139.

For the time stepping we use the leap-frog scheme (3.20). Since $H/h = 2^8$ the CFL

Table 5.1: Computational cost to solve the model problem with $\varepsilon = 2^{-10}$ with a fully resolved FEM and the FE-HMM.

	fully resolved FEM	FE-HMM
mesh size	2^{-13}	2^{-5}
number of elements	2^{14}	2^{6}
time for computing the mass matrix	$7.310 \cdot 10^{-1}$ s	$4.618 \cdot 10^{-3}$ s
number of micro problems	—	192
time for computing the stiffness matrix	1.301 s	$2.698 \cdot 10^{-1}$ s
time step	2^{-16}	2^{-8}
number of time steps	2^{17}	2^{9}
time for time stepping	$2.606 \cdot 10^{2}$ s	$3.609 \cdot 10^{-2}$ s
L^2-difference to u^0	$2.454 \cdot 10^{-4}$	$2.9576 \cdot 10^{-4}$

condition is 2^8 times more stringent for the fully resolved FEM than for the FE-HMM. Hence we set the time step for the FE-HMM 2^8 times greater than the time step for FEM.

In Table 5.1 the results are summarized. The indicated times needed for the computation are the averages of a hundred runs on the same computer. The overall average computation time for the fully resolved FEM is 263 s. For the FE-HMM only 0.311 s are needed in average. Whenever possible the same implementation techniques are used for both the FEM and FE-HMM. Hence the computational gain is not due to an optimized implementation, but inherent in the method itself. This computational gain can be explained as follows: Since fewer elements are needed for the FE-HMM than for a fully resolved FEM, the assembling of the mass matrix is over 150 times faster. In contrast, the computation of the FE-HMM stiffness matrix is only five times faster because it involves the solution of the micro problems. As mentioned above this step could be sped up by solving the micro problems in parallel. The biggest gain in computation time is caused by the time-stepping. On one hand each time iteration is faster since the number of degree of freedoms and hence the size of the matrices is smaller for FE-HMM. On the other hand considerably fewer iterations are needed. The combination of these two effects leads to a speed up of over 7000.

Remark. The cost of the FE-HMM is independent of ε, since the sampling domain I_δ scales with ε. For the standard FEM a decreasing microscopic structure ε of the material must be fully resolved by the mesh, leading to smaller mesh sizes. Due to the CFL condition the time step must be decreased as well. Hence for even smaller ε and in multiple space dimensions the fully resolved FEM may no longer be computable.

5.4 Numerical experiments

In [48–50] we have performed a variety of tests and examples to show the usefulness and versatility of our FE-HMM. In this section we just consider the most prominent examples. First we apply the FE-HMM to the model example of Section 4.1. Then, we

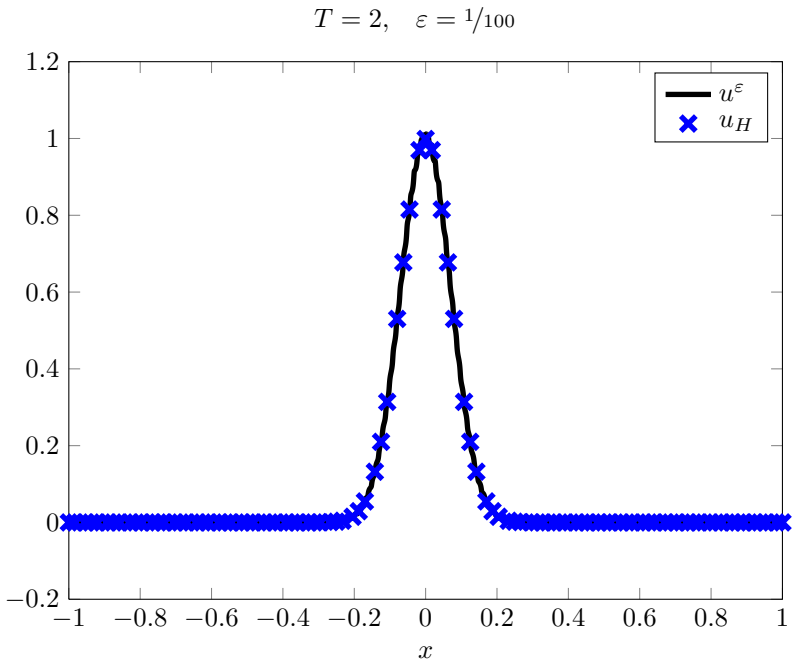

Figure 5.4: Reference solution u^ε and FE-HMM solution u_H of the model example at $T = 2$ for $\varepsilon = 1/100$.

consider one-dimensional wave propagation through a medium, which depends on both scales x and x/ε. Finally we show three two-dimensional examples with different macroscopic solvers. For the first example we used $\mathcal{Q}^1$, for the second $\mathcal{Q}^2$, and for the third $\mathcal{P}^1$ elements. We conclude this section giving some comments on the implementation of the FE-HMM.

Model problem

We apply the FE-HMM with $\mathcal{P}^3$ elements for the macro and the micro solver to our model example. We set $\varepsilon = 1/100$ and choose the discretization parameters as follows:

$$H = 2^{-4} = \frac{1}{16}, \qquad h = \frac{\varepsilon}{100} = \frac{1}{5000}, \qquad \Delta t = \frac{H}{8} = \frac{1}{128}.$$

The macroscopic behavior of u^ε is well described by the FE-HMM scheme, as shown in Figure 5.4. Furthermore the discretized energy of the FE-HMM solution $E_H^{\mathrm{HMM}} \approx 6.238$ is a good approximation of the homogenized energy. The relative error between E_H^{HMM} and the discretized energy of the homogenized solution E_H^0, where the same discretization parameters are used, is

$$\frac{\left|E_H^{\mathrm{HMM}} - E_H^0\right|}{\left|E_H^0\right|} = 1.878 \cdot 10^{-11}.$$

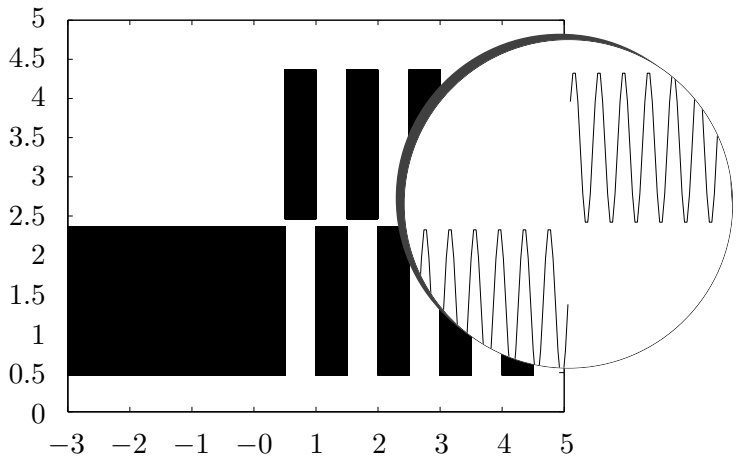

Figure 5.5: The tensor a^ε in the whole computational domain $\Omega = (-3, 5)$ with a zoom of the x-axis at $x = 4.5$.

If the error $e_{\text{HMM}} \to 0$ the convergence $E_H^{\text{HMM}} \to E_H^0$ follows. Note that the modeling error vanishes due to Theorem 3.9 since a^ε is periodic and does only depends on the micro scale $1/\varepsilon$. Hence we have $e_{\text{HMM}} = e_{\text{MIC}}$, which can be bounded using Theorem 3.8.

One-dimensional wave propagation

In contrast to the model example the medium considered now is no longer purely periodic since it depends on the macro and the micro scale. At the micro scale the medium oscillates and is discontinuous at the macro scale.

Let the computational domain $\Omega = (-3, 5)$ and the final time $T = 3$. We consider the problem

$$\begin{cases} \partial_{tt} u^\varepsilon(t;x) - \partial_x \left(a^\varepsilon(x) \partial_x u^\varepsilon(t;x) \right) = 0 & \text{in } \Omega,\ 0 < t < T, \\ u^\varepsilon(t;x) = 0 & \text{on } \partial\Omega,\ 0 < t < T, \end{cases}$$

where the initial condition is a right-moving Gaussian pulse and we set $\varepsilon = 10^{-3}$. The material described by

$$a^\varepsilon(x) = \begin{cases} \sqrt{2} + \sin\left(2\pi \frac{x}{\varepsilon}\right), & x \le 0 \text{ or } x \in [k, k + 0.5),\ k \in \mathbb{N}_0, \\ \sqrt{2} + \sin\left(2\pi \frac{x}{\varepsilon}\right) + 2, & x \in [k + 0.5, k + 1),\ k \in \mathbb{N}_0, \end{cases}$$

is shown in Figure 5.5. In this example we use linear elements to solve either the macro aor the micro problem. To constrain the micro solution a periodic coupling condition was enforced. The discretization parameters of our HMM are set as follows: the macro mesh size $H = 10^{-2}$, the size of the sampling domain $\delta = \varepsilon = 10^{-3}$, the micro mesh size $h = 10^{-4}$, and the time step in the leap-frog scheme $\Delta t = 10^{-3}$. Here we compare the FE-HMM solution with a reference solution (DNS) on a highly refined mesh. On the left-hand side of Figure 5.6 three snapshots of the solution are shown. We see that the

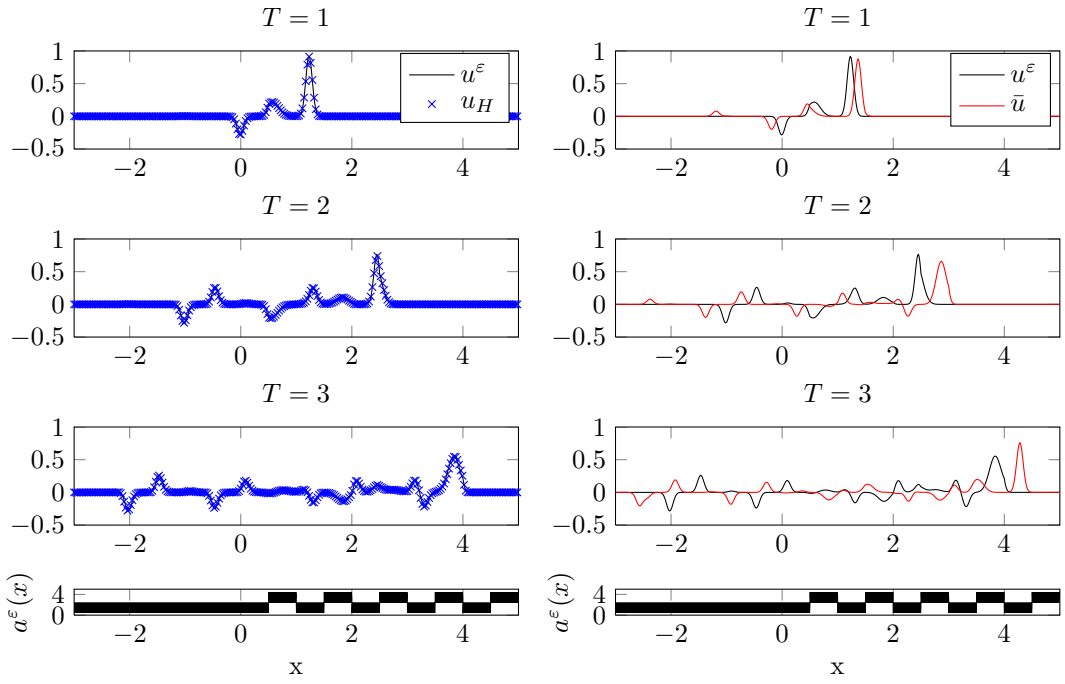

Figure 5.6: One-dimensional example. Three snapshots of the the reference solution u^ε, the FE-HMM solution u_H and the solution $\bar{u}$ computed with an averaged tensor at $T = 1$, 2, and 3 with a sketch of the highly oscillatory tensor a^ε on the bottom.

FE-HMM solution is in good accordance with the reference solution, whereas a naive average of a^ε leads to wrong results. This can be seen from the right-hand side of Figure 5.6.

Two-dimensional wave propagation

Locally isotropic medium with anisotropic effective medium

Let $\Omega = [0,1]^2 \in \mathbb{R}^2$, $T = 0.25$, and $\varepsilon = 1/300$. We now consider the following two-dimensional problem from [37, Section 4.3.2]:

$$\begin{cases} \partial_{tt} u^\varepsilon(t;x) - \nabla \cdot (a^\varepsilon(x) \nabla u^\varepsilon(t;x)) = 0 & \text{in } \Omega,\ 0 < t < T, \\ u^\varepsilon(t;x) = 0 & \text{on } \partial\Omega,\ 0 < t < T, \\ u^\varepsilon(0;x) = \exp\left(-\dfrac{|x - x_M|^2}{\sigma^2}\right) & \text{in } \Omega, \\ \partial_t u^\varepsilon(0;x) = 0 & \text{in } \Omega\,, \end{cases}$$

where $x_M = (0.5, 0.5)$, $\sigma = 0.1$, and $a^\varepsilon(x) = a^\varepsilon(x_1)$ is the 2×2 tensor given by

$$a^\varepsilon(x) = \begin{pmatrix} 1.1 + 0.5\left(\sin 2\pi x_1 + \sin 2\pi \frac{x_1}{\varepsilon}\right) & 0 \\ 0 & 1.1 + 0.5\left(\sin 2\pi x_1 + \sin 2\pi \frac{x_1}{\varepsilon}\right) \end{pmatrix},$$

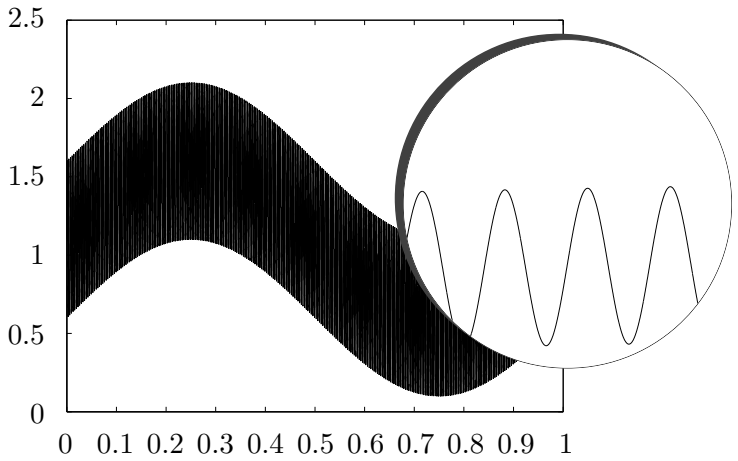

Figure 5.7: Cross section, i.e., fixed second component x_2, of the tensor a^ε through the material.

with $\varepsilon = 1/300$. A cross section through the material is shown in Figure 5.7. In this case the homogenized tensor can be computed analytically by (2.15). It is given by

$$a^0 = \begin{pmatrix} \sqrt{(1.1 + 0.5 \sin 2\pi x_1)^2 - 0.5^2} & 0 \\ 0 & 1.1 + 0.5 \sin 2\pi x_1 \end{pmatrix}.$$

Note that even though a^ε is locally isotropic, the homogenized tensor is not. We compare the HMM solution with the solution of the homogenized problem. For the FE-HMM we used $\mathcal{Q}^1$ elements for solving the macro and the micro problems, again with a periodic coupling condition. We set $H = 1/100$, $\delta = \varepsilon = 1/300$, $h = 1/3000$, and $\Delta t = 1/1000$. As shown in Figure 5.8, both solutions coincide as the initially circular wave front propagates through the stratified medium and becomes increasingly distorted. We recall that in contrast to the direct FE solution of the homogenized wave equation, which requires the a priori analytic derivation of the homogenized tensor a^0, the FE-HMM solution only uses the original fine scale description of the medium, contained in a^ε.

Waveguide example

We now let $\Omega = (0, 3) \times (0, 1) \subset \mathbb{R}^2$ and divide Ω into two distinct subregions (see Figure 5.9):

$$\Omega_1 = \{x = (x_1, x_2) \in \Omega : x_2 \geq x_1 - 1\}$$
$$\Omega_2 = \{x = (x_1, x_2) \in \Omega : x_2 < x_1 - 1\}.$$

We consider the wave equation (1.3) in two space dimensions with zero initial condition, i.e., $u_I = v_I = 0$. The squared velocity field is given by

$$a^\varepsilon(x) = \begin{pmatrix} 1.1 + \delta_{i2} \sin(2\pi \frac{x_1}{\varepsilon}) & 0 \\ 0 & 1.1 + \delta_{i2} \sin(2\pi \frac{x_1}{\varepsilon}) \end{pmatrix} \qquad \text{for } x \in \Omega_i,$$

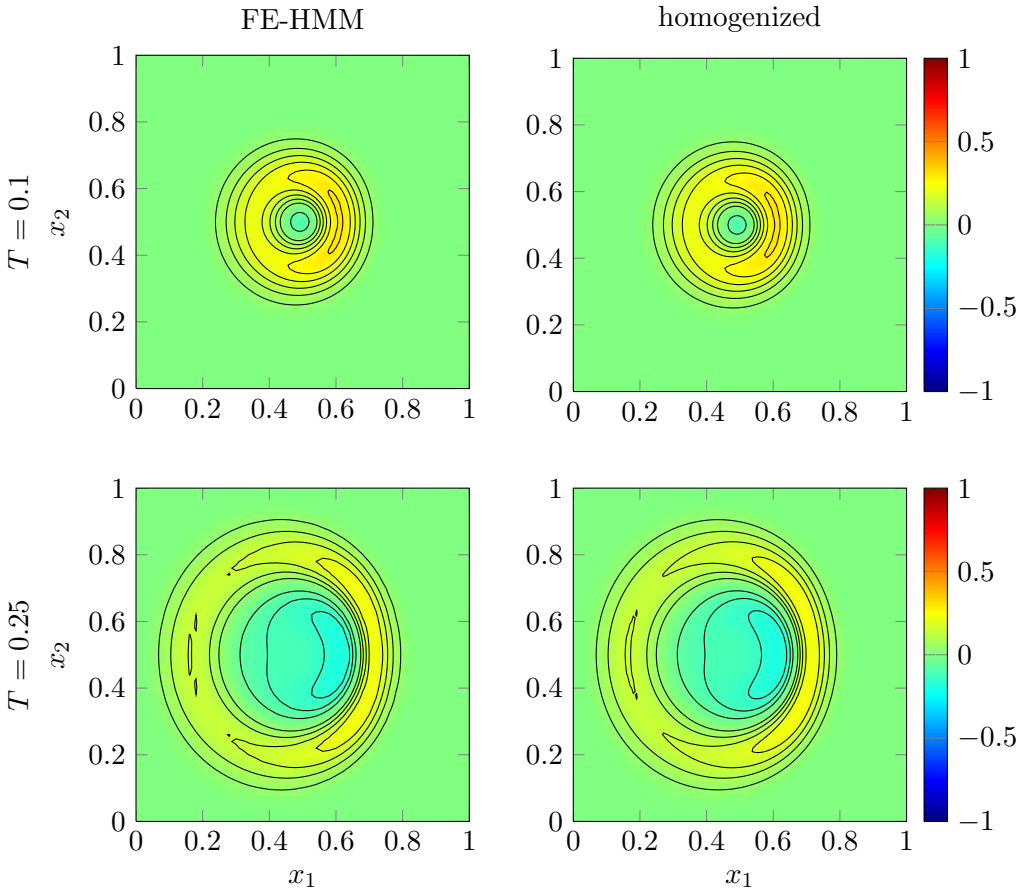

Figure 5.8: Two-dimensional example. Two snapshots of the FE-HMM solution u_H (left) and the homogenized solution u^0 (right) at $T = 0.1$ and $T = 0.25$.

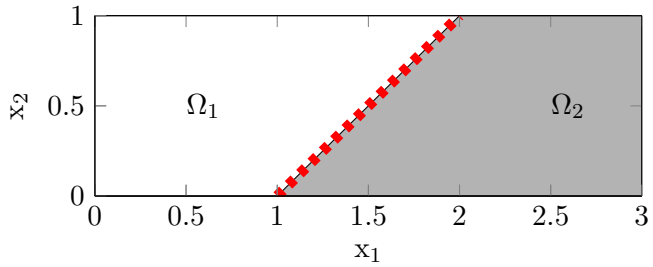

Figure 5.9: The computational domain Ω for the waveguide example.

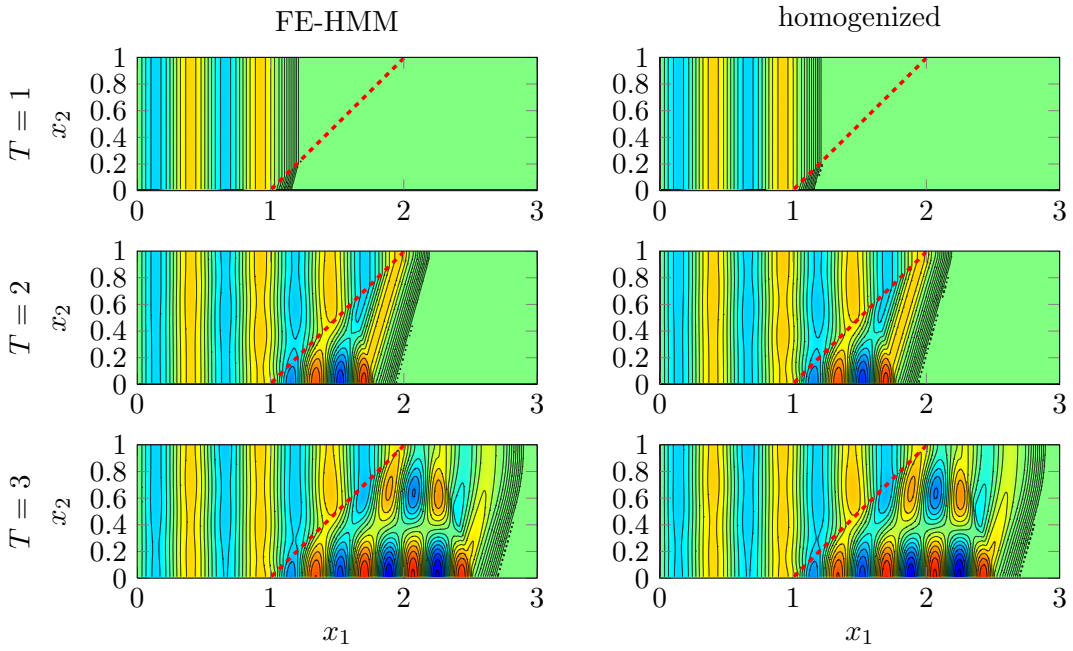

Figure 5.10: Waveguide example. Three snapshots of the FE-HMM solution u_H (left) and the homogenized solution u^0 (right) at $T = 1$, 2, 3.

where $\delta_{12} = 0$ and $\delta_{22} = 1$.

On the upper and lower boundary we impose a homogeneous Neumann and on the right boundary a homogeneous Dirichlet boundary condition. On the left boundary we set the time dependent Dirichlet condition,

$$u^\varepsilon(x,t) = \sin(4\pi t),$$

which corresponds to a plane wave incoming from the left. We set $\varepsilon = 10^{-3}$ and used quadrilateral biquadratic finite elements on a rectangular mesh with mesh size $H = 10^{-2}$. The sampling domains are of size $\delta = \varepsilon$, each partitioned into an equidistant, rectangular submesh with mesh size $h = 10^{-4}$.

In Ω_1, no homogenization is needed, whereas in Ω_2, we can apply again (2.15). For comparison, we compute the FE solution of the wave with the analytically computed homogenized tensor

$$a^0(x) = \begin{cases} \begin{pmatrix} 1.1 & 0 \\ 0 & 1.1 \end{pmatrix} & \text{for } x \in \Omega_1, \\ \begin{pmatrix} \sqrt{0.21} & 0 \\ 0 & 1.1 \end{pmatrix} & \text{for } x \in \Omega_2. \end{cases}$$

Snapshots of the FE-HMM solution u_H and the homogenized solution u^0 are shown in Figure 5.10 at different times. A good correspondance can be observed.

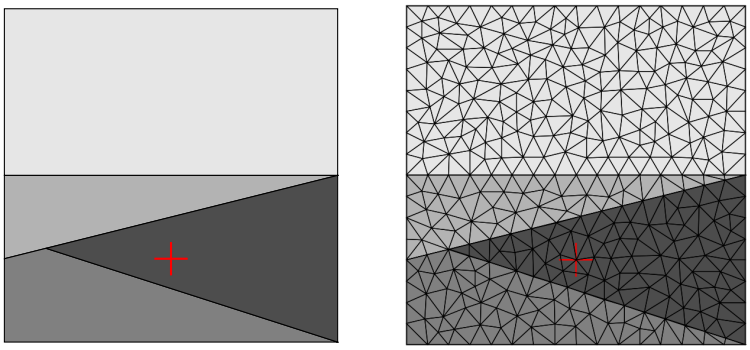

Figure 5.11: Computational domain with subdomains and receiver (red cross) at $(1, -0.5)$ (left), sample triangulation respecting inner interfaces (right)

Rock layer example

Here, we shall now extend the FE-HMM approach to triangular meshes and illustrate its use in complex geometry, reminiscent of rock layers. We consider the computational domain $\Omega = [0, 2] \times [-1, 1] \subset \mathbb{R}^2$, subdivided into four distinct subdomains, as shown in Figure 5.11. The material tensor $a^\varepsilon(x)$ is given by

$$a^\varepsilon(x) = \begin{cases} I_{2\times 2} & \text{for } x \in \Omega_1, \\ \left(\sqrt{2} + \sin\left(2\pi \frac{x_2}{\varepsilon}\right)\right) I_{2\times 2} & \text{for } x \in \Omega_2, \\ \left(\sqrt{2} + \frac{1}{2}\sin\left(2\pi x_2\right) + \sin\left(2\pi \frac{x_2}{\varepsilon}\right)\right) I_{2\times 2} & \text{for } x \in \Omega_3, \\ 2I_{2\times 2} & \text{for } x \in \Omega_4, \end{cases}$$

where $I_{2\times 2} = \left(\begin{smallmatrix} 1 & 0 \\ 0 & 1 \end{smallmatrix}\right)$ and $\varepsilon = 10^{-3}$. To achieve uniqueness, initial and boundary conditions need to be imposed. As initial condition we choose a downward moving Gaussian plane wave centered at $y = 0.5$ and set homogeneous Neumann boundary conditions on the entire boundary.

To solve the wave equation (1.3) numerically we choose $\mathcal{P}^1$ finite elements for the macro solver, $\mathcal{Q}^1$ finite elements for the micro solver, and a leap-frog time stepping scheme. The macro mesh we use has 63,498 elements and respects the inner interfaces of the medium, similar to the mesh shown on the right of Figure 5.11. Further discretization parameters are

$$\delta = \varepsilon = \frac{1}{1000}, \quad h = \frac{1}{7000}, \quad \Delta t = \frac{1}{1000}.$$

If we would use a fully resolved triangular mesh with the fine mesh size h, we would need almost 400 millions elements.

In Figure 5.12 we show three snapshots of the wave at different times. We depict not only the FE-HMM solution but also the numerical solution of the analytically homogenized problem, due to (2.15). Finally we show the solution where a^ε has been replaced by its local average. We observe that the HMM solution and the homogenized solution coincide, whereas the naively averaged solution displays errors both in phase and in am-

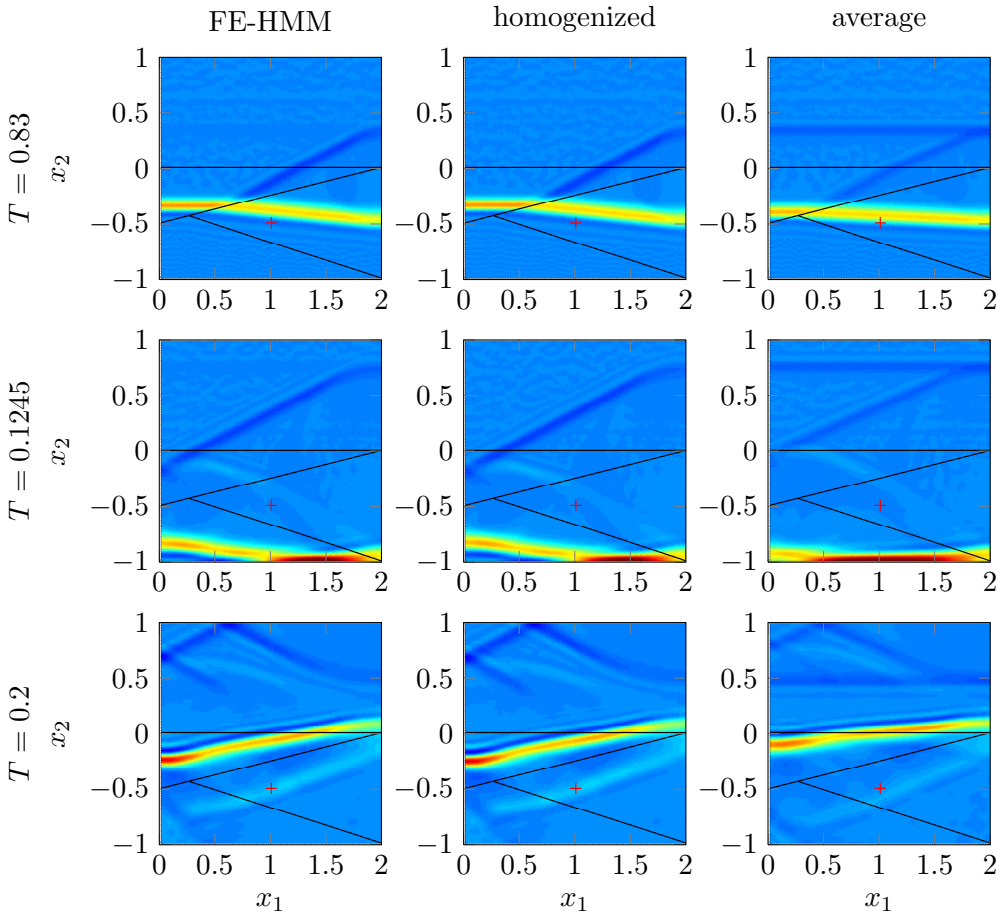

Figure 5.12: Rock layer example. Three snapshot of FE-HMM solution u_H (left), the homogenized solution u^0 (middle), and the solution $\bar{u}$ computed with an averaged tensor (right) at $T = 0.83$, 0.12456 and 0.2.

plitude. In Figure 5.13 we compare the three numerical solutions at the receiver location at $x^* = (1, -0.5)$; it is marked with a red cross in Figures 5.11 and 5.12.

5.5 Alternative FE-HMM formulations

In the FE-HMM scheme (5.1) the use of elliptic micro problems to compute the FE-HMM bilinear form B_H is probably surprising. The explanation thereof relies on homogenization theory; see Chapter 4. The homogenized tensor a^0 is computed in the same manner for elliptic and for hyperbolic homogenization problems. This observation is the starting point for the design of this FE-HMM scheme. Nevertheless, the most obvious idea to design a FE-HMM scheme consists in solving the wave equation on space-time sampling domains to estimate the missing data in the macro scale model. Following this

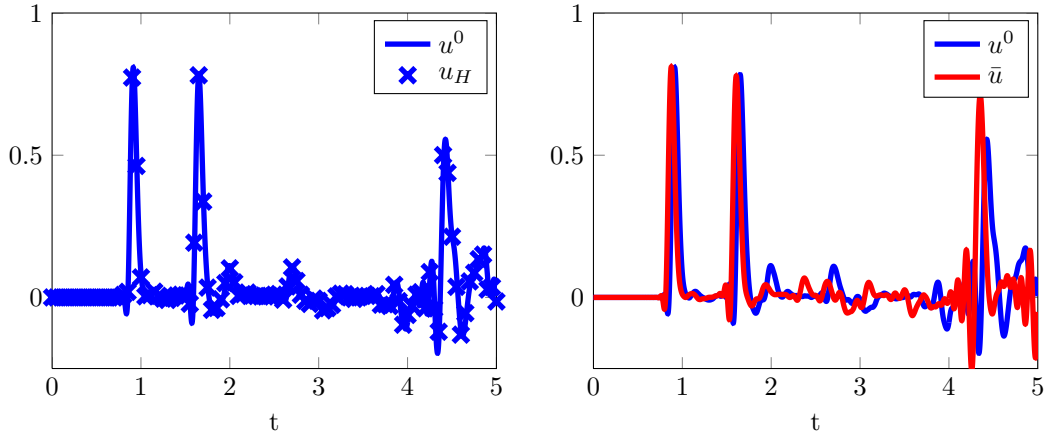

Figure 5.13: The homogenized solution $u^0(t;x^*)$, the FE-HMM solution $u_H(t;x^*)$ and the solution $\bar{u}$ computed with an averaged tensor at $x^* = (1,-0.5)$ for $t \in [0,5]$. The solutions u^0 and u_H coincide (left), whereas naively averaging the tensor a^ε leads to a wrong solution (right).

approach, a FD-HMM for the wave equation was proposed in [35, 37]. There, solutions of the wave equation are used to estimate an effective flux. Inspired by this FE-HMM scheme, we propose an alternative to our standard FE-HMM, which we call the the flux-averaging FE-HMM scheme. The direct application of the ideas of [35, 37] leads to a bilinear form, which is in general not symmetric. This non-symmetry is unfavorable since we know from homogenization theory that the analytically homogenized tensor a^0 is symmetric, as mentioned in the remark on page 15. Moreover, the energy conservation and the proof of the general a priori error estimates use the symmetry of the involved bilinear forms. For that reason we propose a second alternative, which is symmetric and uses hyperbolic micro problems. We show a close relation between this hyperbolic FE-HMM scheme and the standard FE-HMM proposed in Section 5.1.

Flux-averaging FE-HMM

While in an FD discretization the flux appears naturally, it is usually not considered in an FE discretization. Therefore we rewrite the bilinear form B^ε by

$$B^\varepsilon(v,w) = \int_\Omega [F^\varepsilon(v)](x) \cdot \nabla w(x)\, dx,$$

where $[F^\varepsilon(v)](x) = a^\varepsilon(x)\nabla v(x)$. Similarly we can rewrite the homogenized bilinear form by

$$B^0(v,w) = \int_\Omega [F^0(v)](x) \cdot \nabla w(x)\, dx,$$

where the homogenized flux is given by $[F^0(v)](x) = a^0(x)\nabla v(x)$ and a^0 is the usual homogenized tensor defined in (2.11). Note that we have only introduced the notation

of the flux. So far everything is equivalent to the earlier considerations.

The definition of the flux-averaging FE-HMM is similar the to standard FE-HMM. Only the definition of the bilinear form changes. Everything else, e.g., the triangulation $\mathcal{T}_H$, the finite element space $S_0^\ell(\Omega, \mathcal{T}_H)$, or the quadrature formula $\{x_{K,j}, \omega_{K,j}\}$ remains unchanged. The flux-averaging FE-HMM is given by the following problem: Find $u_H^{\mathrm{fl}} \colon [0,T] \to S_0^\ell(\Omega, \mathcal{T}_H)$ such that

$$\begin{cases} \left(\partial_{tt} u_H^{\mathrm{fl}}, v_H\right) + B_H^{\mathrm{fl}}\left(u_H^{\mathrm{fl}}, v_H\right) = (f, v_H) & \text{for all } v_H \in S_0^\ell(\Omega, \mathcal{T}_H),\ 0 \le t \le T, \\ u_H^{\mathrm{fl}}(0) = I_H(u_I) & \text{in } \Omega, \\ \partial_t u_H^{\mathrm{fl}}(0) = I_H(v_I) & \text{in } \Omega, \end{cases} \tag{5.2}$$

where B_H^{fl} is given by

$$B_H^{\mathrm{fl}}(v_H, w_H) = \sum_{K \in \mathcal{T}_H} \sum_{j=1}^{J} \omega_{K,j} [F_H(v_H)](x_{K,j}) \cdot \nabla w_H(x_{K,j}),$$

and the averaged flux is given by

$$[F_H(v_H)](x_{K,j}) = \int_{-\tau}^{\tau} \int_{I_\delta(0)} k_\tau(t) k_\eta(x) a^\varepsilon(x_{K,j} + x) \nabla \tilde{v}_h(t; x)\, dx\, dt, \tag{5.3}$$

where $\tilde{v}_h$ is the solution of the following hyperbolic micro problem: Find $\tilde{v}_h : [-\tau, \tau] \to S^q(I_\delta, \mathcal{T}_h)$ such that

$$\begin{cases} (\partial_{tt} \tilde{v}_h, z_h) + B^\varepsilon(\tilde{v}_h, z_h) = 0 & \text{for all } z_h \in S^q(I_\delta, \mathcal{T}_h),\ -\tau \le t \le \tau, \\ \tilde{v}_h(0) = Q(v_H) & \text{in } \Omega, \\ \partial_t \tilde{v}_h(0) = 0 & \text{in } \Omega. \end{cases} \tag{5.4}$$

Here δ and τ are the size of the sampling domain in space and time. Furthermore, k_τ and k_η are averaging kernels and $Q(v_H)$ is the macro-to-micro coupling operator, used to initialize the micro problem.

For the kernel we introduce the kernel spaces $\mathbb{K}^{p',q'}$ by

$$k \in \mathbb{K}^{p',q'} \Leftrightarrow \begin{cases} k \in C^{q'}(\mathbb{R}), \\ \operatorname{supp} k \subset [-1,1], \\ \int_{\mathbb{R}} k(x)\, dx = 1, \\ \int_{\mathbb{R}} k(t) t^r\, dx = 0, \quad 1 \le r \le p', \end{cases}$$

and set $k_\nu(x) := {}^1\!/\!_\nu k({}^x\!/\!_\nu)$ for any $\nu > 0$. Averaging kernels were introduced in [40] for an HMM scheme to solve stiff ordinary equations and used in [35–37, 39] to estimate an effective flux. In this thesis we consider only symmetric polynomial kernels and we write $k_\nu \in \mathbb{K}^{p',q'}$ if there exists a $k \in \mathbb{K}^{p',q'}$ such that $k_\nu(x) = {}^1\!/\!_\nu k({}^x\!/\!_\nu)$. Due to the initial condition $\partial_t \tilde{v}_h(0) = 0$, the micro solution $\tilde{v}_h$ is symmetric in time. Hence we have

$$[F_H(v_H)](x_{K,j}) = 2 \int_{0}^{\tau} \int_{I_\delta(0)} k_\tau(t) k_\eta(x) a^\varepsilon(x_{K,j} + x) \nabla \tilde{v}_h(t; x)\, dx\, dt,$$

and it is enough to solve the micro problem only forward in time. For an actual implementation a time stepping scheme must again be applied.

Note that the support $[-\eta, \eta]$ of the averaging kernel must be inside the sampling domain I_δ, hence we let $\eta \leq \delta/2$. Furthermore, we choose δ to be large enough, such that no information propagates from the boundary into the averaging area. This is possible because of the finite speed of propagation of the wave equation. Hence the choice of the boundary condition of the micro problem does not influence the scheme.

Here we restrict ourself to a linear coupling given by

$$[Q(v_H)](x) = v_H(x_{K,j}) + \nabla v_H(x_{K,j}) \cdot x. \tag{5.5}$$

We will discuss the use of higher order coupling conditions later in Section 6.4.

For the analysis we consider the semidiscrete case as-well. Here $\tilde{v}_h$ is replaced by the exact solution $\tilde{v}$ of the exact micro problem: Find $\tilde{v} : [-\tau, \tau] \to H^1(I_\delta)$ such that

$$\begin{cases} (\partial_{tt}\tilde{v}, z) + B^\varepsilon(\tilde{v}, z) = 0 & \text{for all } z \in H^1(I_\delta),\ -\tau \leq t \leq \tau, \\ \tilde{v}(0) = Q(v_H) & \text{in } \Omega, \\ \partial_t \tilde{v}(0) = 0 & \text{in } \Omega. \end{cases} \tag{5.6}$$

We denote the corresponding bilinear form by $\bar{B}_H^{\mathrm{fl}}$ and the corresponding flux by $\bar{F}_H$.

In the following we show that the difference between $\bar{B}_H^{\mathrm{fl}}$ and the homogenized bilinear form can be bounded, but first we show two properties of the fluxes F_H and $\bar{F}_H$.

Lemma 5.2 (Linearity of fluxes, cf. [37, Section 2.2])**.** *The operators $F_H, \bar{F}_H : S_0^\ell(\Omega, \mathcal{T}_H) \to \mathbb{R}^d$ are linear.*

Proof. This proof works for both fluxes F_H and $\bar{F}_H$. The micro problem we have to solve is a linear wave equation, which is linear with respect to its initial data. Due to the linearity of Q the micro solution $\tilde{w}_h$ corresponding to the macro function

$$w_H = \alpha v_H + \beta v'_H$$

is given by

$$\tilde{w}_h = \alpha \tilde{v}_h + \beta \tilde{v}'_h,$$

where $\tilde{v}_h$ and $\tilde{v}'_h$ are the micro solutions corresponding to v_H and v'_H, respectively. Averaging consists of computing a weighted integral, which is again a linear operation and so is the entire flux. □

From [37, Theorem 3.1] we have the following convergence result.

Lemma 5.3 (Convergence of $\bar{F}_H$)**.** *Let F^0 and $\bar{F}_H$ be the homogenized flux and the HMM flux with an exact solution of the micro problem respectively, $a^\varepsilon(x) = a(x/\varepsilon)$, where a is Y-periodic, symmetric, positive definite, and smooth. Moreover, suppose $k \in \mathbb{K}^{p',q'}$, the initial data being smooth, and $\eta = \tau$. Then,*

$$\left\| [F^0(v)](x) - [\bar{F}_H(v)](x) \right\| \leq C \left| \nabla v(x) \right| \left(\frac{\varepsilon}{\eta} \right)^{q'},$$

where C is independent of ε, η, p', and q'.

From this we find a bound for the difference of the bilinear form $\bar{B}_H^{\mathrm{fl}}$ compared with B^0.

Corollary 5.4. *Suppose that the assumptions of Lemma 5.3 and the assumptions* (3.16), (3.17), *and* (3.18) *on the quadrature formula $\{x_{K,j}, \omega_{K,j}\}$ hold. Then we have*

$$\left| B^0_{\mathrm{QF}}(v_H, w_H) - \bar{B}^{\mathrm{fl}}_H(v_H, w_H) \right| \leq C \left(\frac{\varepsilon}{\eta}\right)^{q'} \|\nabla v_H\|_{L^2(\Omega)} \|\nabla w_H\|_{L^2(\Omega)} .$$

Proof. We have

$$\begin{aligned}
&\left| B^0_{\mathrm{QF}}(v_H, w_H) - \bar{B}^{\mathrm{fl}}_H(v_H, w_H) \right| \\
&\quad \leq \sum_{K\in\mathcal{T}_H} \sum_{j=1}^{J} \omega_{K,j} \left| [F^0(v_H)](x_{K,j}) - [\bar{F}_H(v_H)](x_{K,j}) \right| |\nabla w_H(x_{K,j})| \\
&\quad \leq C \left(\frac{\varepsilon}{\eta}\right)^{q'} \sum_{K\in\mathcal{T}_H} \sum_{j=1}^{J} \omega_{K,j} |\nabla v_H(x_{K,j})| \, |\nabla w_H(x_{K,j})| \\
&\quad \leq C \left(\frac{\varepsilon}{\eta}\right)^{q'} \left(\sum_{K\in\mathcal{T}_H} \sum_{j=1}^{J} \omega_{K,j} |\nabla v_H(x_{K,j})|^2 \right)^{\frac{1}{2}} \left(\sum_{K\in\mathcal{T}_H} \sum_{j=1}^{J} \omega_{K,j} |\nabla w_H(x_{K,j})|^2 \right)^{\frac{1}{2}} \\
&\quad \leq C \left(\frac{\varepsilon}{\eta}\right)^{q'} \|\nabla v_H\|_{L^2(\Omega)} \|\nabla w_H\|_{L^2(\Omega)} .
\end{aligned}$$

We use the positivity of the quadrature weights and the triangle inequality in the first, Lemma 5.3 in the second, the Cauchy-Schwartz inequality in the third, and the assumption on the quadrature formula in the last inequality. □

This corollary implies that the assumptions (3.11) and (3.12) are fulfilled for $\tilde{B} = B^0$ and $\tilde{B}_H = \bar{B}^{\mathrm{fl}}_H$. However, we cannot apply Theorems 3.1 and 3.2, because $\bar{B}^{\mathrm{fl}}_H$ is not symmetric in general. To show this, let us first introduce some notation. It is easy to see that the fluxes $[\bar{F}_H(v_H)](x_{K,j})$ and $[\bar{F}_H(w_H)](x_{K,j})$ are equal, if the gradients of v_H and w_H at $x_{K,j}$ are the same. More precisely we have for the one-dimensional case

$$[\bar{F}_H(v_H)](x_{K,j}) = \bar{F}_{H;K,j} \partial_x v_H(x_{K,j}), \tag{5.7}$$

where $\bar{F}_{H;K,j} = [\bar{F}_H(x)](x_{K,j})$. For the d-dimensional case let e_i be the i-th unit vector and denote by

$$\bar{F}^{(i)}_{H;K,j} = [\bar{F}_H(x \cdot e_i)](x_{K,j})$$

the i-th component of the flux. Then we have

$$[\bar{F}_H(v_H)](x_{K,j}) = \bar{F}_{H;K,j} \nabla v_H(x_{K,j}),$$

where

$$\bar{F}_{H;K,j} = [\bar{F}^{(1)}_{H;K,j}, \bar{F}^{(2)}_{H;K,j}, \dots, \bar{F}^{(d)}_{H;K,j}].$$

Note that we could use the same techniques to study F_H.

Lemma 5.5 (Symmetry of $\bar{B}^{\mathrm{fl}}_H$)**.** *The bilinear form $\bar{B}^{\mathrm{fl}}_H$ is symmetric, if the matrices $\bar{F}_{H;K,j}$ are symmetric.*

Proof. This lemma follows immediately from the equation

$$\begin{aligned}\bar{B}^{\mathrm{fl}}_H(v_H, w_H) &= \sum_{K\in\mathcal{T}_H}\sum_{j=1}^{J} \omega_{K,j}[\bar{F}_H(v_H)](x_{K,j})\cdot\nabla w_H(x_{K,j}) \\ &= \sum_{K\in\mathcal{T}_H}\sum_{j=1}^{J} \omega_{K,j}F_{H;K,j}\nabla v_H(x_{K,j})\cdot\nabla w_H(x_{K,j}).\end{aligned}$$

□

If $d = 1$, $\bar{F}_{H;K,j}$ is a scalar, hence obviously symmetric and therefore the symmetry of $\bar{B}^{\mathrm{fl}}_H$ follows. But for higher dimensions the flux $\bar{F}_{H;K,j}$ is in general not symmetric. For example, notice that

$$u_1(t;x) = x_1 + t^2x_2, \qquad u_2(t;x) = x_2,$$

are solutions of the two-dimensional wave equation with $a(x) = \left(\begin{smallmatrix} 2x_1x_2+c & 0 \\ 0 & 1\end{smallmatrix}\right)$ and initial data

$$\begin{aligned} u_1(0) &= x_1, & u_2(0) &= x_2, \\ \partial_t u_1(0) &= 0, & \partial_t u_2(0) &= 0.\end{aligned}$$

The constant c is chosen such that $a(x)$ remains positive definite for all x. The flux of the first solution is $A\nabla u_1 = (2x_1x_2, t^2)^T$, whereas the flux of the second solution is $A\nabla u_2 = (0,1)^T$. With Lemma 5.5 we can deduce that the corresponding bilinear form is not symmetric. Due to this lack of symmetry we do not further investigate the general d-dimensional case, but only the restriction to $d = 1$.

To conclude the presentation of the flux-averaging FE-HMM scheme (5.2), we apply it to our model example with $\varepsilon = 1/100$. The parameters are chosen as on page 54. Additionally, we set $\eta = \tau = 5\varepsilon$. The size of the sampling domain was chosen such that no information from the boundary intrudes into the averaging domain. We set

$$\delta = \eta + \tau\left(\sup_{x\in\Omega}|a^\varepsilon(x)|\right)^{\frac{1}{2}}.$$

To average the flux we used kernels in $\mathbb{K}^{9,9}$; see [53]. In Figure 5.14 we see that the homogenized solution is recovered as it is for the FE-HMM scheme (5.1). The maximal difference between the solutions u^{fl}_H and u_H of the two schemes is 7.16×10^{-6}.

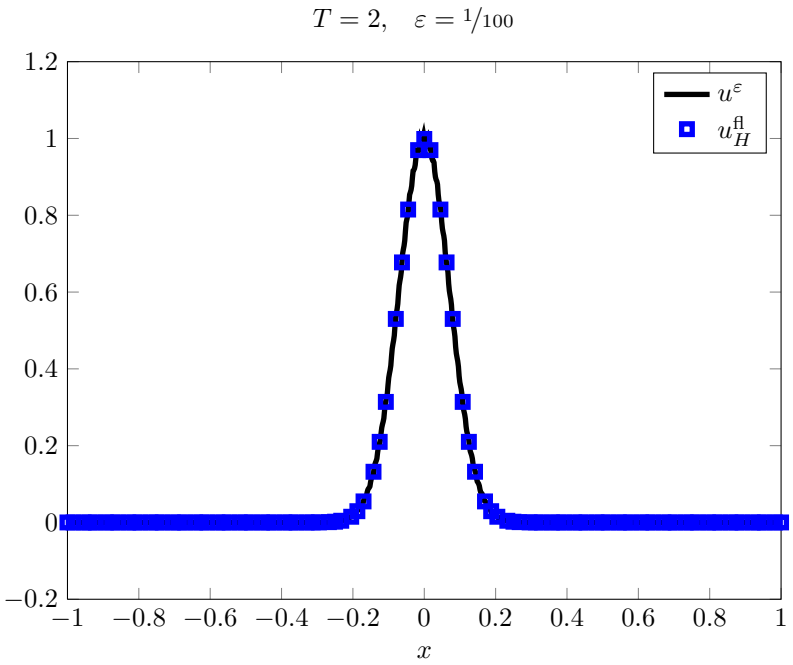

Figure 5.14: Reference solution u^ε and flux-averaging FE-HMM solution u_H^{fl} of the model example at $T = 2$ for $\varepsilon = 1/100$.

Hyperbolic FE-HMM

The second alternative that we propose is a combination between the standard and the flux-averaging FE-HMM. It uses the hyperbolic micro problem (5.4), but averages the micro solution and not the flux. It is given as follows: Find $u_H^{\mathrm{hyp}} \colon [0,T] \to S_0^\ell(\Omega, \mathcal{T}_H)$ such that

$$\begin{cases} \left(\partial_{tt} u_H^{\mathrm{hyp}}, v_H\right) + B_H^{\mathrm{hyp}}\left(u_H^{\mathrm{hyp}}, v_H\right) = (f, v_H) & \text{for all } v_H \in S_0^\ell(\Omega, \mathcal{T}_H),\ 0 \le t \le T, \\ u_H^{\mathrm{hyp}}(0) = I_H(u_I) & \text{in } \Omega, \\ \partial_t u_H^{\mathrm{hyp}}(0) = I_H(v_I) & \text{in } \Omega, \end{cases} \tag{5.8}$$

where

$$B_H^{\mathrm{hyp}}(v_H, w_H) = \sum_{K \in \mathcal{T}_H} \sum_{j=1}^{J} \omega_{K,j} \int_{I_\delta(0)} k_\eta(x) a^\varepsilon(x_{K,j} + x) \nabla \bar{v}_h(x) \cdot \nabla \bar{w}_h(x)\, dx \tag{5.9}$$

and $\bar{v}_h$ and $\bar{w}_h$ are given by

$$\bar{v}_h(x) = \int_{-\tau}^{\tau} k_\tau(t) \tilde{v}_h(t; x)\, dt, \tag{5.10}$$

with the obvious changes for $\bar{w}_h$. Again, $\tilde{v}_h$ is the solution of (5.4) with a linear coupling condition Q. Because we average the solution $\tilde{v}_h$ over the time interval $[-\tau, \tau]$ the micro solution $\bar{v}_h$ and $\bar{w}_h$ are time independent.

Furthermore, if we choose simple averages for the kernels, i.e.,

$$k_\eta(x) = \frac{1}{|I_\delta(0)|}\chi_{I_\delta(0)}(x) \quad \text{and} \quad k_\tau(t) = \frac{1}{2\tau}\chi_{[-\tau,\tau]}(t),$$

where χ denotes the characteristic function of the set indicated by the subscript, the bilinear form B_H^{hyp} becomes in this setting

$$B_H^{\text{hyp}}(v_H, w_H) = \sum_{K\in\mathcal{T}_H}\sum_{j=1}^{J}\frac{\omega_{K,j}}{|I_\delta|}\int_{I_\delta(0)} a^\varepsilon(x_{K,j}+x)\nabla\bar{v}_h(x)\cdot\nabla\bar{w}_h(x)\,dx.$$

We consider now the semidiscrete case where the micro problems are solved exactly. Let $\tilde{v}$ be the solution of the continuous hyperbolic micro problem (5.6) and

$$\bar{v}(x) = \int_{-\tau}^{\tau} k_\tau(t)\tilde{v}(t;x)\,dt.$$

Under sufficient smoothness we have

$$\begin{aligned}
-\nabla\cdot(a^\varepsilon(x_{K,j}+x)\nabla\bar{v}(x)) &= -\frac{1}{2\tau}\int_{-\tau}^{\tau}\nabla\cdot(a^\varepsilon(x_{K,j}+x)\nabla\tilde{v}(t;x))\,dt\\
&= -\frac{1}{2\tau}\int_{-\tau}^{\tau}\partial_{tt}\tilde{v}(t;x)\,dt\\
&= -\frac{1}{2\tau}\left(\partial_t\tilde{v}(\tau;x) - \partial_t\tilde{v}(-\tau;x)\right)\\
&= -\frac{1}{\tau}\partial_t\tilde{v}(\tau;x),
\end{aligned}$$

where we used the symmetry if $\tilde{v}$. We conclude, that $\bar{v}$ solves the continuous version of the elliptic micro problem (3.26), where the right-hand side is disturbed by a term of order $\Omega(1/\tau)$. Hence $\bar{v}$ approximates the solution of the elliptic micro problem v_h as τ increases. This shows the close relation between the hyperbolic and the standard FE-HMM scheme.

As for the flux-averaging FE-HMM scheme, we apply the hyperbolic FE-HMM scheme to our model problem. All the parameters are set as before for the flux-averaging FE-HMM scheme; see page 66. Again, we approximate well the homogenized solution u^0.

5.6 Comments on the implementation of the FE-HMM

The examples shown in Section 5.4 were computed by different implementations of the the FE-HMM. In this section we comment on the features of these different implementations. We do not explain the whole code, but give a brief overview.

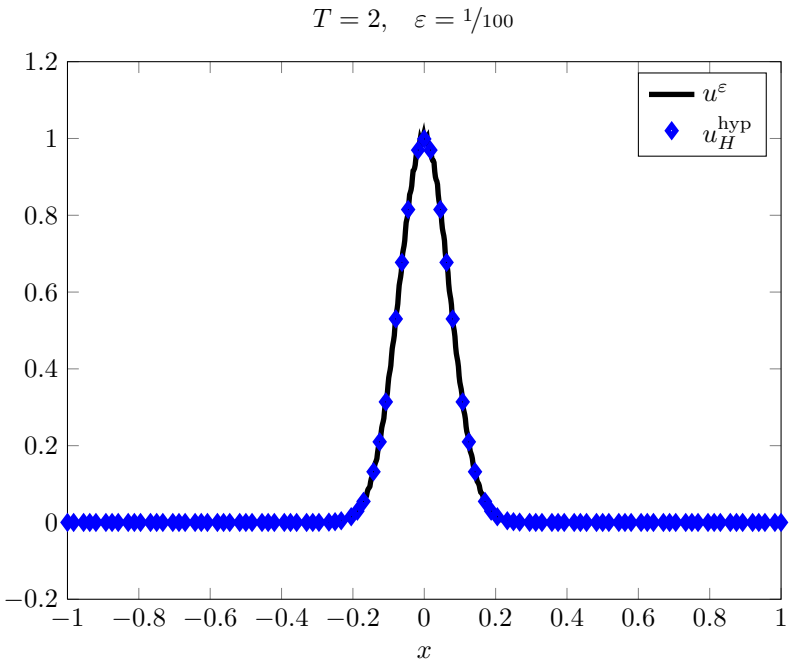

Figure 5.15: Reference solution u^ε and hyperbolic FE-HMM solution u_H^{hyp} of the model example at $T = 2$ for $\varepsilon = 1/100$.

One-dimensional FE-HMM

All the one-dimensional examples were computed with our own implementation of the FE-HMM scheme written in MATLAB. To be able to test various ideas and slight modifications of the FE-HMM easily we used a modular implementation. There are three main modules, one for the computation of the mass matrix, one for the computation of the stiffness matrix, and one for the time stepping scheme. The input parameters for the first two modules are the description of the material a^ε as a function handle, a description of the (macro) FEM, the quadrature formula that we use, and a list of the coordinates and the elements. The list of coordinates is a vector containing all interpolation nodes. In the list of elements every line contains the indexes of the nodes in a specific element. This representation follows the idea of [9] applied to the one-dimensional case. Although we use only uniform meshes for the examples shown in this thesis, nonuniform meshes could be used as well. The output is either the mass or the stiffness matrix.

Since we only consider affine-equivalent FE it is enough to prescribe the location of the interpolation nodes in the reference element $[0, 1]$ and the FE reference basis functions. For example, the nodes for linear FEM are given by `refElementNodes = [0,1]` and for quadratic FEM by `refElementNodes = [0,0.5,1]`. All reference basis functions are given as a single function handle, where each row is the evaluation of one basis function. For example, we have

```
phi_linear = @(x) [x; 1-x]
```

for linear FE and

```
phi_quad = @(x) [2*x.^2 - 3*x + 1; -4*x.^2 + 4*x; 2*x.^2 - x]
```

for quadratic FE. In addition we pass the derivatives of the basis function similarly. For the quadrature formula we pass two row vectors, the first one contains the quadrature node for the reference element and the second one contains the corresponding weights. For the trapezoidal quadrature these two vectors are `quadNodes = [0,1]` and `quadWeights = [0.5,0.5]` and for the Simpson rule `quadNodes = [0,0.5,1]` and `quadWeights = [1/6,2/3,1/6]`. The last input parameter is a function handle pointing to a routine that describes how to compute the element mass or stiffness matrix, respectively. The global mass and stiffness matrix are assembled elementwise, where a loop through all elements is implemented in the main module. In each iteration the necessary data are passed to the routine to compute the contribution of the current element. This design allows use of the same main module for different schemes. The only difference between standard FEM, FE-HMM, and flux-averaging FE-HMM is the computation of the element stiffness matrix. Therefore, the majority of the code can be reused.

For the time stepping we implemented both the second order leap-frog and the forth order modified equation scheme. Both schemes take the mass matrix, the stiffness matrix, and the initial data as input parameters and compute an approximation at the final time T. To reduce memory burden we do not save all time steps, but only the last two are stored. If the solution is not only needed at T but, for example, in addition at an intermediate time $\tilde{T} < T$, we run the time stepping scheme for 0 to $\tilde{T}$. After saving the needed data, we can continue starting from $\tilde{T}$. We do not have to recompute the time iteration from 0 to $\tilde{T}$ since leap-frog and ME can both be written as a three term recurrence relation. Hence we only use the last two time-steps.

Two-dimensional FE-HMM

To solve two-dimensional problems we use two different implementations. Our implementation uses the ideas from the implementation for one-dimension described above, but only rectangular elements on uniform meshes are supported. The code is a mixture of MATLAB and C combined by the MEX facility of MATLAB. The first two examples in two-dimensions shown in Section 5.4 are computed using this implementation.

The third example is computed with an adaption and extension of the FE-HMM implementation described in [7]. This MATLAB code is designed to solve multiscale elliptic or parabolic problems in two or three space dimensions with FE-HMM. It is freely available from `http://anmc.epfl.ch/abdulle.html`.

Since the estimation of the bilinear form is the same for elliptic, parabolic, or hyperbolic problems, we were able to use the part of the code which is devoted to the solution of the micro problems and the assembling of the stiffness matrix. To assemble the mass matrix we could profit from the implementation for the parabolic case. To the contrary,

the time stepping scheme is entirely new. We use a leap-frog scheme to solve the occurring second order system of ordinary differential equations. Because this implementation handles only linear and bilinear elements on a triangular, respectively a quadrilateral mesh, the chosen time stepping scheme is in accordance with the spatial solver, since it provides the same order of convergence. The quadrature formula is set fixed to be the barycenter rule for triangular and a Gauss-Legendre two points quadrature rule for quadrilateral elements.

Because of the ability to use nonregular meshes we use this code to compute the FE-HMM solution in complex computational domains, e.g., the last example in Section 5.4. In this example the computational domain is partitioned into subdomains respected by the triangulation. Each subdomain has its own tensor a^ε, but not all of them display a microscopic behavior. To decrease the computational cost we use FE-HMM only in the nonhomogeneous domains, whereas for the homogeneous subdomains standard FEM is used. To this goal we modified the code such that it can be prescribed whether FE-HMM or FEM is used for each subdomain.

Six

FE-HMM for the wave equation for long time

In Section 4.3 we have seen that the homogenized wave equation is not accurate enough for long-time intervals, since it neglects macroscopic dispersive effects, which do not influence the macroscopic behavior of the solution in the short run, but accumulate over time. Since the macro scale model of both HMM schemes presented in Chapter 5 is the homogenized wave equation we do not expect that these schemes recover the long-time dispersive effects. This is in fact true as can be seen from Figure 6.1. On the left we show the solution of the standard and on the right the solution of the flux-averaging FE-HMM scheme.

To design an FE-HMM scheme accurately for both time regimes the macro scale model needs to be changed. In Chapter 4 we have seen that the linearized Boussinesq

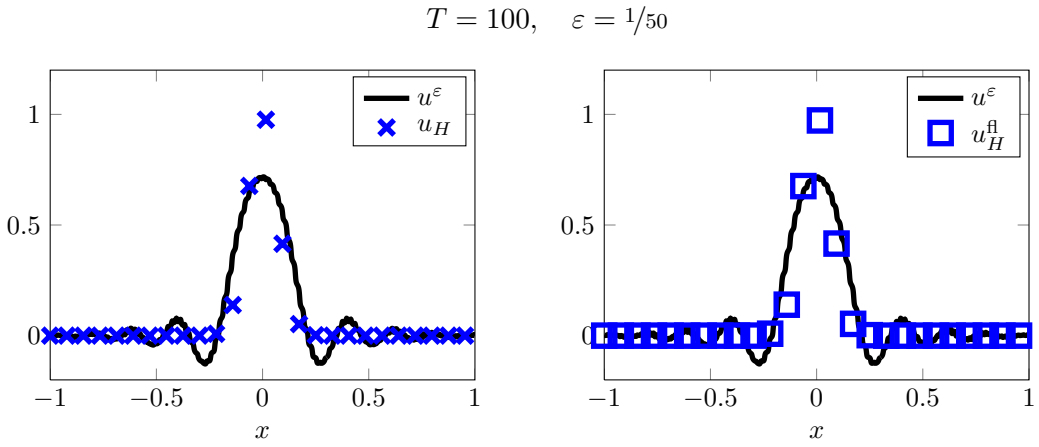

Figure 6.1: Reference solution u^ε, standard FE-HMM solution u_H, and flux-averaging FE-HMM solution u_H^{fl} of the model example at $T = 100$ for $\varepsilon = 1/50$. Both FE-HMM schemes do not recover the long-time dispersive effects.

equation is a suitable model. We will first focus on the linearized "improved" Boussinesq equation (4.9). In Section 6.4 we present two alternative formulations, where the first is based on the linearized "bad" Boussinesq equation (4.8).

6.1 Description of the multiscale method

We first consider the weak formulation of the one-dimensional linearized improved Bousinesq equation (4.9): Find $u\colon [0,T] \to H^1_0(\Omega)$ such that

$$\begin{cases} \partial_{tt}(u(t),v)^{\text{eff}} + B^\varepsilon(u(t),v) = (f(t),v) & \text{for all } v \in H^1_0(\Omega),\ 0 \le t \le T, \\ u(0) = u_I & \text{in } \Omega, \\ \partial_t u(0) = v_I & \text{in } \Omega, \end{cases} \tag{6.1}$$

where B^0 is the homogenized bilinear form defined in (4.7) and $(\cdot\,,\cdot)^{\text{eff}}$ is the sum of the standard L^2 inner product and a correction term

$$(v,w)^{\text{eff}} = (v,w) + (v,w)^{\text{cor}} \quad \text{for all } v,w \in H^1_0(\Omega).$$

The correction is given by

$$(v,w)^{\text{cor}} = \varepsilon^2 \int_\Omega \frac{b^0}{a^0} \partial_x v(x) \cdot \partial_x w(x)\, dx \quad \text{for all } v,w \in H^1_0(\Omega).$$

This correction is symmetric, bilinear, and positive semidefinite. Moreover it only depends on the spatial derivatives of its arguments and is of order $\mathcal{O}\big(\varepsilon^2\big)$.

We propose an FE-HMM scheme that uses (6.1) as a macro model. In contrast to the FE-HMM schemes of Chapter 5 we do not only need to estimate an effective bilinear form, but in addition we have to estimate the effective inner product $(\cdot\,,\cdot)^{\text{eff}}$, respectively, the correction $(\cdot\,,\cdot)^{\text{cor}}$. Since the bilinear form is the same for (6.1) and for the homogenized wave equation (4.6), we will use again the standard FE-HMM bilinear form B_H defined in (3.29). To not increase the computational cost of the method, we reuse the solution of the micro problems (3.26) to compute the FE-HMM correction of the L^2 inner product. The method described below lies in the FE-HMM framework described in Section 3.2 and can be seen as an extension of the FE-HMM for the wave equation described in Section 5.1. We do not repeat all the notation, since they remain unchanged.

The solution u_H of the FE-HMM scheme for long time (FE-HMM-L) is given by he following variational problem: Find $u_H\colon [0,T] \to S^\ell_0(\Omega,\mathcal{T}_H)$ such that

$$\begin{cases} (\partial_{tt} u_H, v_H)_H + B_H(u_H,v_H) = (f,v_H) & \text{for all } v_H \in S^\ell_0(\Omega,\mathcal{T}_H),\ 0 \le t \le T, \\ u_H(0) = I_H(u_I) & \text{in } \Omega, \\ \partial_t u_H(0) = I_H(v_I) & \text{in } \Omega, \end{cases} \tag{6.2}$$

where B_H given in (3.29) and

$$(v_H,w_H)_H = (v_H,w_H) + (v_H,w_H)^{\text{cor}}_H. \tag{6.3}$$

The approximation of the correction is given by

$$(v_H, w_H)_H^{\mathrm{cor}} = \sum_{K\in\mathcal{T}_H} \sum_{j=1}^{J} \frac{\omega_{K,j}}{|I_\delta|} \int_{I_\delta} (v_h(x) - v_{H,\mathrm{lin}}(x))(w_h(x) - w_{H,\mathrm{lin}}(x))\,dx, \tag{6.4}$$

where v_h, w_h are the solution of the micro problem (3.26) and $v_{H,\mathrm{lin}}$, $w_{H,\mathrm{lin}}$ are the linearizations of v_H, w_H, respectively, defined in (3.27).

Remark. For a fully discrete scheme in space, we have to evaluate the remaining L^2 inner products in the definition of $(\cdot\,,\cdot)_H$ with a quadrature formula. Again we emphasize that this quadrature formula may differ from the quadrature formula $\{x_{K,j}, \omega_{K,j}\}$.

Form (6.4) it is easy to see that $(\cdot\,,\cdot)_H^{\mathrm{cor}}$ is symmetric. Because all weights $\omega_{K,j}$ are positive it follows immediately that $(\cdot\,,\cdot)_H^{\mathrm{cor}}$ is positive semidefinite. Hence we can conclude in view of Lemma 6.1 that $(\cdot\,,\cdot)_H$ is in fact a true inner product and hence the FE-HMM-L is well defined for all $H, h > 0$.

6.2 Convergence analysis

Before giving an a priori error estimate for FE-HMM-L, we show that the approximation of the correction has the same properties as the true correction itself. The bilinearity, the dependence of the spatial derivatives, and the second order bound in ε follow directly from the following lemma.

Lemma 6.1. *The following identity holds:*

$$(v_H, w_H)_H^{\mathrm{cor}} = \varepsilon^2 \sum_{K\in\mathcal{T}_H} \sum_{j=1}^{J} \omega_{K,j} m_K^{\mathrm{cor}}(x_{K,j}) \nabla v_H(x_{K,j}) \cdot \nabla w_H(x_{K,j}).$$

The $(d\times d)$-matrix $m_K^{\mathrm{cor}}(x_{K,j})$ is symmetric and given by

$$(m_K^{\mathrm{cor}}(x_{K,j}))_{r,s} = \left(\frac{\delta}{\varepsilon}\right)^2 \int_Y \hat{\psi}_h^r(y)\hat{\psi}_h^s(y)\,dy,$$

where $\hat{\psi}_h^s \in S^q\Big(Y, \hat{\mathcal{T}}_h\Big)$ solves

$$\int_Y a_{x_{K,j}}(y)\nabla\hat{\psi}_h^s(y)\cdot\nabla\hat{z}_h\,dy = -\int_Y a_{x_{K,j}}(y)e_s\cdot\nabla\hat{z}_h\,dy \qquad \text{for all } \hat{z}_h \in S^q\Big(Y,\hat{\mathcal{T}}_h\Big), \tag{6.5}$$

and $a_{x_{K,j}}(y) = a^\varepsilon(x_{K,j}+\delta y)$. As before $Y = [-1/2, 1/2]^d$ denotes the centered unit cube and $\hat{\mathcal{T}}_h$ is the scaled and translated micro triangulation $\mathcal{T}_h$ of the sampling domain I_δ given by

$$\hat{\mathcal{T}}_h = \frac{1}{\delta}\mathcal{T}_h - x_{K,j}.$$

Moreover, we have for all $v_H, w_H \in S_0^\ell(\Omega, \mathcal{T}_H)$

$$|(v_H, w_H)_H^{\mathrm{cor}}| \le \tilde{C}\varepsilon^2 \left\|\nabla v_H\right\|_{L^2(\Omega)} \left\|\nabla w_H\right\|_{L^2(\Omega)}, \tag{6.6}$$

where $\tilde{C} = Cd(\delta/\varepsilon)^2(\Lambda/\lambda)$ *with a constant* C *independent of all the mentioned parameters. Note that inequality* (6.6) *gives the correct order in* ε *because* $\delta/\varepsilon = \mathcal{O}(1)$.

Proof. Recalling the definition of the micro problem (3.26) we note that its solution can be expressed as

$$v_h(x) = v_{H,\mathrm{lin}}(x) + \sum_{s=1}^{d} \psi_h^s(x) \nabla v_H(x_{K,j}) \cdot e_s,$$

where ψ_h^s is defined in (3.31). Identifying $x = x_{K,j} + \delta y$ we can write ψ_h^s with the solution of the scaled micro problem (6.5) as

$$\psi_h^s(x) = \delta \hat{\psi}_h^s(y).$$

We can proceed as follows:

$$\begin{aligned}
(v_H, w_H)_H^{\mathrm{cor}} &= \sum_{K\in\mathcal{T}_H} \sum_{j=1}^{J} \frac{\omega_{K,j}}{|I_\delta|} \int_{I_\delta} (v_h(x) - v_{H,\mathrm{lin}}(x))(w_h(x) - w_{H,\mathrm{lin}}(x))\, dx \\
&= \sum_{K\in\mathcal{T}_H} \sum_{j=1}^{J} \frac{\omega_{K,j}}{|I_\delta|} \cdot \\
&\qquad \int_{I_\delta} \left(\sum_{s=1}^{d} \psi_h^s(x) \nabla v_H(x_{K,j}) \cdot e_s \right) \left(\sum_{r=1}^{d} \psi_h^r(x) \nabla v_H(x_{K,j}) \cdot e_r \right) dx \\
&= \sum_{K\in\mathcal{T}_H} \sum_{j=1}^{J} \frac{\omega_{K,j}}{|I_\delta|} \sum_{r,s=1}^{d} \partial_{x_r} v_H(x_{K,j}) \left(\int_{I_\delta} \psi_h^r(x) \psi_h^s(x)\, dx \right) \partial_{x_s} w_H(x_{K,j}) \\
&= \sum_{K\in\mathcal{T}_H} \sum_{j=1}^{J} \omega_{K,j} \sum_{r,s=1}^{d} \partial_{x_r} v_H(x_{K,j}) \left(\delta^2 \int_Y \hat{\psi}_h^r(y) \hat{\psi}_h^s(y)\, dy \right) \partial_{x_s} w_H(x_{K,j}) \\
&= \sum_{K\in\mathcal{T}_H} \sum_{j=1}^{J} \omega_{K,j} \sum_{r,s=1}^{d} \partial_{x_r} v_H(x_{K,j}) \left(\varepsilon^2 \left(m_K^{\mathrm{cor}}(x_{K,j}) \right)_{r,s} \right) \partial_{x_s} w_H(x_{K,j}) \\
&= \varepsilon^2 \sum_{K\in\mathcal{T}_H} \sum_{j=1}^{J} \omega_{K,j} m_K^{\mathrm{cor}}(x_{K,j}) \nabla v_H(x_{K,j}) \cdot \nabla w_H(x_{K,j}).
\end{aligned}$$

To show the second part of the lemma, we use that

$$\left\| \hat{\psi}_h^s \right\|_{H^1(Y)} \leq C \left\| \nabla_y \hat{\psi}_h^s \right\|_{L^2(Y)} \leq C \frac{\lambda}{\Lambda},$$

since $a^\varepsilon \in \mathcal{M}(\lambda, \Lambda)$ and therefore we have for all r and s

$$\left| \left(m_K^{\mathrm{cor}}(x_{K,j}) \right)_{r,s} \right| \leq C \left(\frac{\delta}{\varepsilon} \right)^2 \frac{\Lambda}{\lambda}.$$

Hence the following estimates holds for all $\xi \in \mathbb{R}^d$:

$$|m_K^{\mathrm{cor}}(x_{K,j})\xi| \leq \|m_K^{\mathrm{cor}}(x_{K,j})\|_F \, |\xi| \leq dC \left(\frac{\delta}{\varepsilon}\right)^2 \frac{\Lambda}{\lambda} \, |\xi| \, .$$

Thus we conclude

$$\begin{aligned}(v_H, w_H)_H^{\mathrm{cor}} &\leq \tilde{C}\varepsilon^2 \left(\sum_{K\in\mathcal{T}_H} \sum_{j=1}^{d} \omega_{K,j} \, |\nabla v_H(x_{K,j})|^2 \right)^{\frac{1}{2}} \left(\sum_{K\in\mathcal{T}_H} \sum_{j=1}^{d} \omega_{K,j} \, |\nabla v_H(x_{K,j})|^2 \right)^{\frac{1}{2}} \\ &\leq \tilde{C}\varepsilon^2 \, \|\nabla v_H\|_{L^2(\Omega)} \, \|\nabla w_H\|_{L^2(\Omega)} \, . \end{aligned}$$ □

Again we give a priori bounds for the difference between the homogenized and the HMM solution. In contrast to the convergence analysis in Section 5.2 we use here the FE-HMM-L scheme with the long-time correction of the L^2 inner product, defined in (6.2). This method fits into the setting of Theorems 3.1 and 3.2 which we apply to prove the following convergence result.

Theorem 6.2. *Let u^0 and u_H be the unique solutions of the homogenized wave equation (4.6) and the FE-HMM scheme (6.2), respectively. Suppose that the quadrature formula satisfies (3.16)–(3.18). Provided that $a^\varepsilon \in \mathcal{M}(\lambda, \Lambda)$, $a^0 \in W^{\ell,\infty}(\Omega)$, and the following regularity assumptions hold,*

$$\begin{aligned} &\partial_t^k u^0 \in L^2(0,T; H^{\ell+1}(\Omega)),\ \partial_t^{2+k} u^0 \in L^2(0,T; H^{\ell}(\Omega)) && \text{for } k = 0,1,2, \\ &u_I \in H^{\ell+1}(\Omega),\ v_I \in H^{\tilde{\ell}}(\Omega) && \text{with } \tilde{\ell} = \max\{\ell, 2\}, \end{aligned}$$

we have

$$\left\|\partial_t(u^0 - u_H)\right\|_{L^\infty(0,T;L^2(\Omega))} + \left\|u^0 - u_H\right\|_{L^\infty(0,T;H^1(\Omega))} \leq C\left(H^\ell + e_{\mathrm{HMM}} + \varepsilon^2\right)$$

for all $H \leq H_0$.

If the stronger regularity conditions $a^0 \in W^{\ell+1,\infty}(\Omega)$ and

$$\begin{aligned} &\partial_t^k u^0 \in L^2(0,T; H^{\ell+1}(\Omega)),\ \partial_t^{4} u^0 \in L^2(0,T; H^{\ell}(\Omega)) && \text{for } k = 0,1,2,3, \\ &u_I \in H^{\ell+1}(\Omega),\ v_I \in H^{\tilde{\ell}}(\Omega) && \text{with } \tilde{\ell} = \max\{\ell, 2\} \end{aligned}$$

hold, we have additionally

$$\left\|u^0 - u_H\right\|_{L^\infty(0,T;L^2(\Omega))} \leq C\left(H^{\ell+1} + e_{\mathrm{HMM}} + \varepsilon^2\right).$$

Moreover, if the quadrature formula also satisfies (3.19), we get the same error estimates, even if we replace $(\cdot\,,\cdot)$ with $(\cdot\,,\cdot)_{\mathrm{QF}}$ in the definition (6.3) of $(\cdot\,,\cdot)_H$.

Proof. We proceed as in the proof of Theorem 5.1. First we have to check that the assumptions of Theorems 3.1 and 3.2 are fulfilled with $\tilde{B} = B^0$ and $\{\cdot\,,\cdot\} = (\cdot\,,\cdot)_H$. We have already seen that the assumptions on the bilinear form B^0 hold with $\beta = e_{\mathrm{HMM}}$. Assumptions (3.6)–(3.8) with $\alpha = \tilde{C}\varepsilon^2$ follow immediately from Lemma 6.1. Hence we can apply the two cited theorems. Note that we absorb $\tilde{C}$ into the constant C to get the final result. Using numerical quadrature the coercivity of $(\cdot\,,\cdot)_{\mathrm{QF}}$ due to (3.19); see the remark on page 29. □

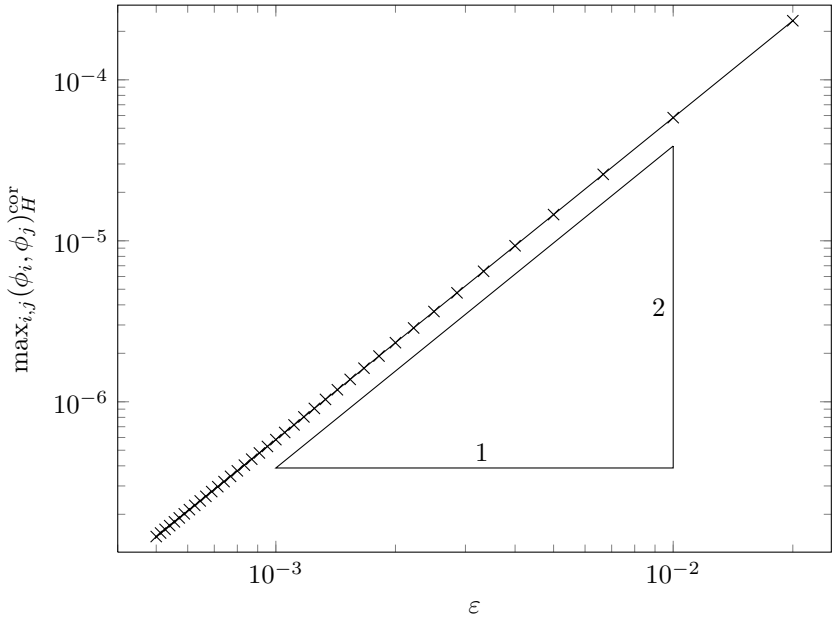

Figure 6.2: Size of the approximated correction $(\cdot\,,\cdot)_H^{\mathrm{cor}}$ for different values of ε. The expected second order dependence on ε is recovered.

Numerical confirmation

We recover the theoretical results of Lemma 6.1 and Theorem 6.2 numerically. First we consider again Ω and a^ε as given for the model example; see Section 4.1. For $\varepsilon = 1/50k$ with $k = 1, 2, \ldots, 40$, we computed $\max_{i,j}(\phi_i, \phi_j)_H^{\mathrm{cor}}$, where the ϕ_i are the standard linear FEM basis functions on a regular mesh with $H = 2^{-5}$. In Figure 6.2 the results are plotted on a log-log-scale against ε and we retrieve the expected second order convergence.

To recover the convergence order of the FE-HMM-L scheme we consider the same example as in Section 5.2 for the FE-HMM scheme. Since there is an additional addend in $\mathcal{O}\big(\varepsilon^2\big)$ in the a priori error estimate of Theorem 6.2 compared with Theorem 5.1, we reduce ε to $1/2000$ such that this additional term does not harm the observed convergence. In Figure 6.3 the L^2- and the H^1-error at $T = 0.6$ are shown for the FE-HMM-L with linear macro and micro solver for simultaneously refined mesh sizes H and h. The second order convergence of the L^2-error between the solution u_H of the FE-HMM-L scheme and the homogenized solution u^0 and the first order convergence of the corresponding H^1-error are clearly evident.

6.3 Numerical experiments

To show the usefulness and versatility of the FE-HMM-L we give some numerical examples. First we apply the FE-HMM-L to the model example. Afterwards we consider two further one-dimensional examples, where a^ε is not ε-periodic, but depends on the

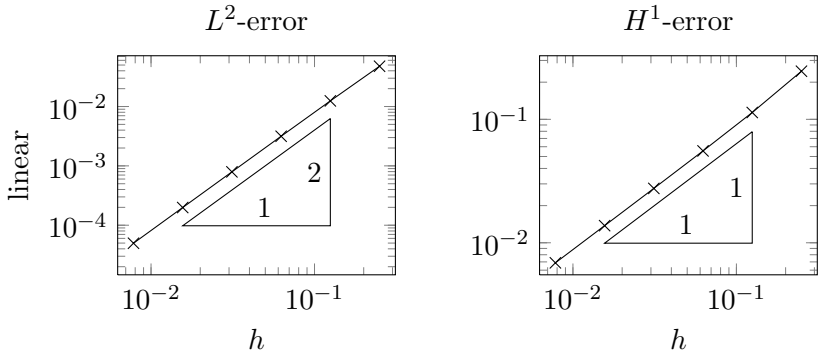

Figure 6.3: L^2- and the H^1-error of the FE-HMM with linear FEM for the macro and the micro solver. The expected orders of convergence are achieved if the macro and micro mesh are refined simultaneously.

macro scale. Note that for the construction of the FE-HMM-L scheme no particular dependence of the microscopic behavior, e.g., periodicity, is assumed. Finally, we show a two-dimensional example.

Model example

We apply the FE-HMM-L with $\mathcal{P}^3$ elements for the macro and the micro solver to our model example; see Section 4.1. For the time integration we use the leap-frog scheme. We set $\varepsilon = 1/50$ and choose the discretization parameters as follows:

$$H = 2^{-8} = \frac{1}{256}, \qquad h = \frac{\varepsilon}{100} = \frac{1}{5000}, \qquad \Delta t = \frac{H}{8} = \frac{1}{2048}.$$

Since we are interested in the long-time behavior of the wave equation, we have to be aware of numerical dispersion. This is why we can not enlarge the macro mesh size H to the same value as for the short-time experiment on page 54. In order not to violate the CFL condition the time step Δt must be adapted accordingly.

In Figure 6.4 we see that the FE-HMM-L solution u_H approximates the solution u^{eff} of the improved linearized Boussinesq equation (4.9). Thus, it is able to capture the long-time dispersive effects.

Explicit macroscale and microscale dependence

In the following two examples the tensor a^ε is no longer ε-periodic. Thus, the theoretical results of [25, 59, 60] mentioned in Section 4.3 are not applicable. Nevertheless, the FE-HMM-L solution coincides well with the reference solution. Similar experiments are considered in [36] to test the FD-HMM scheme for longer times.

For the first example the high frequency oscillation of a^ε is superposed with a low frequency oscillation. The squared wave propagation speed is given by

$$a_1^\varepsilon(x) = \sqrt{2} + \frac{1}{2}\left(\cos\left(\pi x\right) + \sin\left(2\pi\frac{x}{\varepsilon}\right)\right).$$

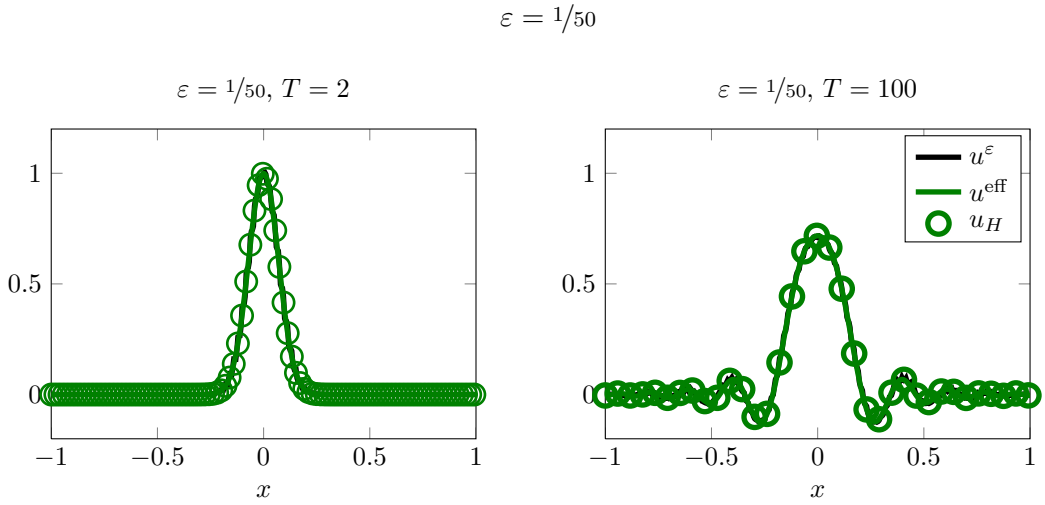

Figure 6.4: Reference solution ε, effective solution u^{eff} of the improved linearized Boussinesq equation, and FE-HMM-L solution u_H of the model example at $T = 2$ and $T = 100$ for $\varepsilon = 1/50$.

For the second example we again consider a fast varying media, where the amplitude of the oscillations changes on a macroscopic level. Here the squared wave propagation speed is given by

$$a_2^\varepsilon(x) = \left(\sqrt{2} + \frac{1}{2}\sin\left(2\pi\frac{x}{\varepsilon}\right)\right)\left((1 + \frac{1}{4}\cos(\pi x)\right).$$

The initial condition is a Gaussian pulse with zero initial velocity as for the model example, the computational domain Ω is $[-1, 1]$, and the boundary conditions are again imposed to be periodic.

In both examples we compare the numerical solution of the FE-HMM-L scheme with a reference solution computed on a fully resolved mesh. We use cubic FE and the leap-frog time stepping scheme. The discretization parameters are

$$\varepsilon = \delta = \frac{1}{50}, \qquad H = 2^{-10}, \qquad h = \frac{\varepsilon}{500}, \qquad \Delta t = \frac{H}{8}.$$

In addition we compute the solution of the standard FE-HMM scheme with the same discretization.

The results are shown in Figure 6.5 for the first example and in Figure 6.6 for the second example. For short times all three solutions coincide. For longer times, however, the standard FE-HMM solution deviates from the reference solution, whereas the FE-HMM-L scheme provides reliable results for short and long times.

Two-dimensional example

We consider two-dimensional wave propagation in a periodic, highly oscillating, anisotropic waveguide. The computational domain is given by $\Omega = [-1, 1] \times [0, 0.25]$.

$$a_1^\varepsilon(x) = \sqrt{2} + \frac{1}{2}\left(\cos\left(\pi x\right) + \sin\left(2\pi\frac{x}{\varepsilon}\right)\right) \text{ for } \varepsilon = \frac{1}{50}.$$

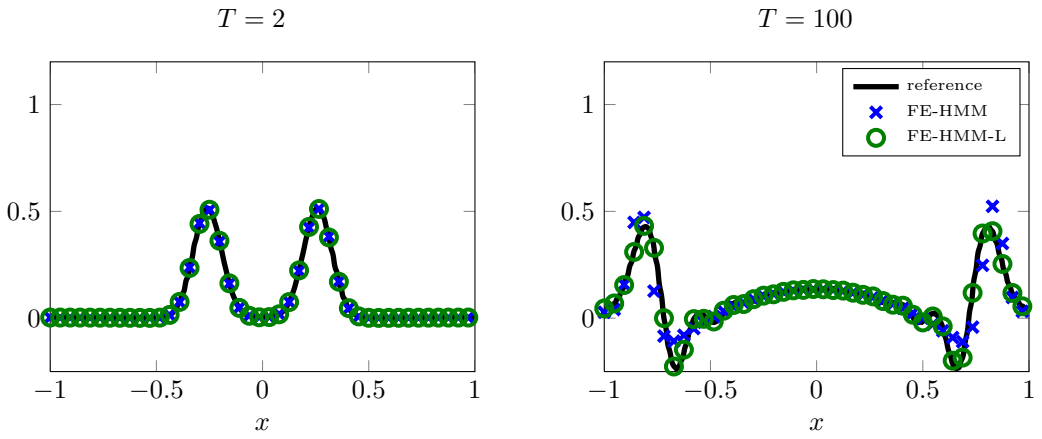

Figure 6.5: Reference, FE-HMM, and FE-HMM-L solution at $T = 2$ and $T = 100$ for $\varepsilon = 1/50$ with tensor a_1^ε.

$$a_2^\varepsilon(x) = \left(\sqrt{2} + \frac{1}{2}\sin\left(2\pi\frac{x}{\varepsilon}\right)\right)\left(1 + \frac{1}{4}\cos(\pi x)\right) \text{ for } \varepsilon = \frac{1}{50}.$$

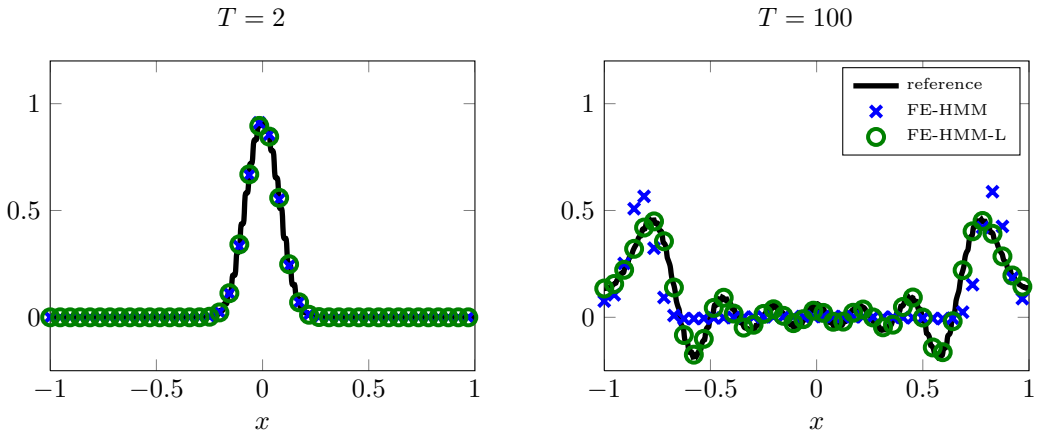

Figure 6.6: Reference, FE-HMM, and FE-HMM-L solution at $T = 2$ and $T = 100$ for $\varepsilon = 1/50$ with tensor a_2^ε.

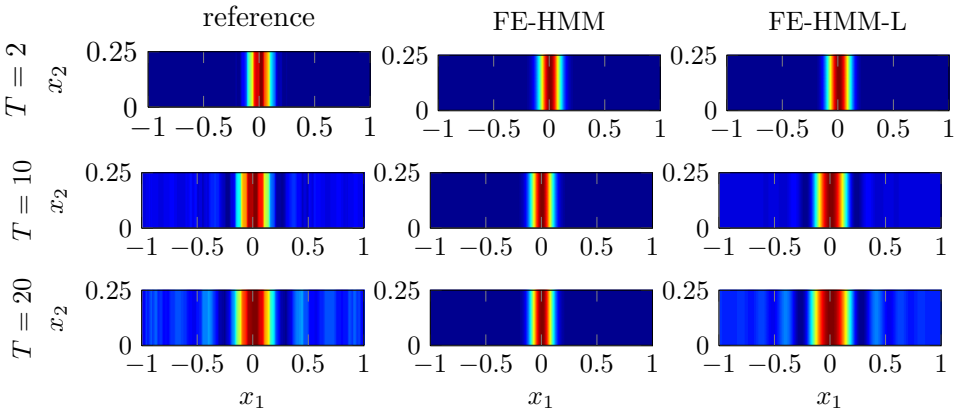

Figure 6.7: Three snapshot of reference solution u^ε (left), the FE-HMM solution (middle), and the FE-HMM-L solution (right) at $T = 2$, 10, and 20 for $\varepsilon = 1/20$.

We impose homogeneous Neumann boundary conditions on the top and bottom and a periodic boundary condition on the left and right. As initial condition we consider a Gaussian pulse in the x_1 direction with zero initial velocity, i.e.,

$$u_I(x) = u_I(x_1) = \exp(-100x_1^2), \qquad v_I(x) = 0.$$

The material is described by the tensor

$$a^\varepsilon(x) = \begin{pmatrix} \sqrt{2} + \sin\left(2\pi\frac{x_1}{\varepsilon}\right) & \\ & 1 + \frac{1}{2}\sin\left(2\pi\frac{x_1}{\varepsilon}\right) \end{pmatrix}$$

with $\varepsilon = 1/20$. Since a^ε only depends on x_1, we can apply formula (2.15) to compute the homogenized tensor

$$a^0(x) = \begin{pmatrix} 1 & 0 \\ 0 & 1 \end{pmatrix}.$$

Because of this particular choice the homogenized solution is given by

$$u^0(t;x) = \frac{1}{2}\left(\exp(-100(x_1 - t)^2) + \exp(-100(x_1 + t)^2)\right)$$

and displays no dispersive behavior. However, the reference solution computed with $\mathcal{Q}^1$ finite elements on a fully resolved grid is dispersive, as can be seen on the left column of Figure 6.7. The standard FE-HMM scheme approximates the u^0 and thus fails to capture these long-time dispersive effects; see the middle column of Figure 6.7. By way of contrast, the FE-HMM-L solution is dispersive as well; see the right column of Figure 6.7. For easier comparison cross sections of the three solutions at $x_2 = 0.1$ are shown in Figure 6.8.

For both schemes we used $\mathcal{Q}^1$ finite elements for the macro and the micro solver with a two points Gauss quadrature rule given on the reference element $[0, 1]^2$ by the nodes

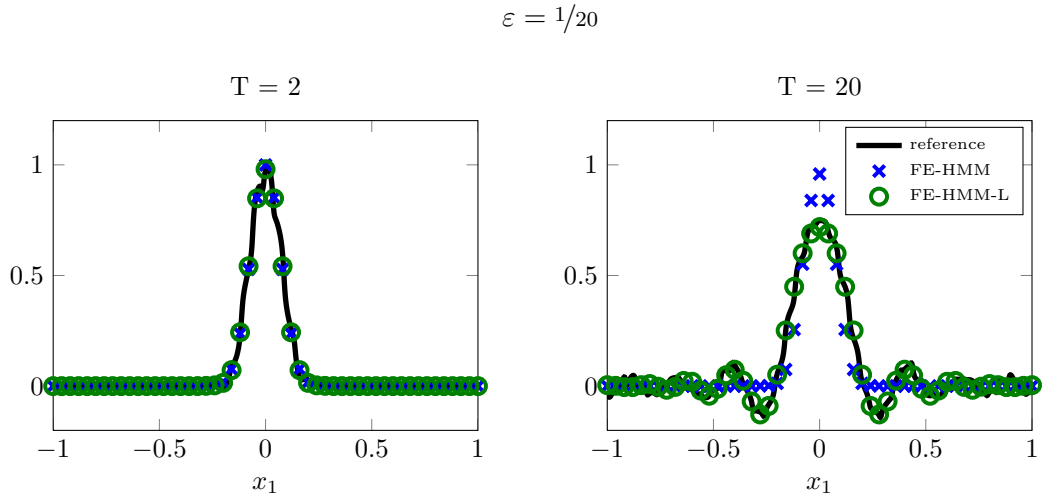

Figure 6.8: Cross section of the reference solution, the FE-HMM solution, and the FE-HMM-L solution at $x_2 = 0.1$ for $T = 2$ and $T = 20$.

$(1/2 \pm \sqrt{3}/6, 1/2 \pm \sqrt{3}/6)$ and the corresponding weights $\hat{\omega}_j = 1/4$ for $1 \leq j \leq 4$. The macro and micro mesh sizes are given by

$$H = \frac{1}{200} \qquad \text{and} \qquad h = \frac{1}{2000}.$$

For the time stepping we used the leap-frog scheme.

6.4 Alternative FE-HMM-L formulations

In [36, 39] the FD-HMM scheme proposed in [35, 37] was modified to recover the long-time dispersive effects. In this method an effective flux is still computed by solving the wave equation on a micro space-time sampling domain. These domains must be larger than the sampling domains used in the original FD-HMM scheme. However, the use of a cubic coupling condition between the macro and the micro solver is the main modification for the new scheme. Because of the enhanced coupling mechanism the flux depends not only on the first, but also on the second and third derivative of the solution.

We present a modification of the flux-averaging FE-HMM scheme, which follows these ideas. The second formulation that we present resembles the FE-HMM-L scheme. Again, an effective linear form is computed, but the micro problem is no longer elliptic, but hyperbolic. Because the symmetry can only be guaranteed for one dimension, see Section 5.5, we restrict ourself to this particular case.

Modification of the flux-averaging scheme

Like the FD-HMM of [36, 39] the macroscopic model which this modification relies on is the linearized "bad" Boussinesq equation (4.8). Multiplying this equation with a

test function v and integrating by parts we get

$$\partial_{tt}\Big(u^{\text{eff}}(t), v\Big) + B^{\text{eff}}\Big(u^{\text{eff}}(t), v\Big) = (f(t), v),$$

where

$$B^{\text{eff}}(v, w) = \int_\Omega (a^0 \partial_x v + \varepsilon^2 b^0 \partial_{xxx} v) \cdot \partial_x w \, dx.$$

The sum in the parentheses can be seen as an effective flux, which we want to estimate by solving hyperbolic problems on small sampling domains. This effective flux depends on the third derivative, whereas the flux-averaging scheme (5.2) only depends on the first derivative of the macroscopic solution u_H; see formula (5.7). This dependence is caused by the linear coupling condition (5.5). To modify the flux-averaging FE-HMM (5.2), such that the flux F_H depends on the third spatial derivatives of u_H, we change the coupling condition to

$$[Q(v_H)](x) = c_0 v_H(x_{K,j}) + c_1 \partial_x v_H(x_{K,j}) \cdot x + c_2 \partial_{xx} v_H(x_{K,j}) \cdot \frac{x^2}{2} + c_3 \partial_{xxx} v_H(x_{K,j}) \cdot \frac{x^3}{6},$$

where c_0, c_1, c_2, and c_3 must be chosen appropriately. This means that the initial data of the micro problem must be consistent with the macroscopic solution, as was pointed out in [36,39]. The change of the coupling condition is the main modification. Otherwise the scheme is given as in (5.2). Since this coupling uses spatial derivatives up to order three of the macroscopic FE solution, such a coupling is only meaningful for FE of order three or higher.

From numerous numerical experiments we have detected the effects of these coefficients: The coefficients c_0 and c_2 do not influence the solution at all. For c_0 this can be explained since only the derivative of the microscale solution is used in the averaging process of the micro fluxes; see (5.3). The coefficient c_2 has no influence because of symmetry, since we only use symmetric kernels and purely periodic ε in our tests. The coefficient c_1 mainly influences the propagation speed of the wave, whereas c_3 determines how dispersive the scheme is. Setting $c_3 = 0$ we could not observe any long-time dispersive effects. Therefore, it is inevitable that a scheme, capable of recovering the long-time dispersive effects of wave propagation through a highly oscillatory medium, has a $c_3 > 0$. On the downside, we saw that the stiffness matrix is no longer symmetric if c_3 is positive. We could not resolve this dilemma of wanting both a symmetric scheme, which is capable of recovering the long-time dispersive effects, with this approach.

Hyperbolic FE-HMM-L

As in the short-time regime we can replace the elliptic with a hyperbolic micro problem. This formulation can be seen as a combination of the FE-HMM-L (6.2) and the hyperbolic FE-HMM scheme (5.8). It reads as follows: Find $u_H^{\text{hyp}} \colon [0, T] \to S_0^\ell(\Omega, \mathcal{T}_H)$

such that

$$\begin{cases} \Big(\partial_{tt} u_H^{\mathrm{hyp}}, v_H\Big)_H^{\mathrm{hyp}} + B_H^{\mathrm{hyp}}\Big(u_H^{\mathrm{hyp}}, v_H\Big) = (f, v_H) & \text{for all } v_H \in S_0^\ell(\Omega, \mathcal{T}_H),\ 0 \le t \le T, \\ u_H^{\mathrm{hyp}}(0) = I_H(u_I) & \text{in } \Omega, \\ \partial_t u_H^{\mathrm{hyp}}(0) = I_H(v_I) & \text{in } \Omega, \end{cases}$$

where B_H^{hyp} is given in (5.9) and

$$(v_H, w_H)_H^{\mathrm{hyp}} = (v_H, w_H) + (v_H, w_H)_H^{\mathrm{cor,hyp}}.$$

The approximation of the correction is given by

$$(v_H, w_H)_H^{\mathrm{cor,hyp}} = \sum_{K \in \mathcal{T}_H} \sum_{j=1}^{J} \omega_{K,j} \int_{I_\delta(0)} k_\eta(x) \bar{v}_h(x) \bar{w}_h(x)\, dx,$$

where $\bar{v}_h$ and $\bar{w}_h$ are the weighted averages over $[-\tau, \tau]$ of the solutions $\tilde{v}_h$ and $\tilde{w}_h$ of the micro problem (5.4); see (5.10). The coupling condition of the micro problem is given by

$$[Q(v_H)](x) = \nabla v_H(x_{K,j}) \cdot x. \tag{6.7}$$

Remark. This coupling condition differs slightly from (5.5) where a constant term is added. Note that this difference has no influence for the computation of the bilinear form B_H^{hyp} since only the spatial derivatives of $\bar{v}_h$ and $\bar{w}_h$ are used. Hence the additional constant cancels out. However, for the computation of $(\cdot\,, \cdot)_H^{\mathrm{cor,hyp}}$ the choice of the coupling condition is crucial. By choosing (6.7) we can use the same solution of the micro problem for both computations. Therefore, every micro problem needs to be solved only once.

The hyperbolic FE-HMM-L behaves comparably to the standard FE-HMM scheme: with the correction of the L^2 inner product it is not only accurate for short time, but captures the long-time dispersive effects as well. To demonstrate this we consider again the model problem for $\varepsilon = 1/50$; see Figure 6.9. We set $\eta = \tau = 10\varepsilon$ and $k_\eta, k_\tau \in \mathbb{K}^{9,9}$.

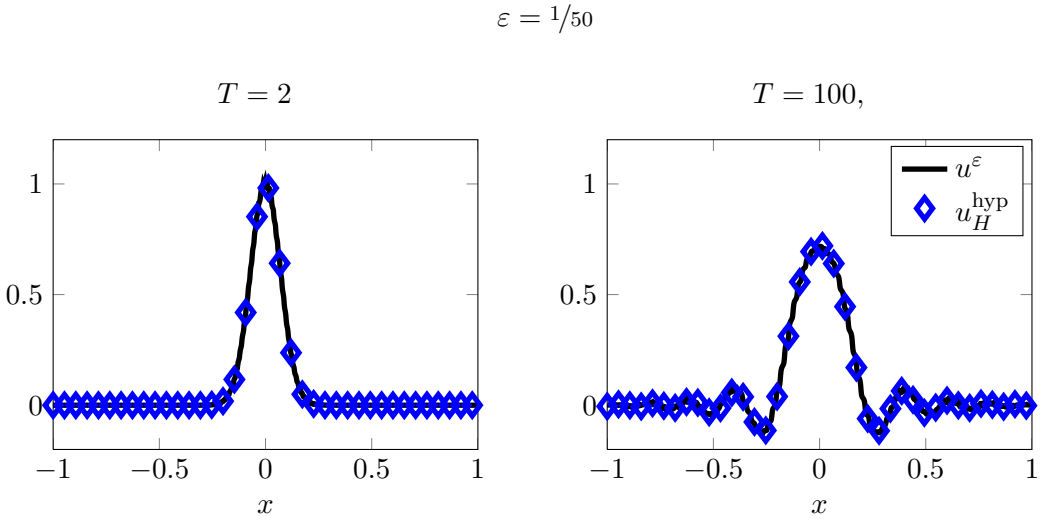

Figure 6.9: Reference solution u^ε and hyperbolic FE-HMM-L solution u_H^{hyp} of the model example at $T = 2$ and $T = 100$ for $\varepsilon = 1/50$. Similarly to standard FE-HMM-L, hyperbolic FE-HMM-L recovers the long-time dispersive effects.

Part III

Conclusions and Future Work

Seven

Conclusions and Future Work

7.1 Conclusions

In this thesis we have shown that the HMM framework can be used to simulate acoustic wave propagation in a highly oscillatory medium. We focused on FEM because of its ability to handle complex geometry easily and its profound theoretical foundation. The standard FE-HMM approximates the solution of the homogenized wave equation without precomputation of any effective coefficients. We have shown that this approach leads to a significant reduction of CPU time as well as a reduction in memory reduction, since we only need to fully resolve the medium on small sampling domains. To solve the arising system of second order ordinary differential equations we used the second order leap-frog or the fourth order modified equation scheme. Here, the computational gain from the fact that the triangulation for the macro solver does not need to resolve the micro structure of the medium is twofold. On one side the number of degrees of freedom and hence the sizes of the mass matrix and the stiffness matrix are substantially reduced. On the other side we can use a greater time step due to the CFL condition.

The overall behavior of the wave is well described by the homogenized wave equation, but for longer times the true solution deviates as a large secondary wave train develops. This dispersive behavior is not captured by classical homogenization theory. Since the FE-HMM converges to the homogenized solution, it does also not recover the dispersion. To get a reliable approximation of the true solution even in this long-time regime we modified the method. This modification is based on the improved linearized Boussinesq equation, which was shown to serve as an effective model for short and long times. In addition to the estimation of the homogenized bilinear form we estimated a small correction of the L^2 inner product. We have shown that this correction is of order ε^2 and only depends on the gradient of the macroscopic solution. This is consistent with our expectations raised from the effective model. The FE-HMM scheme with the L^2 correction, called FE-HMM-L, is well-posed and stable for all H, h, and ε.

We have proven convergence to the solution of the homogenized wave equation for both methods, FE-HMM and FE-HMM-L, in the L^2 and the energy norm. The proof relies on new Strang-type results for the wave equation. It covers not only the case

where the L^2 product is computed analytically, but also the use of a quadrature formula is comprised. This is of special interest since it justifies the use of mass lumping techniques for the FE-HMM. Note that mass lumping leads to a diagonal mass matrix and thus its inversion, which is needed in every time step, becomes trivial. The proof of the Strang-type results follows and generalizes ideas from convergence proofs for standard FEM with numerical quadrature. Its key ingredient is the consideration of an adequately defined elliptic projection. The imposed assumptions can be considered as conventional, since they are used for standard FEM with numerical quadrature as well. The order of dependence of the macro solver is conserved, but only if the micro mesh is refined accordingly. For the main convergence theorem no special assumptions such as periodicity of the medium are needed. As it is usual for FE-HMM, however, additional assumptions are needed to bound the HMM error e_{HMM}.

Various numerical experiments show the usefulness and versatility of the methods. In particular we retrieved the expected order of convergence numerically. In this thesis we restricted ourselves to examples in one and two dimensions, but the extension of the method to three-dimensional problems is straightforward. A model problem served as a test case to simplify the comparison between the different methods. We applied FE-HMM and FE-HMM-L to problems not covered by homogenization theory, especially in the long-time regime, where only results for ε-periodic materials are available. Nevertheless, we found good agreement between the HMM solutions and the reference solution computed on a fully resolved mesh.

We proposed alternative formulations of the FE-HMM and the FE-HMM-L method, where the elliptic micro problems are replaced by hyperbolic ones. More precisely we solved the wave equation on small space-time sampling domains. Since averaging the fluxes of the micro solution leads to a nonsymmetric stiffness matrix, except for the short-time one-dimensional case, we prefer to average the micro solution itself. The symmetry of the stiffness matrix is important, because the convergence proofs are not easily generalizable to nonsymmetric bilinear forms. Moreover, the symmetry gives rise to the conservation of a discretized energy. The time average of the micro solution over the sampling domain is time independent, which reveals a close relation between the hyperbolic and the standard FE-HMM. The L^2 long.-time correction can also be incorporated into this alternative formulation.

7.2 Future work

In this section we comment on open questions, present possible extensions of our work, and describe lines of research that could be pursued.

While the connection of the FE-HMM solution and the homogenized equation is well understood, an a priori error estimate between the effective solution and the solution of the Boussinesq-type effective model is still missing. Probably an extension of the general convergence Theorems 3.1 and 3.2 is needed. Instead of replacing the L^2 inner product involving second time derivatives by a nonstandard inner product in only one of the two wave equations, the case where both of these L^2 inner products are replaced should be

considered. Very recent theoretical results [25] might help to gain closer insight.

Furthermore, by revocation of restrictions one encounters new problems. While we considered wave propagation fields that vary rapidly in space, we always assumed that the tensor a^ε is time independent. Removing this assumption one has to distinguish between two cases; see [13, Chapter 2, Section 3]. In the first case a^ε changes only slowly over time, whereas in the second case a^ε oscillates on a microscopic time scale of order ε. For the first case we could apply FE-HMM and FE-HMM-L, but we would have to recalculate the stiffness matrix and the L^2 correction in every time step. Hence, we have to solve the micro problems over and over again, which is computationally costly. The natural question in this context is how tho reduce the computational work. In the context of time dependent tensors we refer to [8], where FE-HMM methods have been applied to parabolic problems. For the second case, however, the use of elliptic micro problems is unlikely to result in a reliable method. Here hyperbolic FE-HMM seems to be a more promising approach.

In this thesis only the tensor a^ε displays a multiscale nature, whereas the initial conditions vary only at the macroscale. In [38] an HMM scheme for one-dimensional wave-propagation with high frequency initial condition in a smooth, nonoscillatory medium is proposed. For the combination, i.e., wave propagation in a highly oscillatory medium with high frequency initial condition, no HMM scheme seems to be available.

Besides considering highly oscillatory media one could try to adapt FE-HMM such that it is applicable to perforated domain. The notion of H-convergence was generalized to perforated domains and called H^0-convergence; see [17]. This generalization was applied to the acoustic wave equation in [26]. An extension of our FE-HMM based on this theoretical framework would enlarge the number of treatable applications. There are HMM methods to solve elliptic problems in perforated domains, see, e.g., [52], which could be a starting point for the design of FE-HMM for acoustic wave propagation in such domains.

I hope that this thesis might be used as a sound basis for further research in multiscale methods for wave phenomena.

Bibliography

[1] Assyr Abdulle. On a priori error analysis of fully discrete heterogeneous multiscale fem. *Multiscale Modeling & Simulation*, 4(2):447–459, 2005.

[2] Assyr Abdulle. The finite element heterogeneous multiscale method: a computational strategy for multiscale pdes. *GAKUTO International Series, Math. Sci. Appl.*, 31:133–182, 2009.

[3] Assyr Abdulle. Discontinuous Galerkin finite element heterogeneous multiscale method for elliptic problems with mutiple scales. *Math. Comp.*, 81(278):687–713, 2012.

[4] Assyr Abdulle, Weinan E, Björn Engquist, and Eric Vanden-Eijnden. The heterogeneous multiscale method. *Acta Numerica*, 21:1–87, 2012.

[5] Assyr Abdulle and Marcus J. Grote. Finite element heterogeneous multiscale method for the wave equation. *Multiscale Model. Simul.*, 9(2):766–792, 2011.

[6] Assyr Abdulle, Marcus J. Grote, and Christian Stohrer. FE-HMM for the wave equation: Long time effects. *in preparation*, 2013.

[7] Assyr Abdulle and Achim Nonnenmacher. A short and versatile finite element multiscale code for homogenization problems. *Comput. Methods Appl. Mech. Engrg.*, 198(37–40):2839–2859, 2009.

[8] Assyr Abdulle and Gilles Vilmart. Coupling heterogeneous multiscale FEM with Runge-Kutta methods forparabolic homogenization problems: a fully discrete space-time analysis. *Math. Models Methods Appl. Sci.*, 22(6):1250002, 2012.

[9] Jochen Alberty, Carsten Carstensen, and Stefan A. Funken. Remarks around 50 lines of Matlab: short finite element implementation. *Numerical Algorithms*, 20:117–137, 1999.

[10] Grégoire Allaire. Homogenization and two-scale convergence. *SIAM J. Math. Anal.*, 23(6):1482–1518, 1992.

[11] Garth A. Baker. Error estimates for finite element methods for second order hyperbolic equations. *SIAM Journal on Numerical Analysis*, 13(4):564–576, 1976.

[12] Garth A. Baker and Vassilios A. Dougalis. The effect of quadrature errors on finite element approximations for second order hyperbolic equations. *SIAM Journal on Numerical Analysis*, 13(4):577 – 598, 9 1976.

[13] Alain Bensoussan, Jacques-Louis Lions, and George Papanicolaou. *Asymptotic Analysis for Periodic Structures*. AMS Chelsea Publishing, Providence, RI, 2011. Corrected reprint of the 1978 original.

[14] Felix Bloch. Über die Quantenmechanik der Elektronen in Kristallgittern. *Zeitschrift für Physik A Hadrons and Nuclei*, 52(7):555–600, 1929.

[15] Dietrich Braess. *Finite Elemente*. Springer-Verlag, dritte, korrigierte und ergänzte Auflage edition, 2003.

[16] Safia Brahim-Otsmane, Gilles A. Francfort, and François Murat. Correctors for the homogenization of the wave and heat equations. *J. Math. Pures Appl.*, 71:197–231, 1992.

[17] Marc Briane, Alain Damlamian, and Patrizia Donato. H-convergence for perforated domains. In *Nonlinear partial differential equations and their applications. Collège de France Seminar, Vol. XIII (Paris, 1994/1996)*, volume 391 of *Pitman Res. Notes Math. Ser.*, pages 62–100. Longman, Harlow, 1998.

[18] Russel E. Caflisch. Editoral policy. *Multiscale Model. Simul.*

[19] Wen Chen and Jacob Fish. A dispersive model for wave propagation in periodic heterogeneous media based on homogenization with multiple spatial and temporal scales. *Journal of Applied Mechanics*, 68(2):153–161, 2001.

[20] Philippe G. Ciarlet. *The Finite Element Method for Elliptic Problems*, volume 40 of *Classics in Applied Mathematics*. Society for Industrial and Applied Mathematics (SIAM), Philadelphia, PA, 2002. Reprint of the 1978 original.

[21] Philippe G. Ciarlet and Pierre-Arnaud Raviart. The combined effect of curved boundaries and numerical integration in isoparametric finite element methods. In *The mathematical foundations of the finite element method with applications to partial differential equations*, 1972.

[22] Doina Cioranescu and Patrizia Donato. *An Introduction to Homogenization*. Number 17 in Oxford lecture Series in Mathematics and its Application. Oxford, University Press, 1999.

[23] Gary C. Cohen. *Higher-order numerical methods for transient wave equations*. Scientific Computation. Springer-Verlag, Berlin, 2002.

[24] Richard Courant, Kurt Friedrichs, and Hans Lewy. Über die partiellen Differenzengleichungen der mathematischen Physik. *Math. Ann.*, 100(1):32–74, 1928.

[25] Thomas Dohnal, Agnes Lamacz, and Ben Schweizer. Dispersive effective equations for waves in heterogeneous media on large time scales. arXiv, 2013.

[26] Patrizia Donato and Florian Gaveau. Homogenization and correctors for the wave equation in non periodic perforated domains. *Networks and hetergeneous media*, 3(1):97 – 124, 2008.

[27] Qiao-Li Dong and Li-Qun Cao. Multiscale asymptotic expansions and numerical algorithms for the wave equations of second order with rapidly oscillating coefficients. *Applied Numerical Mathematics*, 59(12):3008 – 3032, 2009.

[28] Rui Du and Pingbing Ming. Heterogeneous multiscale finite element method with novel numerical integration schemes. *Communications in Mathematical Sciences*, 8(4):863–885, 2010.

[29] Todd Dupont. L^2-estimates for galerkin methods for second order hyperbolic equations. *SIAM Journal on Numerical Analysis*, 10(5):880–889, 1973.

[30] Weinan E and Bjorn Engquist. The heterogeneous multiscale methods. *Commun. Math. Sci*, 1(1):87–132, 2003.

[31] Weinan E, Bjorn Engquist, Xiantao Li, Weiqing Ren, and Eric Vanden-Eijnden. Heterogeneous multiscale methods: A review. *Communications in Computational Physics*, 2(3):367–450, 2007.

[32] Weinan E, Pingbing Ming, and Pingwen Zhang. Analysis of the heterogeneous multiscale method for elliptic homogenization problems. *J. Amer. Math. Soc.*, 18(1):121–156, 2005.

[33] Yalchin Efendiev and Thomas Y. Hou. *Multiscale Finite Element Methods*, volume 4 of *Surveys and Tutorials in the Applied Mathematical Sciences*. Springer New York, 2009.

[34] Hanafi El-Zoheiry. Numerical study of the improved Boussinesq equation. *Chaos Solitons Fractals*, 14(3):377–384, 2002.

[35] Björn Engquist, Henrik Holst, and Olof Runborg. Multiscale methods for the wave equation. *Proc. Appl. Math. Mech.*, 7(1):1140903–1140904, 2007.

[36] Björn Engquist, Henrik Holst, and Olof Runborg. Analysis of hmm for one dimensional wave propagation problems over long time, nov 2011.

[37] Björn Engquist, Henrik Holst, and Olof Runborg. Multi-scale methods for wave propagation in heterogeneous media. *Comm. Math. Sci.*, 9(1):33–56, 2011.

[38] Björn Engquist, Henrik Holst, and Olof Runborg. Multiscale methods for one dimensional wave propagation with high frequency initial data. Technical report, KTH Royal Institute of Technology, School of Computer Science and Communication, 2011. TRITA-NA-2011:7.

[39] Björn Engquist, Henrik Holst, and Olof Runborg. Multiscale methods for wave propagation in heterogeneous media over long time. In Björn Engquist, Olof Runborg, and Yen-Hsi Richard Tsai, editors, *Numerical Analysis of Multiscale Computations*, volume 82 of *Lecture Notes in Computational Science and Engineering*, pages 167–186. Springer, 2012.

[40] Björn Engquist and Yen-Hsi Tsai. Heterogeneous multiscale methods for stiff ordinary differential equations. *Mathematics of Computation*, 74(252):1707–1742, 2005.

[41] Lawrence C. Evans. *Partial Differential Equation*, volume 19 of *Graduate Studies in Mathematics*. American Mathematical Society, 1998.

[42] Jacob Fish and Wen Chen. Higher-order homogenization of initial/boundary-value problem. *Journal of Engineering Mechanics*, 127(12):1223–1230, dec 2001.

[43] Jacob Fish and Wen Chen. Uniformly valid multiple spatial-temporal scale modeling for wave propagation in heterogeneous media. *Mechanics of Advanced Materials and Structures*, 8(2):81–99, 2001.

[44] Jacob Fish and Wen Chen. Space-time multiscale model for wave propagation in heterogeneous media. *Computer methods in applied mechanics and engineering*, 193(45-47):4837–4856, 2004.

[45] Jacob Fish, Wen Chen, and Gakuji Nagai. Non-local dispersive model for wave propagation in heterogeneous media: multi-dimensional case. *International journal for numerical methods in engineering*, 54(3):347–363, 2002.

[46] Jacob Fish, Wen Chen, and Gakuuji Nagai. Non-local dispersive model for wave propagation in heterogeneous media. part 1: one-dimensional case. *International journal for numerical methods in engineering*, 54(3):331–346, 2002.

[47] Jean Charles Gilbert and Patrick Joly. Higher order time stepping for second order hyperbolic problems and optimal CFL conditions. In *Partial differential equations*, volume 16 of *Comput. Methods Appl. Sci.* Springer, Dordrecht, 2008.

[48] Marcus J. Grote and Olaf Schenk. Multiscale analysis and simulation of waves in strongly heterogeneous media. Technical report, SNF Projekt 117703, 2010. Schlussbericht.

[49] Marcus J. Grote and Olaf Schenk. Multiscale analysis and simulation of waves in strongly heterogeneous media. Technical report, SNF Projekt 130050, 2011. Zwischenbericht.

[50] Marcus J. Grote and Olaf Schenk. Multiscale analysis and simulation of waves in strongly heterogeneous media. Technical report, SNF Projekt 130050, 2012. Schlussbericht.

[51] Houssem Haddar and Jan S. Hesthaven. Waves 2005 conference. *J. Comput. Appl. Math.*, 204(2):197 – 198, 2007. Special Issue: The Seventh International Conference on Mathematical and Numerical Aspects of Waves (WAVES'05).

[52] Patrick Henning and Mario Ohlberger. The heterogeneous multiscale finite element method for elliptic homogenization problems in perforated domains. *Numerische Mathematik*, 113:601–629, 2009.

[53] Henrik Holst. Algorithms and codes for wave propagation problems. Technical report, KTH Royal Institute of Technology, School of Computer Science and Communication, 2011. TRITA-NA 2011:6.

[54] Labib Iskandar and Padam C. Jain. Numerical solutions of the improved Boussinesq equation. *Proc. Indian Acad. Sci. Sect. A Math. Sci.*, 89(3):171–181, 1980.

[55] Hossein Jafari, Abdollah Borhanifar, and S. A. Karimi. New solitary wave solutions for the bad Boussinesq and good Boussinesq equations. *Numer. Methods Partial Differential Equations*, 25(5):1231–1237, 2009.

[56] Lijian Jiang, Yalchin Efendiev, and Victor Ginting. Analysis of global multiscale finite element methods for wave equations with continuum spatial scales. *Applied Numerical Mathematics*, 60(8):862–876, 2010.

[57] V. V. Jikov, S. M. Kozlov, and O. A. Oleinik. *Homogenization of Differential Operators and Integral Functionals*. Springer-Verlag, Berlin, 1994. Translated from the Russian by G. A. Yosifian.

[58] Oskana Korostyshevskaya and Susan E. Minkoff. A matrix analysis of operator-based upscaling for the wave equation. *SIAM J. Numer. Anal.*, 44(2):586–612, 2006.

[59] Agnes Lamacz. Dispersive effective models for waves in heterogeneous media. *Mathematical Models and Methods in Applied Sciences*, 21(9):1871–1899, 2011.

[60] Agnes Lamacz. *Waves in heterogeneous media: Long time behavior and dispersive models*. PhD thesis, TU Dortmund, June 2011.

[61] Jacques-Louis Lions and Enrico Magenes. *Non-Homogeneous Boundary Value Problems and Applications. Vol. I*, volume 181 of *Die Grundlehren der mathematischne Wissenschaften*. Springer-Verlag, 1972. Translated from the French by P. Kenneth.

[62] François Murat and Luc Tartar. *Topics in the Mathematical Modelling of Composite Materials*, volume 31 of *Progress in Nonlinear Differential Eequations and Their Applications*, chapter H-Convergence. Birkhäuser Boston, 1997.

[63] Gabriel Nguetseng. A general convergence result for a functional related to the theory of homogenization. *SIAM J. Math. Anal.*, 20(3):608–623, 1989.

[64] Houman Owhadi and Lei Zhang. Homogenization of parabolic equations with a continuum of space and time scales. *SIAM J. Numer. Anal.*, 46(1):1–36, 200.

[65] Houman Owhadi and Lei Zhang. Metric-based upscaling. *Comm. Pure Appl. Math.*, 60(5):675–723, 2007.

[66] Houman Owhadi and Lei Zhang. Numerical homogenization of the acoustic wave equation with a continuum of scales. *Computer Methods in Applied Mechanics and Engineering*, 198(3–4):397–406, 2008.

[67] Pierre-Arnaud Raviart. The use of numerical integration in finite element methods for solving parabolic equations. In *Topics in numerical analysis*, pages 233–264, 1972.

[68] Fadil Santosa and William W. Symes. A dispersive effective medium for wave propagation in periodic composites. *SIAM J. Appl. Math.*, 51(4):984–1005, 1991.

[69] Gregory R. Shubin and John B. Bell. A modified equation approach to constructing fourth order methods for acoustic wave propagation. *SIAM J. Sci. Statist. Comput.*, 8(2):135–151, 1987.

[70] Sergio Spagnolo. Sul limite delle soluzioni di problemi di Cauchy relativi all'equazione del calore. *Ann. Sc. Norm. Sup. Pisa*, 21(4):657–699, 1967.

[71] Tetyana Vdovina and Susan E. Minkoff. An a priori error analysis of operator upscaling for the acoustic wave equation. *International Journal of Numerical Analysis and Modeling*, 5(4):543–569, 2008.

[72] Tetyana Vdovina, Susan E. Minkoff, and Oskana Korostyshevskaya. Operator upscaling for the acoustic wave equation. *Multiscale Model. Simul.*, 4(4):1305–1338, 2005.

[73] Gerald B. Whitham. *Linear and nonlinear waves.* Wiley-Interscience [John Wiley & Sons], New York, 1974. Pure and Applied Mathematics.

[74] Calvin H. Wilcox. Theory of bloch waves. *Journal d' analyse mathématique*, 33:146–167, 1978.

[75] Xingye Yue and Weinan E. The local microscale problem in the multiscale modeling of strongly heterogeneous media: Effects of boundary conditions and cell size. *Journal of Computational Science*, 222(2):556–572, 2007.